



POLITECNICO
MILANO 1863

SCUOLA DI INGEGNERIA INDUSTRIALE
E DELL'INFORMAZIONE

Title:

Wireless Power Transfer Methods

**TESI DI LAUREA MAGISTRALE IN
ELECTRICAL ENGINEERING - INGEGNERIA ELETTRICA**

Author: Ahmed Abdelwahid Abdelmoniem Abdelaziz

Student ID: 941908

Advisor: Prof. Roberto Perini

Academic Year: 2022-07

ABSTRACT

Recently, there is emerging demand for safe and convenient conductive chargers, hence wireless charging systems are predicted to be efficient and sufficient option for satisfying this demand whereas the maturity status of this technology that is accompanied with wide range of applications of wireless chargers, specifically within changing the trend in transportation toward electrified ones has induced change toward higher power, power density, modularity, and scalability of designs

Various methods classified in various categories are used in such a technology. They can be categorized by either range or the physical principle it uses to transfer the electric energy. A comparison between their advantages and disadvantages has been discussed in this work.

In addition to increasing concerns for the safe and convenient power supply, there is a rapid-increasing interest in wireless power transfer (WPT) for industrial devices, consumer electronics, and electric vehicles (EVs). As the resonant circuit is one of the cores of both the near-field and far-field WPT systems, it is a pressing need for researchers to develop a high-efficiency high-frequency resonant circuit, especially for the mid-range near-field WPT system.

The modern attempts in magnetic and capacitor couplers designs, compensation networks, power electronics converters, are tackled. Wireless charging systems are considered where serious variations in their designs and applications are highlighted. On that basis, the comparisons between different solutions and design considerations are stated as the essential elements and technology roadmap that will be necessary to support large-scale deployment of high-power wireless charging systems.

While Resonant Inductive Power Transfer (RIPT) charging is a substantially resilient concept with the possibility of charging at any opportunity and is highly versatile for vehicles of all sizes. It faces some major problems, especially in regard to misalignment that may affect Mutual Inductance and Resonance Frequency, this work analyses this problem and the effect it may cause.

Moreover, Resonant Converters has been categorised and illustrated in detail. Selecting the most useful one in the process, with a proposed modification on the topology and a tuning method that they increase the efficiency of the conventional setting.

Keywords: Coupling, Mutual Inductance, Compensation, Frequency, Converters.

SOMMARIO

Recentemente è emersa una domanda di caricabatterie condutti sicuri e convenienti, per cui si prevede che i sistemi di ricarica senza fili siano un'opzione efficiente e sufficiente per soddisfare questa domanda, mentre lo stato di maturità di questa tecnologia, accompagnato da un'ampia gamma di applicazioni dei caricabatterie wireless, in particolare nell'ambito del cambiamento della tendenza dei trasporti verso quelli elettrificati, ha indotto un cambiamento verso una maggiore potenza, densità di potenza, modularità e scalabilità dei progetti.

In questa tecnologia vengono utilizzati diversi metodi classificati in varie categorie. Possono essere classificati in base alla portata o al principio fisico utilizzato per trasferire l'energia elettrica. In questo lavoro è stato discusso un confronto tra i loro vantaggi e svantaggi.

Oltre alle crescenti preoccupazioni per un'alimentazione sicura e conveniente, l'interesse per il trasferimento di energia senza fili (WPT) per i dispositivi industriali, l'elettronica di consumo e i veicoli elettrici (EV) è in rapido aumento. Poiché il circuito risonante è uno dei fulcri dei sistemi WPT in campo vicino e in campo lontano, è urgente per i ricercatori sviluppare un circuito risonante ad alta efficienza e ad alta frequenza, soprattutto per il sistema WPT in campo vicino di fascia media.

Vengono affrontati i moderni tentativi di progettazione di accoppiatori magnetici e condensatori, reti di compensazione e convertitori elettronici di potenza. Vengono presi in considerazione i sistemi di ricarica wireless, per i quali sono state evidenziate le gravi variazioni nei progetti e nelle applicazioni. Su questa base, il confronto tra le diverse soluzioni e le considerazioni progettuali sono indicate come gli elementi essenziali e la roadmap tecnologica che sarà necessaria per supportare la diffusione su larga scala dei sistemi di ricarica wireless ad alta potenza.

La ricarica con trasferimento di potenza induttivo risonante (RIPT) è un concetto sostanzialmente resiliente, con la possibilità di ricaricare in qualsiasi momento e altamente versatile per veicoli di tutte le dimensioni. Il presente lavoro analizza questo problema e l'effetto che può avere sulla frequenza di risonanza e sull'induttanza reciproca.

Inoltre, i convertitori risonanti sono stati classificati e illustrati in dettaglio. La selezione di quello più utile è stata effettuata con una proposta di modifica della topologia e un metodo di regolazione che aumenta l'efficienza dell'impostazione convenzionale.

Parole Chiave: Accoppiamento, Induttanza Reciproca, Compensazione, Frequenza, Convertitori.

ACKNOWLEDGEMENT

بعد الحمد لله والثناء عليه لما وفقنا له وما كنا لننجح لولا ان من الله علينا من عظيم فضله ووسيع رحمته

Words cannot express my gratitude to Professor Roberto Perini for his patience and feedback, I could not have taken this journey without his guidance and his expertise in the field of power electronics. Additionally, he kept pushing me to improve myself and my work as well. I will be deeply indebted to him for his supervision of this work.

I am also grateful to the academic staff of both Politecnico di Milano and University of Khartoum, who added precious skills and knowledge that will be reflected on my professional Career, and helped me achieve one of my targets in life graduating as an Electrical Mobility Engineer.

I would like to express my deepest appreciation to my late grandmother; Fathy Hassan Taha, who died before she can witness our success in life. I would like to dedicate my graduation with a Master Degree in Electrical Engineering to her soul. She remains the reason I keep pushing forward in the academic sector, her love and appreciation for science and knowledge remains the sparkle in my heart that encourages me to acquire knowledge every single day.

This endeavor would not have been possible without the unconditional love and support from all my family members, my dad, Engineer Abdelwahid Abdelmoniem; whom was my inspiration to join the engineering field. To my Mom, Amani Abdelgabbar; who kept believing in me and encouraged me consistently to accomplish my objectives. To my aunt Inaam, whom I look up to, I would like to express my deepest gratitude for taking care of the whole family and for your continuous devotion to patronage me at every possible opportunity; we will always love you. Special thanks to Iglal and Uncle Alaa, for being the cool adults and for showing me how to enjoy my stay in Europe.

To the family Doctors, my siblings Rawan Omer and hopefully the latest edition; Raghd thank you for your back-up throughout the journey, I know we are far in distance but we stayed as close as possible, I wish we gather in a better place soon; keep working hard and you will make it eventually.

I would like to extend my sincere thanks to Abdelhadi Abdelgabbar and Hamad Elneel Abdelgabbar for being the reasonable uncles I return to, and for standing with me during the hard time of the pandemic. Thanks should also go to Uncles: Hassan Abdelgabbar, Abdelhakeem Abdelmoniem, and Abdelfattah Abdemoniem. And aunts: Rajaa Abdelmoniem and Eiman Abdelgabbar- for always keeping me in their minds and their sincere prayers of my well being.

I could not have undertaken this journey without my friends, all of them continued their unmatched cheering. Special Mention to Emad Eldeen Elsideeg and Khalid Ali. Albeit we three have different characters and personalities; yet somehow we were unified. The absolute trust we grew in each other will be the absolute best acquisition I had during my degree and I am definitive that it will continue for years to come if not decades.

I would be remiss in not mentioning the martyrs of the Sudanese Revolution; my people were killed and are still dying for Freedom, Peace and Justice. I believe the dawn for Sudan will come and till that day and after it, we will remember those who fell down in our deepest thoughts; because they are the torch that lights our darkest nightmares. I would like to end up by mentioning this Arabic poem which represents the strength of will in facing difficulties, which was mentioned by my friend, the martyr: Elfatih Omer Elnomair just a day before he were killed

لما سرت رعيرد يكيل خدوه شهد لسر

TABLE OF CONTENTS

| | |
|--|----|
| Abstract..... | 2 |
| Sommario..... | 4 |
| Acknowledgement | 6 |
| Table of Contents..... | 7 |
| List of Figures | 9 |
| List of Tables | 12 |
| 1 Introduction | 13 |
| 1.1 History..... | 13 |
| 1.2 Methods..... | 14 |
| 1.3 Applications..... | 14 |
| 1.3.1 Charging Medical Implants | 14 |
| 1.3.2 Charging Household Appliances | 15 |
| 1.3.3 Charging Electric Vehicles | 15 |
| 1.4 Problems With Wireless Power Transfer Systems..... | 15 |
| 1.4.1 Foreign And Live Objects (FO/LO)..... | 16 |
| 1.4.2 Misalignment | 16 |
| 1.4.3 Interoperability | 16 |
| 1.5 Thesis Objective | 16 |
| 1.6 Thesis Layout..... | 16 |
| 2 Chapter 2: Wireless Power Transfer | 17 |
| 2.1 Definition | 17 |
| 2.2 Principles..... | 17 |
| 2.2.1 Radiative (Far Field) | 17 |
| 2.2.2 Coupling (Near Field) | 18 |
| 2.2.3 Comparison Between Principles | 20 |
| 2.3 Near Field Wireless Power Transfer..... | 22 |
| 2.3.1 Inductive Power Transfer IPT | 22 |
| 2.3.2 Capacitive Power Transfer CPT | 32 |
| 2.3.3 Maximum Achievable Efficiency In Large Air-Gap Inductive And Capacitive Wpt Systems | 38 |
| 2.3.4 Comparison Between IPT And CPT In Large Air-Gap | 40 |
| 3 Chapter 3: Resonant Inductive Coupling | 43 |
| 3.1.1 Models | 44 |
| 3.1.2 Compensation Networks..... | 46 |

| | | |
|-------|--|----|
| 3.1.3 | Influence Of The Quality Factor On The Power Transferred | 52 |
| 3.1.4 | Effect Of Misalignment On RIPT..... | 52 |
| 3.2 | The Need Of Power Converters | 61 |
| 4 | Chapter 4: Power Converter Modelling | 62 |
| 4.1 | Non-Resonant Converters With Resonant Tank | 62 |
| 4.1.1 | Single-Phase AC-AC Converter..... | 62 |
| 4.1.2 | <i>Three-Phase AC-AC Converter</i> | 63 |
| 4.1.3 | <i>DC Fed Energy Injection Converter</i> | 63 |
| 4.1.4 | Comparison Between Non-Resonant Converters | 64 |
| 4.2 | Resonant Inverters With Resonant Tank | 65 |
| 4.2.1 | Class E Resonant Inverter..... | 65 |
| 4.2.2 | Class D Resonant Inverter | 66 |
| 4.2.3 | Class DE Resonant Inverter | 67 |
| 4.2.4 | Class EF _n Resonant Inverter | 67 |
| 4.2.5 | Other Resonant Converters | 68 |
| 4.3 | Comparison of Resonant Circuits..... | 69 |
| 4.4 | Push-Pull Current-Fed Resonant Inverter | 70 |
| 4.4.1 | Basic Structure | 71 |
| 4.4.2 | Gate Signal Analysis | 71 |
| 4.4.3 | Startup Analysis..... | 73 |
| 4.5 | Proposed Model For Push-Pull Current Fed Resonant Inverter. | 75 |
| 4.6 | Resonance Tuning For Push–Pull Parallel-Resonant Inverter..... | 76 |
| 5 | Conclusion And Future Work | 81 |
| 5.1 | Conclusion..... | 81 |
| 5.2 | Future Work | 82 |
| | References | 83 |

LIST OF FIGURES

| | |
|--|----|
| FIGURE 1.1 DIAGRAM OF ONE OF TESLA'S WIRELESS POWER EXPERIMENTS WITH THE ORIGINAL HANDWRITTEN NOTES | 13 |
| FIGURE 1.2 BASIC STRUCTURE OF WIRELESS POWER TRANSFER..... | 13 |
| FIGURE 1.3 APPLICATION OF RESONANT COUPLED WPT IN MEDICAL DEVICES: (A) LVAD AND (B) PACEMAKERS | 14 |
| FIGURE 1.4 WITRICITY SYSTEM | 15 |
| FIGURE 1.5 ELECTRIC VEHICLE CHARGING BY WITRICITY | 15 |
| FIGURE 2.1 DIAGRAM OF WPT BASED ON MICROWAVE TECHNOLOGY | 18 |
| FIGURE 2.2 BLOCK DIAGRAM OF AN OPTICAL WPT. | 18 |
| FIGURE 2.3 INDUCTIVE COUPLING..... | 19 |
| FIGURE 2.4 CAPACITIVE COUPLING..... | 19 |
| FIGURE 2.5 MAGNETIC RESONANCE COUPLING | 20 |
| FIGURE 2.6 OPERATION RANGE AND FREQUENCY OF DIFFERENT WPT METHODS. | 20 |
| FIGURE 2.7 INDUCTIVE WPT COUPLER WITH PRIMARY-SIDE AND SECONDARY-SIDE COILS (THE FERRITE BLOCK ON THE SECONDARY-SIDE IS NOT SHOWN FOR THE PURPOSE OF CLARITY)..... | 22 |
| FIGURE 2.8 THEVENIN EQUIVALENT FOR IPT | 23 |
| FIGURE 2.9 A CIRCUIT SCHEME OF AN IPT SYSTEM, USED AS A MEANS OF WIRELESS POWER TRANSFER. | 24 |
| FIGURE 2.10 TRANSFORMER MODEL OF LOOSELY COUPLED TRANSFORMER THAT INCLUDES THE PRIMARY LEAKAGE, SECONDARY LEAKAGE, AND THE PHYSICAL TURNS' RATIO. | 25 |
| FIGURE 2.11 TRANSFORMER MODEL THAT REFLECTS ALL LEAKAGE AND MAGNETIZING INDUCTANCE TO THE PRIMARY SIDE, AND N_e REPRESENTS THE EQUIVALENT TURNS' RATIO. | 25 |
| FIGURE 2.12 CIRCUIT DIAGRAM OF THE MUTUAL INDUCTANCE MODEL. | 25 |
| FIGURE 2.13 TYPICAL LAYOUT OF A CIRCULAR PAD. | 28 |
| FIGURE 2.14 TYPICAL FIELD GENERATED IN CIRCULAR PAD..... | 28 |
| FIGURE 2.15 TYPICAL LAYOUT OF SOLENOID PAD. | 29 |
| FIGURE 2.16 SIMPLIFIED MODEL OF DD PAD. | 29 |
| FIGURE 2.17 TYPICAL MODEL OF DDQ POLARISED PAD..... | 30 |
| FIGURE 2.18 TYPICAL MODEL OF BIPOLAR POLARISED PAD. | 30 |
| FIGURE 2.19 A TYPICAL A TRIPOLAR PAD WITH ARROWS SHOWING THE FLOW OF CURRENT IN PHASE. | 31 |
| FIGURE 2.20 CPT SYSTEM WITH PRIMARY-SIDE PLATES AND SECONDARY-SIDE PLATES..... | 32 |
| FIGURE 2.21 EQUIVALENT THEVENI MODEL OF CPT, | 32 |
| FIGURE 2.22 TYPICAL CPT SYSTEM CONFIGURATION. | 33 |
| FIGURE 2.23 SIX CAPACITOR MODEL..... | 33 |
| FIGURE 2.24 ICS MODEL..... | 34 |
| FIGURE 2.25 SIMPLIFIED EQUIVALENT MODEL OF COUPLING CAPACITORS THE Π MODEL. | 35 |
| FIGURE 2.26 HCC STRUCTURE..... | 36 |
| FIGURE 2.27 COUPLING MECHANISM OF HCC..... | 36 |
| FIGURE 2.28 VCC STRUCTURE..... | 37 |
| FIGURE 2.29 COUPLING MECHANISM OF VCC..... | 37 |
| FIGURE 2.30 INTERLEAVED CAPACITIVE COUPLER STEREOGRAM. | 38 |
| FIGURE 2.31 INTERLEAVED CAPACITIVE COUPLER FRONT VIEW..... | 38 |
| FIGURE 2.32 TOPOLOGY OF IPT SYSTEM. | 39 |
| FIGURE 2.33 TOPOLOGY OF CPT SYSTEM..... | 39 |
| FIGURE 2.34 RATIO OF POWER TRANSFER CAPABILITIES OF AN INDUCTIVE AND A CAPACITIVE WPT SYSTEM HAVING THE SAME AIR-GAP AND SAME COUPLING AREA..... | 41 |
| FIGURE 2.35 EFFICIENCY OF AN INDUCTIVE AND A CAPACITIVE SYSTEMS WITH 100 KHZ. | 41 |
| FIGURE 2.36 EFFICIENCY OF AN INDUCTIVE AND A CAPACITIVE SYSTEMS WITH 1 MHZ. | 42 |
| FIGURE 2.37 EFFICIENCY OF AN INDUCTIVE AND A CAPACITIVE SYSTEMS WITH 10 MHZ. | 42 |
| FIGURE 3.1 FREQUENCY SPLITTING PHENOMENA IN RIPT AND IPT..... | 44 |
| FIGURE 3.2 EQUIVALENT CIRCUIT MODEL OF SYSTEM ARCHITECTURE WITH TWO COILS. | 44 |

| | |
|--|----|
| FIGURE 3.3 SIMPLIFIED CIRCUIT MODEL BY REFERRING THE SECONDARY COIL TO BE THE EQUIVALENT IMPEDANCE IN THE PRIMARY SIDE..... | 45 |
| FIGURE 3.4 THE TOPOLOGIES OF THE BASIC COMPENSATION TECHNIQUES OF THE PRIMARY AND THE SECONDARY | 47 |
| FIGURE 3.5 SS LCC TOPOLOGY | 50 |
| FIGURE 3.6 PP LCL TOPOLOGY | 51 |
| FIGURE 3.7 EFFECT OF THE DIMENSIONLESS QUALITY FACTOR, Q, ON THE MAXIMUM CURRENT IN A CIRCUIT..... | 52 |
| FIGURE 3.8 LCL BASED RIPT SYSTEM | 53 |
| FIGURE 3.9 SIZE, SHAPE AND POSITION OF PICKUP COIL. (A) HORIZONTAL MISALIGNMENT. (B) VERTICAL MISALIGNMENT..... | 55 |
| FIGURE 3.10 COUPLING COEFFICIENT AGAINST MISALIGNMENT (A) HORIZONTAL MISALIGNMENT. (B) VERTICAL MISALIGNMENT..... | 56 |
| FIGURE 3.11 VOLTAGE AND CURRENT WAVEFORM OF THE INDUCTIVE TRACK AT $M = 14 \mu\text{H}$ AND $f = 85 \text{ kHz}$ | 57 |
| FIGURE 3.12 VOLTAGE AND CURRENT WAVEFORM OF THE INDUCTIVE TRACK AT $M = 25 \mu\text{H}$ AND $f = 87.7 \text{ KHz}$ | 57 |
| FIGURE 3.13 VOLTAGE AND CURRENT WAVEFORM OF INDUCTIVE TRACK AT $M = 25\mu\text{H}$ WHILE TUNING..... | 58 |
| FIGURE 3.14 OPERATING FREQUENCY CORRESPONDING TO COUPLING COEFFICIENT | 58 |
| FIGURE 3.15 OPERATING FREQUENCY AGAINST MISALIGNMENT (A) HORIZONTAL MISALIGNMENT. (B) VERTICAL MISALIGNMENT..... | 59 |
| FIGURE 3.16 POWER TRANSFER LEVEL CORRESPONDING TO THE MISALIGNMENT. (A) VERTICAL(B)HORIZONTAL. | 59 |
| FIGURE 4.1 CLASSIFICATION OF RESONANCE CIRCUIT | 62 |
| FIGURE 4.2 SINGLE-PHASE AC-AC CONVERTER. | 62 |
| FIGURE 4.3 THREE-PHASE AC-AC CONVERTER. | 63 |
| FIGURE 4.4 DC FED ENERGY INJECTION CONVERTER. | 64 |
| FIGURE 4.5 CLASS E INVERTER WITH AN INDUCTIVE LINK. | 66 |
| FIGURE 4.6 PARALLEL FULL-BRIDGE CLASS D RESONANT INVERTER. | 66 |
| FIGURE 4.7 CASCADED FULL-BRIDGE CLASS D RESONANT INVERTER. | 67 |
| FIGURE 4.8 CLASS DE RESONANT INVERTER. | 67 |
| FIGURE 4.9 CLASS EFN RESONANT CONVERTER. | 68 |
| FIGURE 4.10 CURRENT-FED PUSH-PULL RESONANT INVERTER. | 69 |
| FIGURE 4.11 BIDIRECTIONAL RESONANT INVERTER | 69 |
| FIGURE 4.12 EQUIVALENT CIRCUIT FOR PUSH-PULL CURRENT FED INVERTER..... | 71 |
| FIGURE 4.13 CONCEPTUAL ILLUSTRATION OF GATE SIGNALS OPERATION FOLLOWING THE FREQUENCY OF THE RESONANT TANK..... | 72 |
| FIGURE 4.14 BASIC GATE DRIVING CIRCUIT WITH SPEEDUP CAPACITOR..... | 73 |
| FIGURE 4.15 FLOWCHART OF THE AUTONOMOUS REGENERATIVE PROCESS | 74 |
| FIGURE 4.16 SIMPLIFIED CIRCUIT FOR CURRENT-FED CONVERTER | 74 |
| FIGURE 4.17 PROPOSED INVERTER TOPLOGY | 75 |
| FIGURE 4.18 SCHEMATIC OF CONVENTIONAL PUSH-PULL PARALLEL-RESONANT INVERTER..... | 76 |
| FIGURE 4.19 WHEN LTX IS DETUNED TO LOW VALUE. THE EFFECTIVE OUTPUT VOLTAGE OF INVERTER IS LOW, VOLTAGE STRESS ON M_1 IS HIGH..... | 76 |
| FIGURE 4.20 WHEN LTX IS DETUNED TO HIGH VALUE. THE V_{d1} DOES NOT DROP TO ZERO BEFORE GATE TURNS ON, WHICH CAUSES ZERO-VOLTAGE SWITCHING FAILURE | 77 |
| FIGURE 4.21 PROPOSED TUNING CONTROL FOR PARALLEL-RESONANT INVERTER. (A) WHEN MPWM1 IS ON, LTX RESONATES BOTH WITH CTX AND CPWM1. V_d1 AND COMPARATOR'S OUTPUT VCOMP. (B) AT PERFECT RESONANT CONDITION. (C) WHEN LTX IS DETUNED TO A LOWER VALUE. (D) WHEN LTX IS DETUNED TO A HIGHER VALUE..... | 77 |
| FIGURE 4.22 WAVEFORMS OF AUTOTUNING INVERTER..... | 78 |
| FIGURE 4.23 VARIATION OF LTX AND COUPLING k WITH RESPECT TO TX-RX DISTANCE..... | 78 |
| FIGURE 4.24 RX POWER WITH RESPECT TO DISTANCE. | 79 |

| | |
|--|----|
| FIGURE 4.25 TX-TO-RX EFFICIENCY COMPARISON BETWEEN THE CONVENTIONAL..... | 79 |
| FIGURE 4.26 LOSS BREAK DOWN AT TX-RX DISTANCE OF 4 CM..... | 79 |
| FIGURE 4.27 LOSS BREAK DOWN AT TX-RX DISTANCE OF 6 CM..... | 79 |

LIST OF TABLES

| | |
|---|----|
| TABLE 2.1 PRINCIPLES COMPARISON OF WIRELESS POWER TRANSFER | 22 |
| TABLE 2.2 FEATURES OF COIL TOPOLOGIES | 31 |
| TABLE 3.1 COMPARISON BETWEEN DIFFERENT RESONANCE COMBINATIONS. | 49 |
| TABLE 3.2 CIRCUIT PARAMETER AND VALUES. | 54 |
| TABLE 3.3 EFFICIENCY CORRESPONDING TO THE VERTICAL MISALIGNMENT UNDER VARIOUS OPERATING FREQUENCIES. | 60 |
| TABLE 3.4 EFFICIENCY CORRESPONDING TO THE HORIZONTAL MISALIGNMENT UNDER VARIOUS OPERATING FREQUENCIES. | 60 |
| TABLE 4.1 COMPARISON OF NON-RESONANT CONVERTERS WITH RESONANT TANK FOR WPT SYSTEM. | 65 |
| TABLE 4.2 COMPARISON OF RESONANT CIRCUITS FOR WPT | 70 |
| TABLE 4.3 LOGIC OF THE ZVS CIRCUIT FOR PUSH-PULL CONVERTER | 72 |

1 INTRODUCTION

1.1 HISTORY

Wireless Power Transfer (WPT) is not a brand-new notion. In ref [1], the author categorized the history of WPT into three main periods.

First period was related to Maxwell and Hertz. Maxwell first proposed an equation for the transmission of electromagnetic energy in free space in 1873. Hertz tested and verified Maxwell's hypotheses and the existence of electromagnetic radiation between 1885 and 1889.

Second period is dedicated to Nikola Tesla and his futuristic vision of having WWS (World Wireless System) in which he desired to transfer energy to any point on our earth by using our earth and its atmosphere as a conductor [1]. He began experimenting with the potential around the end of the 19th century [2] [3], with the use of microwaves. However, his tests, like the one shown in Figure 1.1, entailed unacceptably large electric fields. [4].

Third period is the current era, which started during World War II, in that time researchers used curved reflectors to concentrate energy into one small area. With time, this technology evolved into a viable alternative to cable charging methods. According to Figure 1.2, this technology has the ability to replace the plug-in interface with transmitters and receivers, enabling electricity to flow in a contactless manner via electromagnetic or static waves. Through power electronic converters, the receiver in WPT systems transfers power to the batteries or desired system.

The main drawback of wireless charging system is its charging time. That can be resolved by different changes in the system. Another concern with WPT is its leakage EMF radiation at higher frequencies. This radiation is restricted by using proper shielding to make it safer [5].

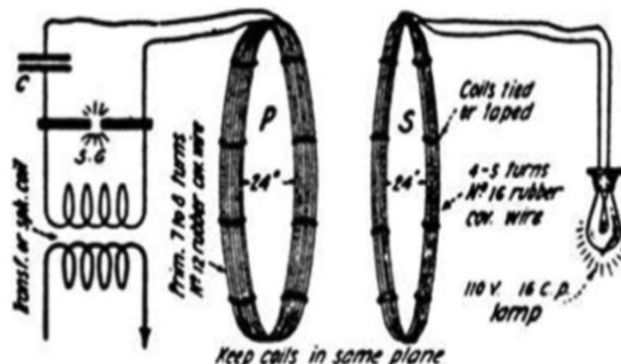


Figure 1.1 Diagram Of One Of Tesla's Wireless Power Experiments With The Original Handwritten Notes [6]

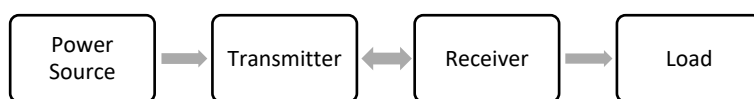


Figure 1.2 Basic Structure Of Wireless Power Transfer

1.2 METHODS

The different methods of WPT can be divided either based on the range of their transmission, or by the principles upon which they are realized. Which will be further discussed in 2.2 below.

This research will be concerned about Magnetic Resonance Coupling and the possible options available of keeping track of the resonance frequency of the circuit.

1.3 APPLICATIONS

1.3.1 Charging Medical Implants

Designing a WPT system in the presence of living things necessitates taking into account how the system interacts with biological tissue, which might change the field distributions and have an impact on the magnetic link. Because biological tissue conducts electricity differently than air or vacuum, WPT systems' high frequency magnetic fields can cause eddy currents to form inside the tissue.

In order to minimize harmful thermal (energy absorption in biological tissue) and non-thermal (nervous system stimulation) health impacts and meet safety criteria, additional design limits must be placed on a system. These design techniques are especially important when creating WPT systems that transmit power to implantable medical devices by using a power receiver coil inside the body of the patient.

Currently, embedded batteries are used to power the majority of implanted medical equipment and sensors. WPT technology reduces the requirement for an embedded power source and a hard-wired power network, enabling these medical devices to operate on their own.

The particular wireless charging system is still being developed for use in powering implanted medical equipment such pacemakers, infusion pumps, left ventricular assist device (LVAD) cardiac assist pumps, Figure 1.3 and others. By employing a resonant coupling technique through the skin with an operational range substantially greater than the skin thickness, such implanted medical equipment and sensors can be effectively activated. As a result, the WPT system really eliminates the need for a driver to enter the human body, allowing for the delivery of energy to devices implanted deep within the body.

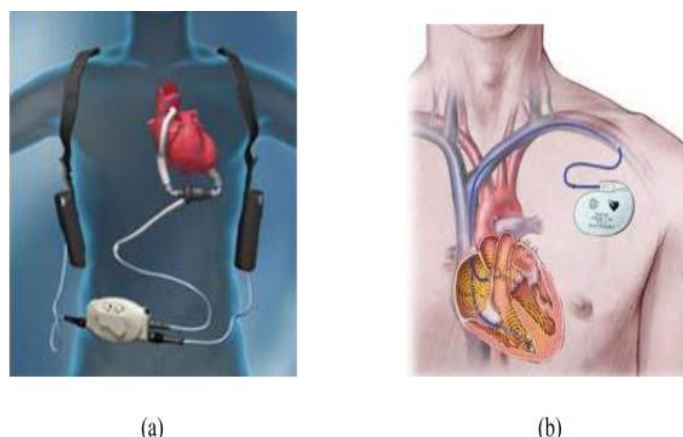


Figure 1.3 Application Of Resonant Coupled WPT In Medical Devices: (A) LVAD And (B) Pacemakers .[7]

1.3.2 Charging Household Appliances

Figure 1.4 shows how Wireless Power Transfer provides practical ways to charge home equipment. Some traditional plug-and-socket applications, such as a blow-dryer in a bathroom, are dangerous when used in a household setting. WPT is appealing because it offers a charging technique that electrically isolates the two transmitter and receiver circuits from one another, creating safer operating situations.



Figure 1.4 Witricity System [8]

1.3.3 Charging Electric Vehicles

There is a growing demand for non-fossil fuel based and safe electric vehicles. These vehicles bring high investment in fast-charging applications [5]. WPT as a way to charge electric vehicles promises more independence from the cost and the inconvenience of the battery and its charging.

The future outlook is even more ambitious. WPT systems are considered for the charging of EVs on-the-go. To extend the cruising range, some portion of the road needs to be equipped with transmitter (Tx) pads [9].

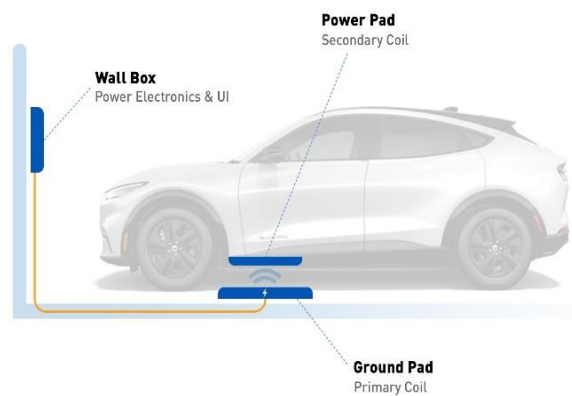


Figure 1.5 Electric Vehicle Charging By Witricity [10]

1.4 PROBLEMS WITH WIRELESS POWER TRANSFER SYSTEMS

WPT systems, are much more complicated systems than the traditional plug-and-socket cable charging solutions, WPT suffer from lower efficiency, greater costs, restricted flexibility, and safety problems due to the current magnetic fields, in addition to this equivalent complexity [11].

More problems are listed as follows:

1.4.1 Foreign And Live Objects (FO/LO)

The possibility of the electromagnetic field being absorbed by close foreign (metallic) or live items exists when the idea of transporting power via air using magnetic fluxes is considered. Not only does this result in losses by requiring the primary to transmit higher levels of power, but the risk these scenarios can introduce is in the considerable heating of the intrusive bodies [12]. Even systems of power transmission of as low as 5W can heat objects to levels unaccepted by the ISO safety standard levels [13].

1.4.2 Misalignment

Receiving coils must not only be close to transmitter coils but also properly aligned with them in order for magnetic fluxes to be picked up in order for proper power transfer to take place. Misalignment is a major issue in WPT [6],[14],[15], and introduces considerable losses to the system. A measure of the effectiveness of the coupling between the coils is the mutual inductance between them, denoted M .

This problem will be illustrated in details in 3.1.4 below, showing the effects of both Vertical and Horizontal Misalignments.

1.4.3 Interoperability

WPT systems are continuously being researched, and approaches to improve their performance are a hot area of study. One path for this optimization is the geometry of the coils, as certain shapes could offer the possibility of better tolerance to misalignment [16]

1.5 THESIS OBJECTIVE

To investigate the ins and outs of wireless power transfer methods and to select the most effective topology among the different options available for power converters, all along with problems that may arise from the misalignment between transmitter and receiver.

1.6 THESIS LAYOUT

Introduction in which a brief preview of the history, applications and problems facing the concept is introduced.

Chapter 2: Wireless Power Transfer discusses the various methods of the phenomena in details and a comparison between near field technologies is conducted.

Chapter 3: Resonant Inductive Coupling elaborates the compensation topologies, in addition to the effect of misalignment on frequency, mutual inductance, power and efficiency.

Chapter 4: Power Converter explains the power electronics switches that are used in the resonant networks in detail, as well as a proposed control method as found in the literature; which is used to tune the frequency of the most useful converter in the author's opinion.

Conclusion And Future Work presents a deduction of the thesis, and an insight of what can be done towards improving this work in the future.

2 CHAPTER 2: WIRELESS POWER TRANSFER

2.1 DEFINITION

Wireless Power Transfer (WPT) is a way of transferring electrical energy from one source to another over an air gap without the direct physical contact [17]. WPT technology has a higher application ease and versatility than traditional conductive power transfer. It is weather resistant and vandalism proof, and it eliminates the need for bulky charging lines and connectors[9]. Furthermore, because the power supply and the powered device are connected by a magnetic field, wireless charging systems provide a high level of operational flexibility, allowing the item to be charged at any time and from any location, even while the vehicle is moving [18].

Contact friction insulation and worn conductor causes concerns in a range of severe settings, including underwater, underground, and aerospace, which greatly enhances the safety and reliability of charging systems [19]

In ref [5], the main characteristics of the WPT system are described as the following:

- The WPT system can be classified into several types based on the transmitting power ranges. WPT systems span a low power range of < 1 kW, a medium range of 1-100 kW, and a high-power range of > 100 kW.
- Power can be transferred unidirectionally and bidirectionally in a WPT system.
- We can transfer power over short distances to vast distances, ranging from a few centimetres to kilometres
- Power can be transferred through a variety of methods.

2.2 PRINCIPLES

The WPT system can be implemented using a variety of physical concepts. The WPT technology is classified into different categories, the categorisation can be based on distance, frequency, or power level. In this work categorisation based on distance is adopted.

According to [5], there are two main categories for the WPT: Far-field (Radiative) and Near-field (Coupling). Radiative System can be categorized into two types: microwave and optical, while Coupling system can be further categorized into Inductive Coupling, Capacitive Coupling and Resonance Inductive Coupling.

2.2.1 Radiative (Far Field)

Radiative WPT coupling, which uses electromagnetic radiation for far-field transmission, like microwave or laser, and it is not particularly convenient for transferring very huge power. However, because of its omnidirectional behaviour, its efficiency is low, making it considerably more useful to transfer information than power [6], [20]

2.2.1.1 *Microwave Power Transfer (MPT)*

A microwave based WPT technology in a far-field context [18], [21]. With minor tweaks, this approach can also be used in the Radiofrequency (RF) range. RF converter is fed by a voltage source, which then generates microwave signal. The microwave signal created by the antenna is sent out and received by the receiving antenna. Rectenna is another name for this receiving antenna. As shown in Figure 2.1, this rectenna comprises of a receiver that includes a matching network and a rectifier that transforms the signal to desired output[5].



Figure 2.1 Diagram Of WPT Based On Microwave Technology.

2.2.1.2 Optical WPT

Optical WPT or Laser-based power transfer emits electromagnetic waves, however they are in the THz range and hence appear as light. The transmitter in this technology consists of a laser diode that creates a light beam with a specific Power and wavelength. Beam director is used to regulate the direction of the light beam by adjusting the laser diode. A Photo-Voltaic (PV) cell and a rectifier make up the secondary side. The PV cell receives light and turns it into a power signal. The rectifier converts the power signal to a DC signal. The DC signal is used to charge a load or a battery[5]. The block diagram of optical WPT is shown in Figure 2.2.

A High Intensity Laser Power Beam (HILPB) system should ideally be capable of transferring power to any place. The system's performance is limited by practical constraints such as conversion efficiencies. The design of the PV cell plays a vital role in the HILPB system for effective conversion of laser power to electricity. For this, the dynamics of laser power, such as wavelength, temperature, and PV cell materials, should be carefully examined [22].

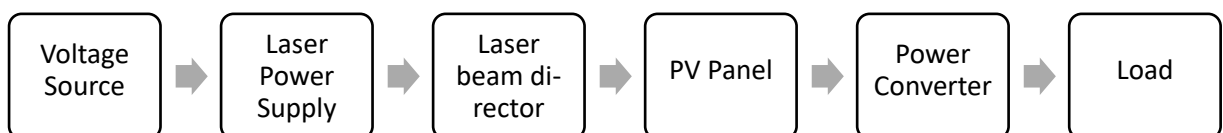


Figure 2.2 Block Diagram Of An Optical WPT.

2.2.2 Coupling (Near Field)

WPT via near-field magnetic coupling is the most widely studied and employed WPT method. The magnetic inductive (Inductive Power Transfer IPT) and magnetic resonance coupling (Resonance Inductive Power Transfer RIPT), the concept is that the magnetic field generated by the high-frequency current in primary coils (Transmitter) is picked up by the secondary coil (Receiver), which converts it to dc current. While on the other hand, Field-coupled electric WPT systems, also known as capacitive power transfer (CPT) systems, use two sets of plates to create an analogous capacitor for power transfer.

2.2.2.1 Inductive Power Transfer (IPT)

A near-field transmission technology which uses a magnetic field to transfer power over an air gap. Transformers, electrical machines, and wireless chargers are electrical devices that uses this technology as well.

Strong magnetic coupling between the coils is required for efficient power transfer. Because axial and angular misalignment between the coils drastically weakens the coupling, IPT is primarily used for high-power transmission over short distances (compared to the dimensions of the coil) [14].

Figure 2.3 shows the reference model. Inductive power transfer (IPT) happens when a primary coil of an energy transmitter generates predominantly varying magnetic field across the secondary coil of the energy receiver within the field, generally less than a wavelength. The near-field magnetic power then induces voltage/current across the secondary coil of the energy receiver within the field. The operating frequency of inductive coupling is typically in the kilo Hertz range [23]. Tuning of secondary coil frequency equal to operating frequency enhance the efficiency of the system [6].

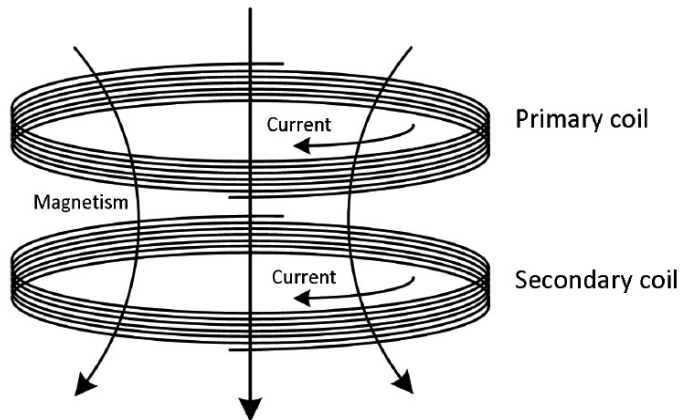


Figure 2.3 Inductive Coupling [23]

2.2.2.2 Capacitive Power Transfer (CPT)

Field-coupled electric field WPT systems, also known as capacitive power transfer (CPT) systems, use two pairs of plates to create an equivalent capacitor for power transfer in the form electrostatic energy. A CPT system can transfer power through the metallic medium since a capacitor is formed from each conductor plate to the metallic surface. Compared to IPT, the CPT system applicable for both low current and high voltage systems. Additional inductors added to capacitor plates on each side to reduce impedance. This is also called as inductive compensation; it enables soft switching operation and increases power transfer efficiency. Exited voltage in secondary side is altered to Direct Current (DC) by rectifier circuit [24].

In Figure 2.4, the electric field lines generated from a primary-side plate links to a secondary-side plate and vice versa. According to [25], theoretically, the capacitive coupling exists between any two conductive objects and a proper excitation voltage would cause power exchange. Therefore, inserting a pair of coupling plates in an AC loop is the most straightforward way to use capacitive coupling.

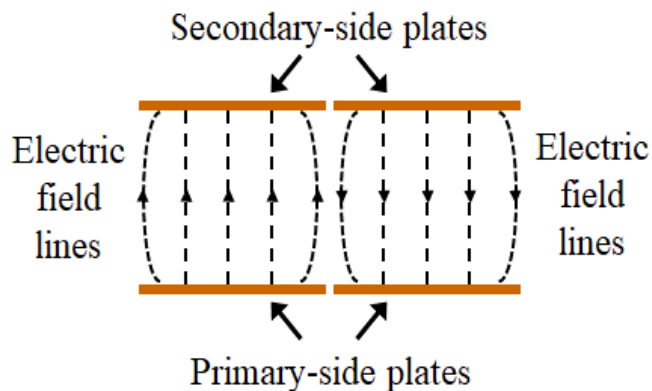


Figure 2.4 Capacitive Coupling [26]

2.2.2.3 Magnetic Resonance Coupling RIPT

Similar to other WPT systems, existed grid voltage is transformed to the High Frequency AC (HFAC) by utilizing power electronics converters. The HFAC signal delivered to the coupler coil. The secondary coupler coil generates voltage by linked magnetic fields. Generated voltage is converted to DC for the powering the battery through power electronics converters and filter circuitry [27].

Compared to IPT system, Compensation networks (capacitors/inductors or both) added in the series or/and parallel formations to both transmitter and receiving side of the coils to form the resonant condition. That helps improve efficiency by reducing additional losses [5]

Magnetic resonance coupling [23], as shown in Figure 2.5, is based on evanescent wave coupling which generates and transfers electrical energy between two resonant coils through varying or oscillating magnetic fields. As two resonant coils, operating at the same resonant frequency, are strongly coupled, high energy transfer efficiency can be achieved with small leakage to non-resonant externalities.

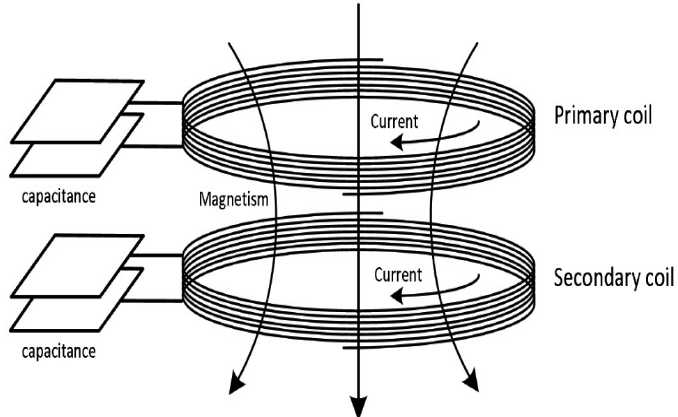


Figure 2.5 Magnetic Resonance Coupling [23]

2.2.3 Comparison Between Principles

With the intention of selecting the most suitable option among different principles; pros and cons should be considered, check Table 2.1. Also, the possibility of applying the topology in accordance with frequency regulation of the system needed, the range of frequencies can be found in Figure 2.6.

Short and medium ranges are the core of this study. Hence, they will be further analysed throughout the research. Their ability to transfer higher power densities make them useful in applications that require high power transfer between transmitters and receivers.

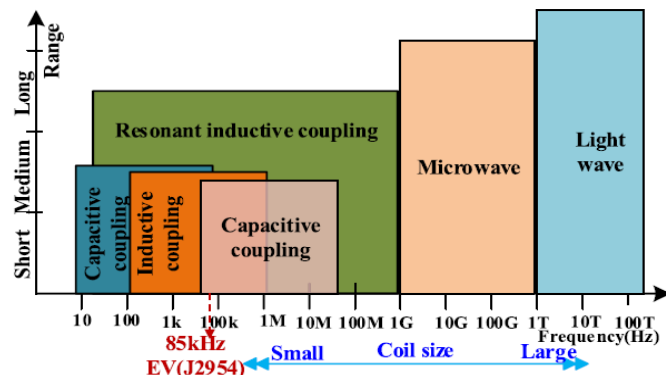


Figure 2.6 Operation Range And Frequency Of Different Wpt Methods [5]

| Principle | Type | Advantages | Disadvantages |
|--|------------|---|--|
| Microwave Power Transfer (MPT) | Far Field | <ul style="list-style-type: none"> Power can be transferred up to several km. Dynamic power transfer is possible (for moving loads). Possible to transfer power up to several kilowatts power. Higher efficiency achieved at beam forming. Compatibility with existing communication system | <ul style="list-style-type: none"> Low efficiency compared to inductive and capacitive methods. Very difficult to implement. Unidirectional power flow. Unsafe for living things when exposed to microwave beam. Size of the antennas increases with power transfer capability increases. |
| Optical Power Transfer | Far Field | <ul style="list-style-type: none"> Effective gap in kms Dynamic power transfer is possible (for moving loads). Capacity to transfer several kilowatts power. Transmitter size is small compared to MPT. | <ul style="list-style-type: none"> Low efficiency (around 20% depends upon air gap). Unidirectional power flow. Difficult to operate. No obstacles allowed in way of light beam. Unsafe operation for living beings, if exposed to radiation. |
| Inductive Power Transfer (IPT) | Near Field | <ul style="list-style-type: none"> Implementation is simple. Galvanic isolation provided. Simple control. High efficiency in low air gap (typically less than a coil diameter). Safe operation compared to resonant mode. Bi-directional power transfer possible. | <ul style="list-style-type: none"> Short air gap few millimetres to centimetres. EMI shielding is needed. Very low efficiency at larger air gaps. Heating effect in the presence of metal objects. Tight alignment needed between transmitter and receiver to achieve good efficiency. |
| Capacitive Power Transfer (CPT) | Near Field | <ul style="list-style-type: none"> Offers Medium power transfer (several kilowatts) Power transfer possible through metallic objects. Cheap because of relies on aluminium plates for power transfer. Suitable for air gap up to 10 cm. Restricted electric field: shielding not needed for EMI control. | <ul style="list-style-type: none"> Power transfer capabilities depend upon the gap between transmitter and receiver. Parasitic capacitance forms. Efficiency around 70-80%. |

| Principle | Type | Advantages | Disadvantages |
|------------------------------------|------------|--|--|
| Magnetic Resonance Coupling (RIPT) | Near Field | <ul style="list-style-type: none"> Offers High power transfer compared to other methods. Commercialized technology for EV charging. Able to transfer power in misaligned conditions. Provides galvanic isolation. Bi-directional power transfer possible. | <ul style="list-style-type: none"> Cost of the system increases with power. Extremely sensitive to the obstacles in between coupler coils. (Especially the metallic ones). Shielding is needed for EMI. |

Table 2.1 Principles Comparison Of Wireless Power Transfer As Discussed In [5]

2.3 NEAR FIELD WIRELESS POWER TRANSFER

2.3.1 Inductive Power Transfer IPT

According to [26] Since an inductive WPT system behaves like a loosely coupled transformer, the resultant flux in the primary-side core can be approximated as the magnetizing flux generated by the primary-side coil. If the primary-side coil generates a magnetizing flux ϕ , the flux density in the primary-side core can be expressed as:

$$B = \frac{\phi}{\sqrt{At}} \quad 2.1$$

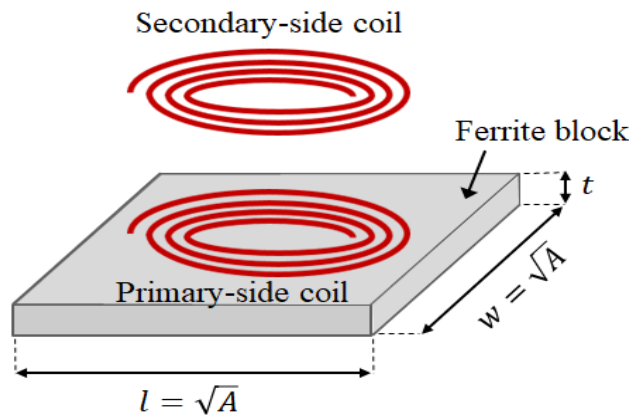


Figure 2.7 Inductive Wpt Coupler With Primary-Side And Secondary-Side Coils (The Ferrite Block On The Secondary-Side Is Not Shown For The Purpose Of Clarity) [26]

Where A is the area of the square-shaped core, and t is the thickness of the core, as shown in Figure 2.7. To analyse power transfer in an inductive WPT system, the dc input voltage, inverter and primary-side matching network is modelled as a Thevenin-equivalent ac voltage source v_{th} in series with a Thevenin impedance Z_{th} and the secondary-side matching network and rectifier and the load are modelled as another impedance Z_{sec} as shown in Figure 2.8.

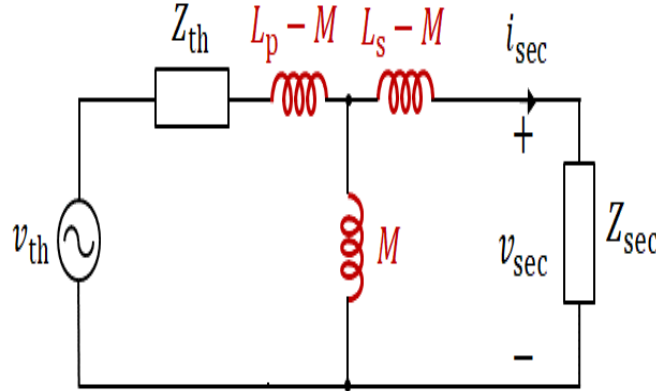


Figure 2.8 Thevenin Equivalent For IPT [26]

For simplicity of the analysis, let us assume that all the reactive compensation is provided by the primary-side matching network, and hence, the impedance looking from the secondary-side of the coupler is purely resistive (i.e., $Z_{sec} = R_{sec} + j0$). Then the voltage generated across the secondary-side coil is given by:

$$V_{sec} = N_2 \left| \frac{d\phi_s}{dt} \right| = 2\pi f_{ipt} N_2 \phi_s \quad 2.2)$$

Where N_2 is the number of turns in the secondary-side coil, f_{ipt} is the operating frequency of the system, and ϕ_s is the portion of the flux generated by the primary-side coil that is linked to the secondary side. Using 2.1) and (2.2) the maximum power transfer capability of the inductive WPT system can be expressed as:

$$P_{ipt,max} = \frac{V_{sec,max}^2}{R_{sec}} = \frac{4\pi^2 f_{ipt}^2 A t^2 \kappa^2 B_{max}^2 N_2^2}{R_{sec}} \quad 2.3)$$

With κ being the coupling coefficient that represents how much fraction of the primary-side generated flux is linked to the secondary side.

2.3.1.1 Models

Inductive Power Transfer-as shown in Figure 2.9-is based on the idea that an electric current driven through a coil induces an electromotive force in an adjacent coil due to the created magnetic flux [5].

Different perspectives exist for understanding WPT systems:

- At the early developing stage of WPT systems, capacitors are deployed on both sides of a loosely coupled WPT coupler, and the operating frequency is tuned to approach the resonance frequency. However, the physical essence of magnetic resonance is not intuitive from a circuit point of view, and the mathematical derivation of a resonator is not straightforward [9]
- Another view considers WPT systems as a conventional resonant converter that utilizes the resonance of an inductor and a capacitor to produce zero-crossing conditions, which

facilitates the device soft-switching [28]. However, the WPT resonant network is typically composed of multiple L and C elements, resulting in multiple resonant modes, which is different from conventional ones that only contain a single LC resonance [9].

- Given the variety of models and methodologies used to describe the system, a simple and straightforward model is required to unify the system's understanding and determine the physical meaning of WPT.

According to [9], there are three models that are used to describe the IPT systems in the time domain, each model has favourable use depending on the application.

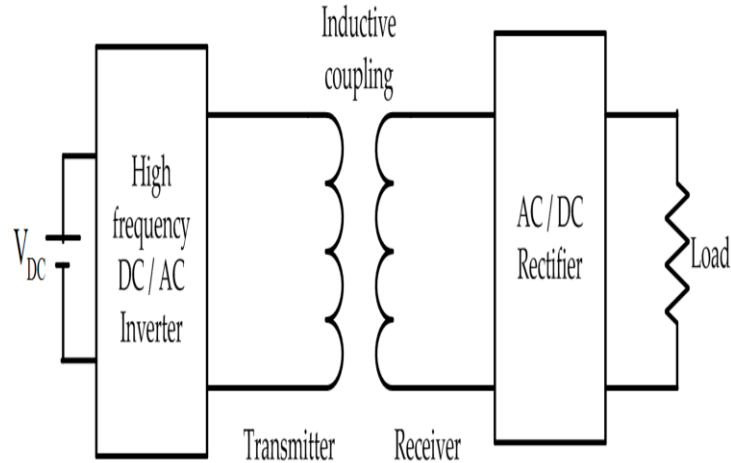


Figure 2.9 A Circuit Scheme Of An IPT System, Used As A Means Of Wireless Power Transfer [29]

2.3.1.1.1 Transformer Model

In the mode analysis of resonant converters, the transformer model is often utilized. The circuit is represented on both sides by a magnetizing inductance, physical turns' ratio, and leakage inductance, as shown in Figure 2.10. It greatly simplifies the analysis of compensation relationships between passive components, allowing for the creation of new compensation topologies that address various design goals. A different type of transformer model is shown in Figure 2.11, in which all parameters are reflected to the primary side. Equivalent leakage, magnetizing inductance, and turns' ratio are represented by the letters L_k , L_{me} , and N_e , respectively. This is frequently observed in the analysis of resonant converters based on ordinary transformers, such as the series resonant LLC converter. Because this model has a small number of elements, choosing the compensation topology and component value is simple.

2.3.1.1.2 Mutual Inductance Model (Coupled Coils' Model)

The mutual inductance model is the most widely used in wireless charging systems, in which the T-type transformer is changed into a two-port network, with the mutual inductance M representing the coupling between the primary and secondary sides, as shown in Figure 2.12. It is more simple than the transformer model because it eliminates the leakage inductance and the turn ratio from the equation, reducing the number of variables.

The following circuit equations can be used to express the mutual inductance model:

$$\begin{bmatrix} V_{inv} \\ 0 \end{bmatrix} = \begin{bmatrix} Z_1 & -j\omega M \\ -j\omega M & Z_2 \end{bmatrix} \begin{bmatrix} I_1 \\ I_2 \end{bmatrix}$$

2.4)

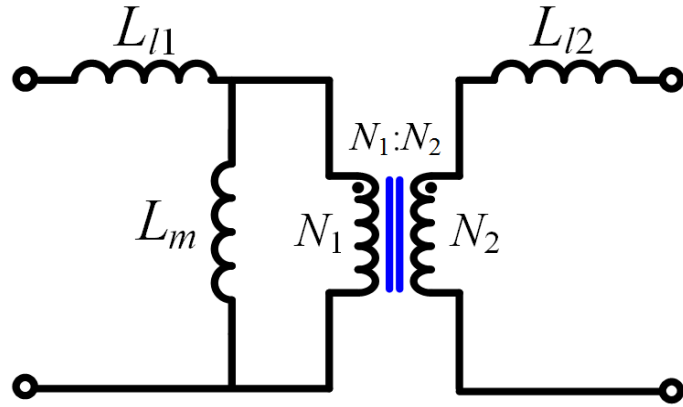


Figure 2.10 Transformer Model Of Loosely Coupled Transformer That Includes The Primary Leakage, Secondary Leakage, And The Physical Turns' Ratio [9]

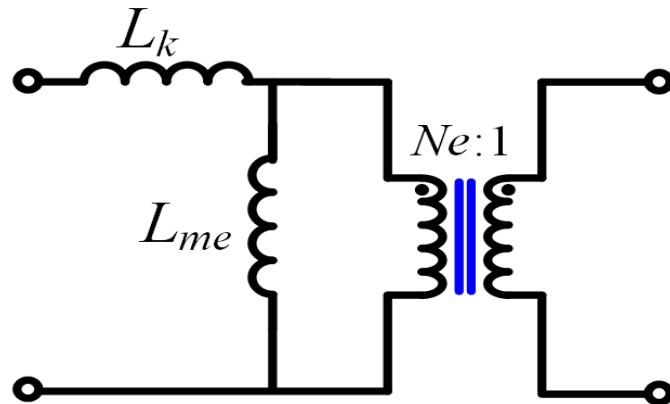


Figure 2.11 Transformer Model That Reflects All Leakage And Magnetizing Inductance To The Primary Side, And Ne Represents The Equivalent Turns' Ratio [9]

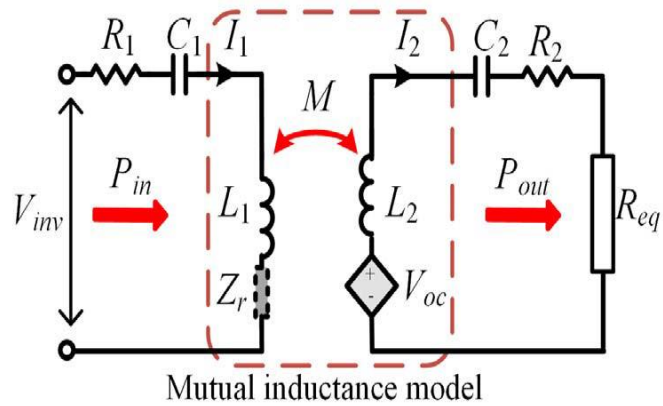


Figure 2.12 Circuit Diagram Of The Mutual Inductance Model [18]

In which the primary-side impedance is simplified as $Z_1 = R_1 + j(\omega L_1 - \frac{1}{\omega C_1})$, and the secondary-side impedance is $Z_2 = R_{eq} + R_2 + j(\omega L_2 - \frac{1}{\omega C_2})$. Therefore, the input impedance of the resonant tank can be solved as:

$$Z_{in} = \frac{V_{inv}}{I_1} = \frac{Z_1 Z_2 + (\omega M)^2}{Z_2} = Z_1 + \frac{(\omega M)^2}{Z_2}$$

2.5)

The second term in 2.5) represents the reflected impedance from the secondary side to the primary side. Based on the abovementioned derivations, the equivalent mutual inductance model can be acquired as shown in Figure 2.12, The reflected impedance Z_r and the secondary open-circuit voltage V_{oc} represent the coupling effect of the primary and secondary sides. With this definition, the input power of the system and the power received by the load are given in the following, respectively:

$$\begin{cases} P_{in} = Re \left(\frac{V_{inv}^2}{Z_{in}} \right) = Re \left(\frac{V_{inv}^2}{Z_1 + \frac{(\omega M)^2}{Z_2}} \right) \\ P_{out} = P_{R_{eq}} = |I_2|^2 R_{eq} = \frac{V_{inv}^2 (\omega M)^2 R_{eq}}{|Z_1 Z_2 + (\omega M)^2|^2} \end{cases}$$

2.6)

The apparent power between the primary side and the secondary side is expressed as:

$$S_{12} = |V_{oc} I_2| = |\omega M I_1 I_2| = \left| \frac{V_{inv}^2 (\omega M)^2 Z_2}{|Z_1 Z_2 + (\omega M)^2|^2} \right| = \frac{P_{out} |Z_2|}{R_{eq}}$$

2.7)

According to (2.7) only when the secondary side is fully compensated as $Z_2 = R_{eq} + jX_2$, purely active power is transferred between two sides. Moreover, the primary side only provides active power when it is fully compensated. Hence, 2.6), and (2.7) present an analytical tool to evaluate the power transfer characteristics and efficiency.

To derive the parametric relationship between two different models, the equivalence of the two models is used. The mutual inductance model and the transformer model can be converted mutually by using Kirchhoff's voltage law (KVL) on both sides and observing from the input and output ports. The following conclusion can be represented in terms of the relationship between self-leakage, and magnetizing inductances and turns' ratio:

M-model to T-model as in Figure 2.10

$$\begin{cases} L_1 = L_{l1} + L_m \\ L_2 = L_{l2} + \frac{L_m}{N^2} \\ L_m = NM \end{cases}$$

2.8)

M-model to T-model as in Figure 2.11

$$\begin{cases} k = M / \sqrt{L_1 L_2} \\ L_k = (1 - k^2) L_1, \quad N_e = k \sqrt{\frac{L_1}{L_2}} \\ L_{me} = k^2 L_1 \end{cases}$$

2.9)

2.3.1.1.3 Coupled-Mode Model

The magnetic resonance WPT model was first proposed by Marin Soljacic's research group at the MIT School of Physics [30]. To accomplish WPT, the magnetic resonant system demonstrated uses two resonant coils with the same resonant frequency to establish a strong resonant coupling. Magnetic resonance WPT, which uses high-Q coils to compensate for the lack of coupling, is more suitable for longer transmission distances when the frequency is increased to the MHz range.

In terms of modelling the power transfer process, magnetic resonant WPT utilizes the coupled-mode theory:

$$\dot{a}_m(t) = -(i\omega_m + \Gamma_m)a_m(t) \sum_{n \neq m} ik_{mn}a_n(t) + F_m(t)$$

2.10)

The subscripts m and n represent individual resonators. $a_m(t)$ is defined as the energy in the m th resonator, ω_m represents the free resonant frequency of the resonator. Γ_m is the inherent attenuation constant (related to ohmic and radiative losses), k_{mn} is the coupling between the resonator m and the resonator n . Finally, $F_m(t)$ is the excitation coefficient of the resonator m .

Resonant frequency, damping factor (load condition), coupling factor, and excitation are all used to describe the energy within the resonators. As a result, it and the mutual inductance model have the same physical meaning. The coupled-mode theory is a mathematical representation of the same WPT process[9].

2.3.1.2 Magnetic Couplers

Non-radiative magnetic coupling WPT can be done using various coupler configurations [31], [32]. They are listed as follows:

1. Circular non polarized Pad (CP)
2. Flux Pipe / Solenoid
3. Double-D polarised Pad (DDP)
4. Double-D Quadrature polarised Pad (DDQP)
5. Bipolar polarized Pad (BPP)
6. Tripolar polarised Pad (TPP)

The coupler consists of transmitter and receiver being the most important part of WPT. The desired characteristics for coupling pads are high Coupling Coefficient 'k', Quality Factor 'Q', and high misalignment tolerance [32]

2.3.1.2.1 Circular Non Polarized Pad (CP)

As mentioned in [32], [33] these are the most commonly used coil structure since early 2000's and it became popular because of the single-sided magnetic field that enters and leave the coil only from the front side.

The single sided nature of flux pattern helps in reducing leakage flux [32]. As shown in Figure 2.13, ferrite bars are presented to the back of the coil pad to facilitate a low reluctant flux path and also reduce the flux leakage [31]. An aluminium plate is placed on the back of the whole coil in order to hold up the flux distribution. This topology gives the advantage that the structure is easy to build with the symmetric flux distribution around the centre but the flux height is proportional to half of the ferrite length is a quarter of pad diameter ($P_d/4$) as mentioned in [33].

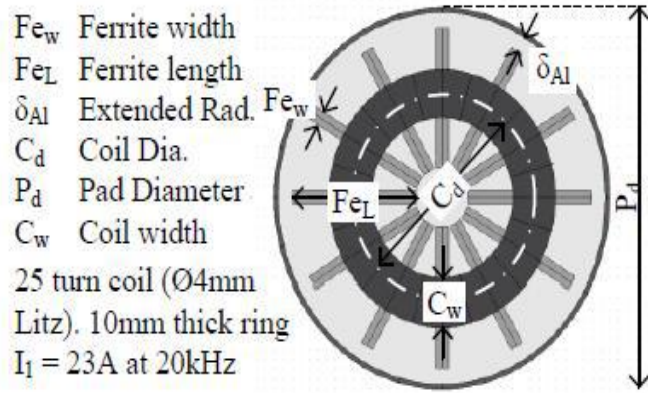


Figure 2.13 Typical Layout Of A Circular Pad [33]

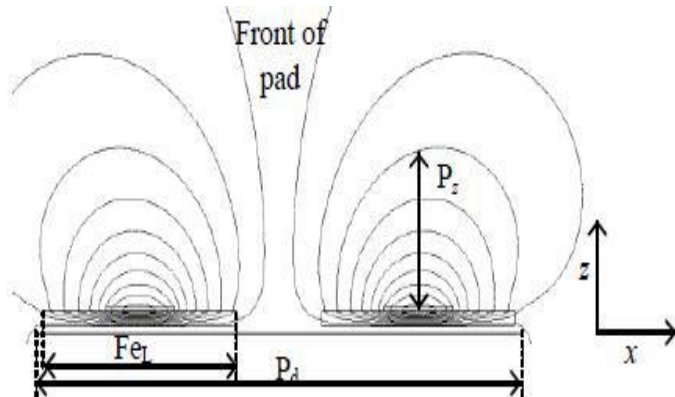


Figure 2.14 Typical Field Generated In Circular Pad [33]

But this configuration has lower tolerance to misalignment which can occur very easily while parking the vehicle and hence there were other configurations that got developed to improve the tolerance to misalignment and also improve the flux height.

2.3.1.2.2 Flux Pipe / Solenoid

The flux pipe consists of two coils positioned at ends of the midsection of a pad as shown in Figure 2.15. The Tx and Rx are the flux transmitting and receiving surfaces, both track and pickup pads are identical. The coils are electrically connected in parallel to lower the impedance and are connected magnetically in series since flux from one coil passes through to the other. The mutual flux between coils links with the pickup pads to couple power [34]. They were developed and used in monorail automated guided vehicle in 90's [33].

Here the fundamental flux path is half of the length of the receiver pad and hence it is better than circular pad. The coefficient of coupling is also similar to the circular pad but the drawback of this design is that the quality factor and the efficiency of the system reduces when aluminium shielding is used [32].

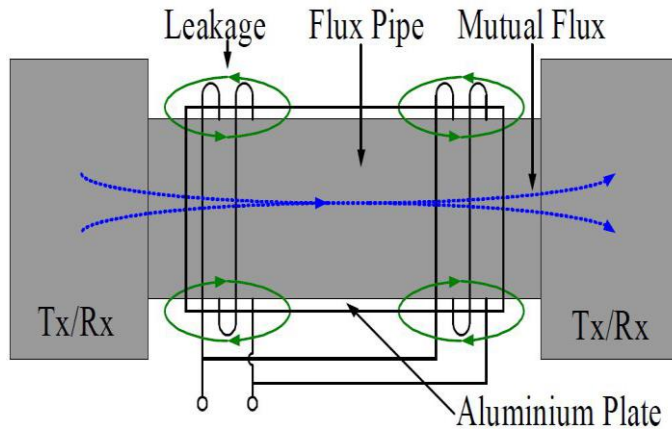


Figure 2.15 Typical Layout Of Solenoid Pad [34]

2.3.1.2.3 Double-D Polarised Pad (DDP)

This is a polarised single-sided flux coupler that combines the advantage of both flux pipe as well as circular pad design [32]. The middle of the DD coil is similar to flux pipe as the coils are connected in series magnetically [32]. Here the coils are placed on top of ferrite and the aluminium shield is placed under the ferrite thus no loss in quality factor. Thus, this DDP design has higher coefficient of coupling, lower losses in aluminium shielding and lower leakage flux also flux height is proportional to half the length of the pad [32]. Therefore, it is a great improvement over the circular pad design.

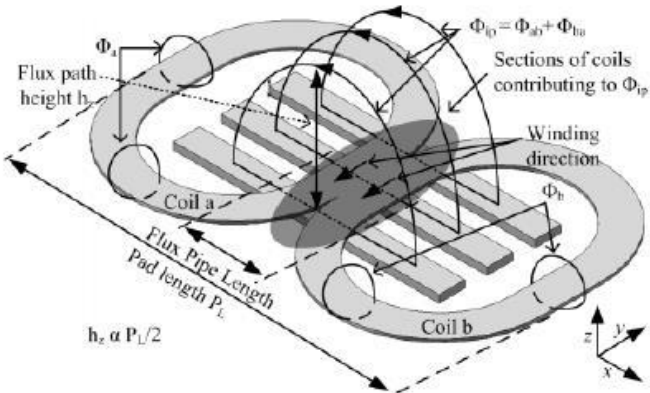


Figure 2.16 Simplified Model Of DD Pad [33]

As a receiver pad the DD coil can only couple horizontal flux component when centred with a transmitter pad, whereas the circular pads can only couple vertical flux component when aligned centrally [33]; also this topology has poor interoperability characteristic when the receiver pad is centrally aligned with the transmitter pad, same goes for the CP topology [31], this led to the development of DDQP pads which can overcome this interoperability issues.

2.3.1.2.4 Double-D Quadrature Polarised Pad (DDQP)

The DDQP topology was designed to generate both parallel and perpendicular magnetic field [31]. In this topology an additional coil is placed on DDP topology, which is shown in Figure 2.17. As the DDQP topology can generate both the polarized and nonpolarized field by regulating the coil current, the flexibility of the system is high than any other topologies, hence higher tolerance to misalignment. But the disadvantage is the increased number of coils, which leads to the increased cost of the topology [31]. This increase in coils is about three times with respect to circular pad [32].

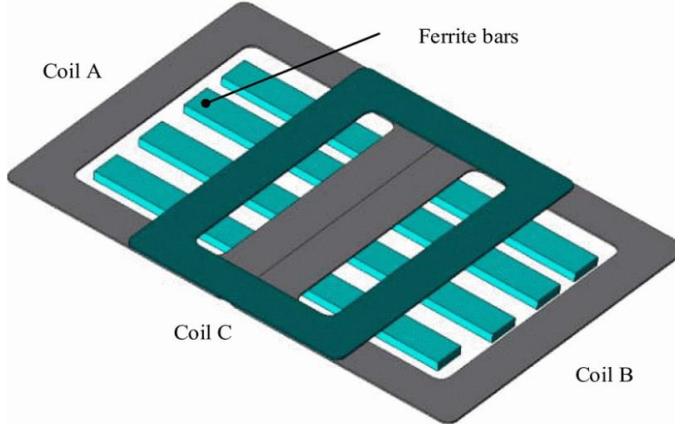


Figure 2.17 Typical Model Of DDQ Polarised Pad [31]

2.3.1.2.5 Bipolar Polarized Pad (BPP)

In this topology coil A and coil B are overlapped in such a manner so that they are mutually decoupled as shown in Figure 2.18. This topology overcomes the added coil structure of DDQP topology hence the copper used here is around 25% to 30% lesser [32] than DDQP topology making this lesser expensive compared to DDQP. And this topology has similar performance to DDQP with regard to misalignment tolerance and higher coefficient of coupling [32]. As per different operation of current direction, BPP can work as CP, single coil or DD mode and thus most suitable for multi-mode secondary pad design [31].

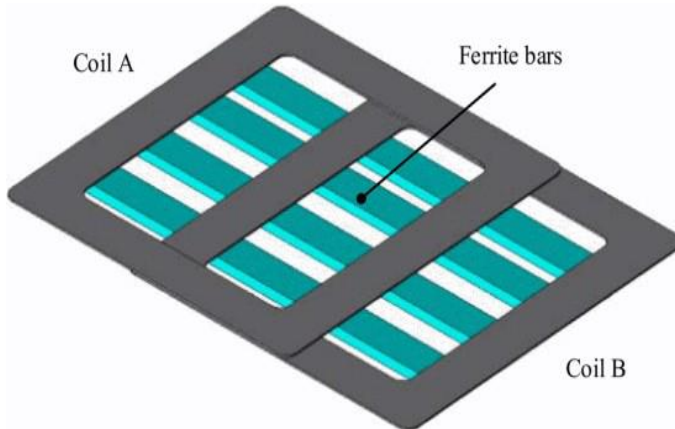


Figure 2.18 Typical Model Of Bipolar Polarised Pad [31]

2.3.1.2.6 Tripolar Polarised Pad (TPP)

Tripolar pad (TPP) is a three-coil coupler arranged in such a way that they are mutually decoupled as shown in Figure 2.19 [35]. This topology allows high tolerance to rotational misalignment of a non-polarized pad [35].

The three mutually decoupled coils are driven independently to achieve highest coupling factor which can be seen in block diagram. As in [35] in this topology allows an increase in effective coefficient of coupling with bipolar and circular pad as the secondary coil. This was accomplished by controlling voltage magnitude and phase of the transmitter coil currents. The apparent power demand is reduced by 45% compared to the circular pad for an air gap of 150 mm [35]. The leakage magnetic field reported is also less. However, the need for three separate inverters to drive three mutually decoupled coils adds to its cost and increases complexity of control [35].

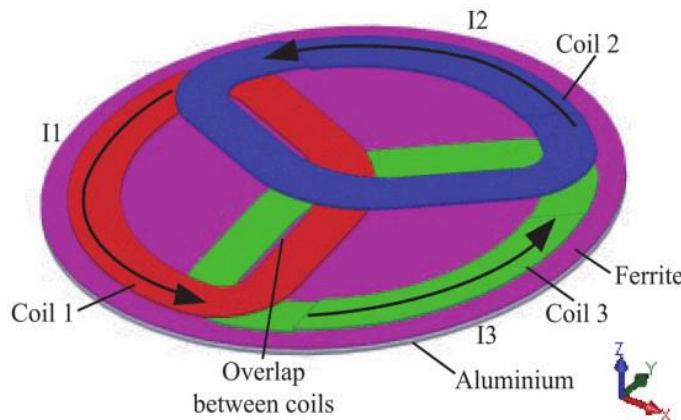


Figure 2.19 A Typical A Tripolar Pad With Arrows Showing The Flow Of Current In Phase [35]

2.3.1.3 Coil Topology Features

In Table 2.2 features of each topology are discussed, showing the preferred use, flux generation and common comparison between selected options.

| Coil Topology | Features |
|---------------------|--|
| Circular Pad | <ul style="list-style-type: none"> • Flux symmetric around CP centre • Non polarised perpendicular field pattern by CP • Commonly used in primary and secondary • Poor interoperability characteristics • Generate and couple perpendicular flux • Flexible application |
| DD Pad | <ul style="list-style-type: none"> • Single sided flux generation • Better performance of interoperability with different topologies • Commonly used in primary • Ferrite bars are easy to saturate at high power rate • No reverse flux to eliminate the unwanted rear flux |
| DDQ | <ul style="list-style-type: none"> • As a secondary the charge zone provide is three time of DD pad • Better performance than DD with different secondary topologies • Commonly used in secondary • Variable excitation modes • Versatile in central coil design to fit the air gap |
| Bipolar Pad | <ul style="list-style-type: none"> • Mutually decoupled partially overlapped structure • Almost same performance and identical power to DDQ • Uses lesser copper than DDQ • Commonly used in secondary. |
| Tripolar Pad | <ul style="list-style-type: none"> • High tolerance to rotational displacement. • All three coils mutually decoupled and overlapped, can be controlled individually. • TPP as primary maintains a high level of uncompensated power regardless of any rotational displacement. |

Table 2.2 Features Of Coil Topologies

2.3.2 Capacitive Power Transfer CPT

In Figure 2.20, The couplers are square-shaped and occupy an area A on both primary and secondary sides.

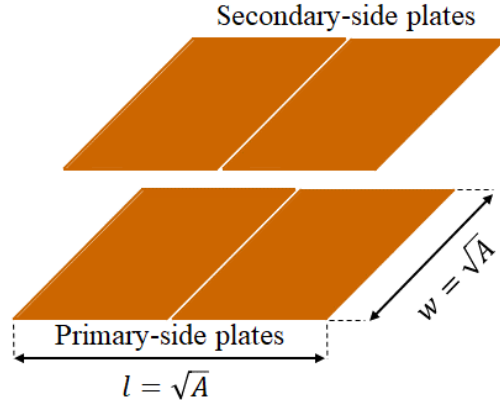


Figure 2.20 CPT System With Primary-Side Plates And Secondary-Side Plates [26]

In a capacitive WPT system, given an air-gap voltage V_{ag} and an air-gap length d , the electric field intensity in the air gap can be approximated by neglecting fringing effect as:

$$E = \frac{V_{ag}}{d} \quad 2.11)$$

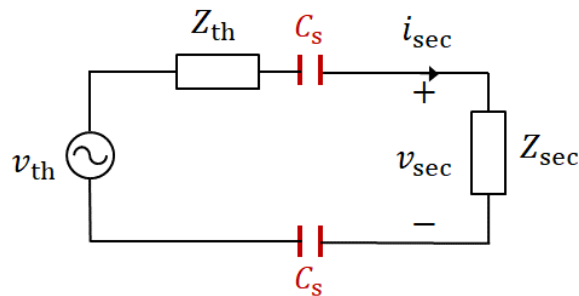


Figure 2.21 Equivalent Thevenin Model Of CPT [26]

In the capacitive WPT system of Figure 2.21, given an air-gap voltage V_{ag} the displacement current through the air-gap i_{ag} can be expressed as:

$$i_{ag} = 2\pi f_{cpt} C_s V_{ag} = \frac{2\pi f_{cpt} \epsilon_0 A}{2d} V_{ag} \quad 2.12)$$

Where f_{cpt} is the operating frequency of the system, and A is the total area of the coupling plates on either the primary or the secondary side. Using 2.11) and 2.12), the maximum power transfer capability of the capacitive WPT system can be expressed as:

$$P_{cpt,max} = i_{ag,max}^2 R_{sec} = \pi^2 f_{cpt}^2 A^2 \epsilon_0^2 E_{max}^2 R_{sec} \quad 2.13)$$

2.3.2.1.1 Models

In Ref [36], A typical CPT system is shown in Figure 2.22 , which includes an inverter, a rectifier, and a properly compensated capacitive coupler. Through the coupling plates, the power is transferred from the TX plates (i.e., P_a and P_b) to the RX plates (i.e., P_c and P_d).

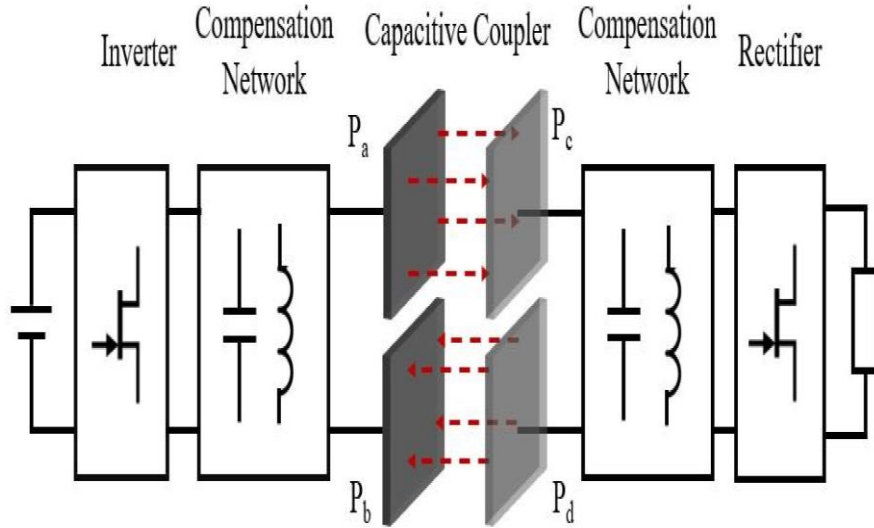


Figure 2.22 Typical Cpt System Configuration [36]

2.3.2.1.1.1 Six Capacitor Model

The coupling mechanism is usually explained by a six-capacitor model as shown in Figure 2.23, and the coupling capacitance between each two plates are represented by C_{ab} , C_{ac} , C_{ad} , C_{bc} , C_{bd} , and C_{cd} [36].

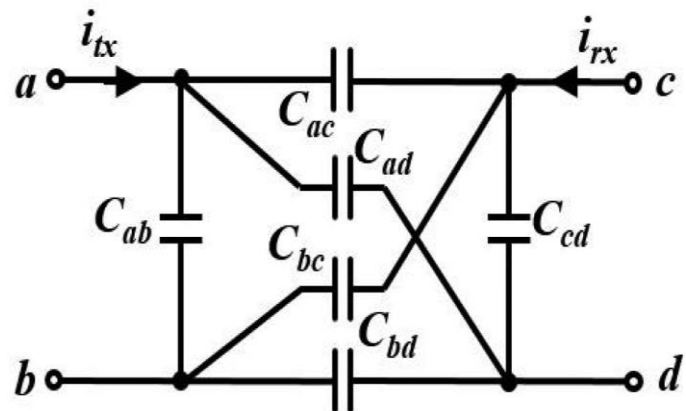


Figure 2.23 Six Capacitor Model [36]

2.3.2.1.1.2 Induced Current Source (ICS)

In order to simplify the circuit analysis, the induced current source (ICS) model is developed as shown in Figure 2.24.

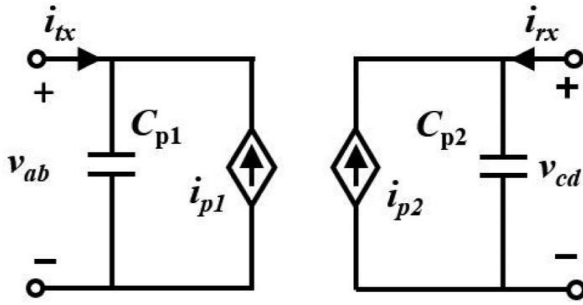


Figure 2.24 Ics Model [36]

And it has:

$$\begin{cases} C_{p1} = C_{ab} + \frac{(C_{ac} + C_{ad})(C_{bc} + C_{bd})}{C_{ac} + C_{ad} + C_{bc} + C_{bd}} \\ C_{p2} = C_{cd} + \frac{(C_{ac} + C_{bc})(C_{ad} + C_{bd})}{C_{ac} + C_{ad} + C_{bc} + C_{bd}} \\ C_{pm} = \frac{C_{bd}C_{ac} - C_{ad}C_{bc}}{C_{ac} + C_{ad} + C_{bc} + C_{bd}} \end{cases} \quad 2.14)$$

This model only needs a pair of self-shunt capacitance (C_{p1} and C_{p2}) and the ICS. With the help of C_{pm} , the power is coupled between TX and RX plates based on the following state equations:

$$\begin{bmatrix} I_{tx} \\ I_{rx} \end{bmatrix} = \begin{bmatrix} j\omega C_{p1} & -j\omega C_{pm} \\ -j\omega C_{pm} & j\omega C_{p2} \end{bmatrix} \begin{bmatrix} V_{ab} \\ V_{cd} \end{bmatrix} \quad 2.15)$$

Where I_{tx} , I_{rx} , V_{ab} , and V_{cd} are the terminal currents and voltages. Which are represented by the phasor form.

Using the ICS model, the coupled power is the product of the induced current and its corresponding voltage, i.e.,

$$P = \text{Re}[V_{ab}(j\omega C_{pm}V_{cd})^*] \quad 2.16)$$

Where * means the conjugate operation and $\text{Re}[\]$ takes the real part. It shows the power transfer capability is proportional to C_{pm} and terminal voltage.

2.3.2.1.1.3 π Model

In ref [25], the equivalent model of the capacitors is further simplified to a π shape, as shown in Figure 2.25. This model is suitable to simplify the parameter calculation in the circuit. It needs to be emphasized that the primary and secondary sides are not separated in the π shape model.

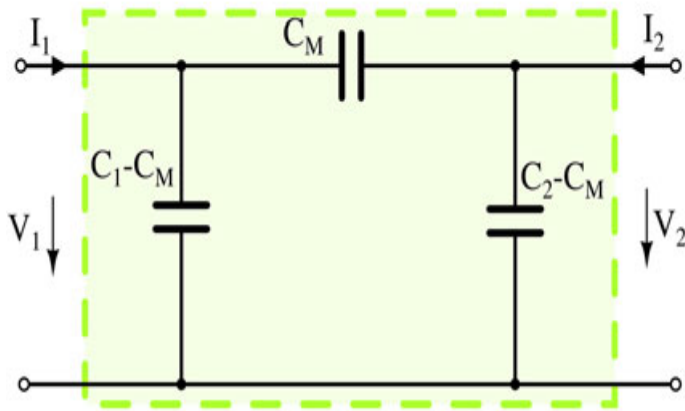


Figure 2.25 Simplified Equivalent Model Of Coupling Capacitors The π Model [25]

Where $V_1 \equiv V_{ab}$, $V_2 \equiv V_{cd}$, $I_1 \equiv I_{tx}$, $I_2 \equiv I_{rx}$, $C_1 \equiv C_{p1}$, $C_2 \equiv C_{p2}$ and $C_M \equiv C_{pm}$. Then equation (2.14) can be reduced into:

$$\begin{cases} I_{tx} = j\omega(C_{p1} - C_{pm}) \cdot V_{ab} + j\omega C_{pm} \cdot (V_{ab} - V_{cd}) \\ I_{rx} = j\omega(C_{p2} - C_{pm}) \cdot V_{cd} + j\omega C_{pm} \cdot (V_{cd} - V_{ab}) \end{cases} \quad 2.17)$$

Similar to that of the coils, the capacitive coupling coefficient k_c of the plates is defined with the parameters from (2.13), as follows:

$$k_c = \frac{C_{pm}}{\sqrt{C_{p1}C_{p2}}} \quad 2.18)$$

2.3.2.1.2 Plates

According on the power level and coupling space, many couplers have currently been created. The well-known coupling process $C = \frac{\epsilon A}{d}$ states that the overlapping area, medium dielectric constant, and distance all affect the coupling capacitance between any two plates. There are two basic coupler structures that are frequently employed; they were created for the same coupling space that is described by l and d . And since the distance d is defined by the application, the only design freedom is to improve the mutual coupling is to enlarge the corresponding overlapping area.

For either of the two, three types of coupling can be defined based on the six-capacitor model. C_{ac} and C_{bd} represent the mutual coupling, and they are helpful for power transfer because a large C_{pm} needs large C_{ac} and C_{bd} [refer to (2.14)]. C_{ab} and C_{cd} are the self-coupling, increasing which will help improve C_{p1} and C_{p2} . C_{ad} and C_{bc} are caused by the cross coupling, and their existence deprecate C_{pm} .

2.3.2.1.2.1 Horizontal Capacitive Couplers (HCC)

When the same-side plates (such as P_a and P_b) are placed horizontally, the mutual coupling is strong, and this structure is defined as HCC, refer to Figure 2.26. For the HCC, the only design variable is the distance (i.e., l_c) between P_a and P_b . Such a structure does benefit C_{pm} , but its C_{p1} is too small [36].

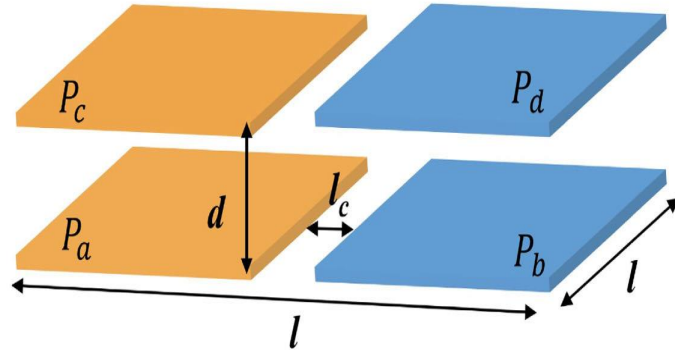


Figure 2.26 HCC Structure [36]

In [37], a horizontal structure was used, the plates at the same side are placed 500 mm away, so the coupling capacitance C_{ab} and C_{cd} are both close to zero. Cross-coupling capacitances C_{ad} and C_{bc} are also close to zero. As a result, the capacitive coupling coefficient is $k_c \approx 1$ [25].

The HCC almost maximizes the mutual coupling and has small cross coupling to ensure large C_{pm} , but its limited self-coupling will significantly depreciate C_{p1} [36]. An illustration to the coupling mechanism is given in Figure 2.27.

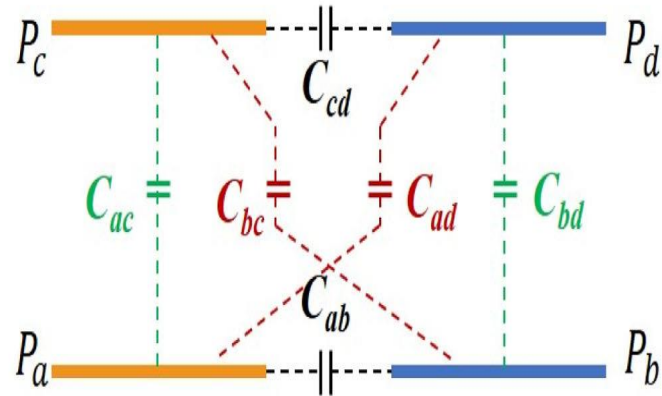


Figure 2.27 Coupling Mechanism Of HCC [36]

2.3.2.1.2.2 Vertical Capacitive Couplers (VCC)

This coupler places same-side plates vertically, and thereby, is named as the Vertical Capacitive Coupling. For VCC, the clearance is ensured by $d_c = 3$ mm, and the only design variable is the length of P_b , i.e., l_s . As shown in Figure 2.28, l_s affects C_{p1} and C_{pm} at the same time. From the power transfer perspective, a design point is chosen to maximize C_{pm} . Even though a maximized C_{pm} still exists, the VCC cannot fully utilize the coupling space like the HCC [36].

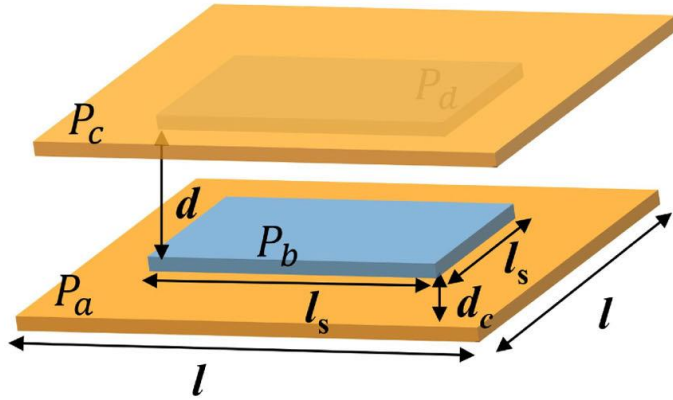


Figure 2.28 VCC Structure [36]

For the vertical structure shown in Figure 2.28, the plate distance d_c is much smaller than the air gap distance d , so C_{ab} and C_{cd} are much larger than C_{ac} and C_{bd} . As a result, the capacitive coupling coefficient $k_c \ll 1$, which means it is a loosely coupled CPT system [25].

The VCC enhance the self-capacitance C_{p1} by increasing the coupling areas between plates P_a, P_b as well as plates P_c, P_d . Even though area between plates P_a, P_c and Plates P_b, P_d remains the same. C_{pm} still decreases because of the decreased mutual coupling effect [36]. The coupling mechanism is explained in Figure 2.29.

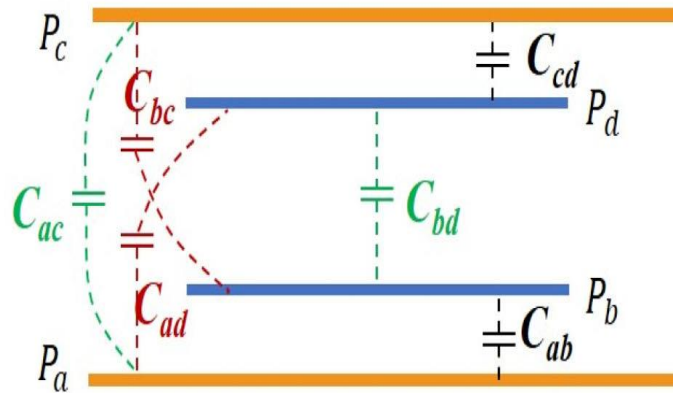


Figure 2.29 Coupling Mechanism Of VCC [36]

2.3.2.1.2.3 Interleaved Capacitive Coupling (ICC)

Reference [36] proposes an additional structure -combining the benefits of the HCC and VCC- shown in Figure 2.30. Both TX and RX sides have four metal plates locating at two layers and all the plates are identical. For either side, the same-layer plates (like P_{a1} and P_{b1}) are disconnected, and plates from different layers are connected through additional wire in an interleaved manner, such as P_{a1} and P_{a2} .

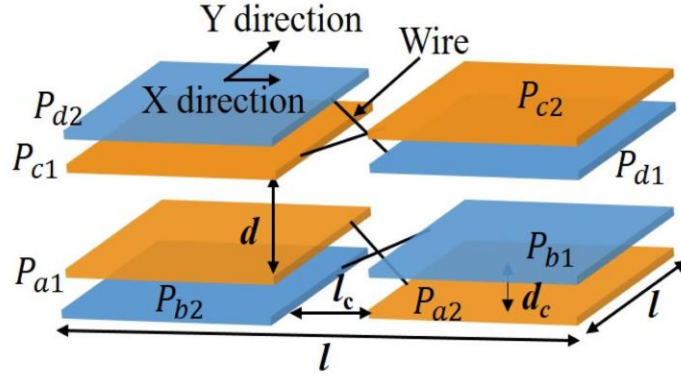


Figure 2.30 Interleaved Capacitive Coupler Stereogram [36]

Compared to the VCC, the ICC has larger C_{p1} due to its larger overlapping area of the same-side plates, because the middle two layers of the VCC is smaller [refer to Figure 2.28 and Figure 2.30]. As for C_{pm} , the VCC must make a trade-off to maximize the C_{pm} [36]. In VCC, the large C_{p1} will sacrifice C_{pm} . However, the ICC will not have this concern when C_{p1} is maximized by the additional plates. In the ICC, the cross-coupling capacitance is determined by:

$$C_{ad} = C_{a1d1} + C_{a2d2} + C_{a1d2} + C_{a2d1} \quad 2.19)$$

In this coupler, the clearance is ensured by l_c and d_c [refer to Figure 2.30]. Like the HCC and VCC, the size parameters can be optimized for the ICC. The large C_{pm} and C_{p1} is achieved simultaneously in the ICC because it can fully utilize the benefits of the HCC and VCC while avoid their downside [36]. The coupling mechanism of this coupler is described in Figure 2.31.

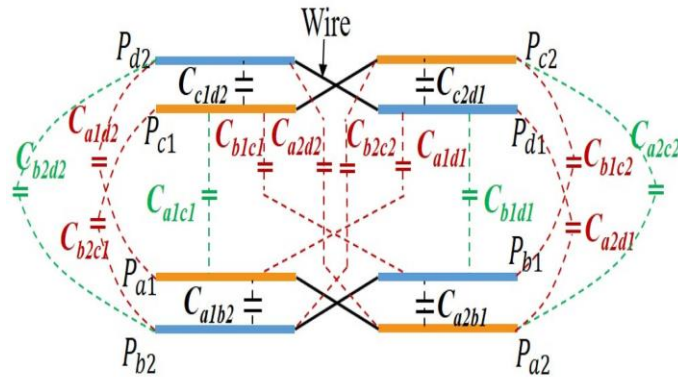


Figure 2.31 Interleaved Capacitive Coupler Front View [36]

2.3.3 Maximum Achievable Efficiency In Large Air-Gap Inductive And Capacitive Wpt Systems

The topology of an inductive and a capacitive WPT system typically utilized in large air-gap applications such as EV charging is shown in Figure 2.32 and Figure 2.33 respectively. In the inductive WPT system, the pair of coupling coils form a loosely coupled transformer, with a primary-side self-inductance L_p , a secondary-side self-inductance L_s , and a mutual inductance M . In the capacitive WPT system, the two pair of coupling plates form two capacitances, shown as C_s . Both the systems comprise resonant matching networks on each side of the coupler that compensate for the coupler's

reactance. These compensations ensure that the impedance seen by the inverter stays near-resistive, enabling effective power transfer with low circulating currents [26].

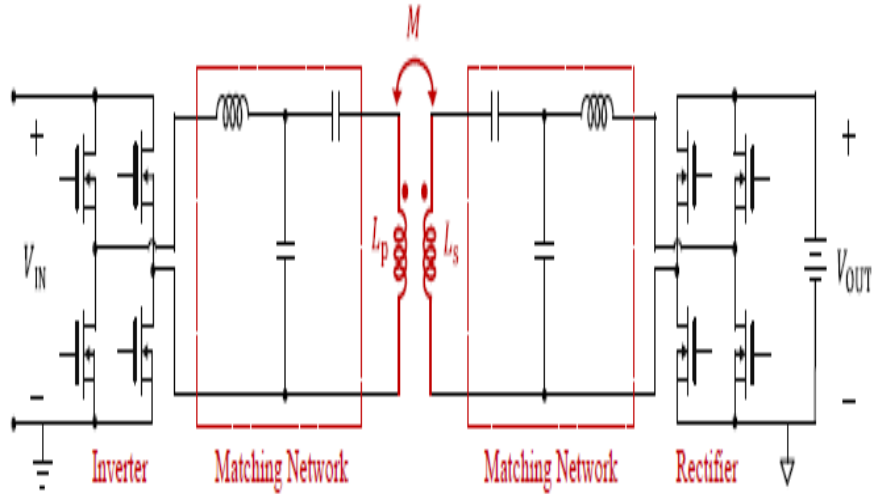


Figure 2.32 Topology Of IPT System [26]

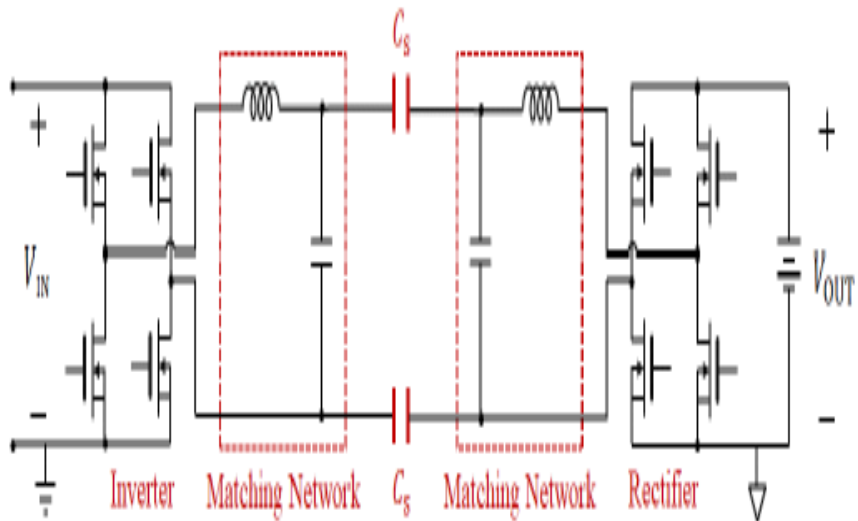


Figure 2.33 Topology Of CPT System [26]

Although operating at a higher frequency increases power transfer capability of both inductive and capacitive WPT systems, it may impact their efficiencies differently [26].

2.3.3.1 Inductive Power Transfer (IPT)

The major source of losses are its matching networks and coupling coils. Assuming that the losses in the inverter and rectifier transistors comparatively very small, and that the matching network capacitors are much more efficient than the inductors [26], the maximum efficiency achievable in the inductive WPT system can be approximated as:

$$\eta_{ipt} \approx 1 - \sqrt{\frac{\pi^2 P_{ipt}}{8V_{IN}V_{OUT}} (\omega_{ipt} M)} - \frac{2}{Q_C} \left(\frac{\sqrt{M}}{L_p L_s} \right)$$

2.20)

Where P_{ipt} is the transferred power, $\omega_{ipt} = 2\pi f_{ipt}$, and $Q_{L,ipt}$ is the unloaded quality factor of its matching network inductors, and Q_C if the unloaded quality factor of the coupling coils. The efficiency expression of 2.20) is obtained by optimally distributing the required compensation among the matching networks.

2.3.3.2 Capacitive Power Transfer (CPT)

The losses in the coupling plates are typically very small compared to matching network losses [26]. Under this assumption and applying similar optimal design approach as IPT, the maximum efficiency achievable in the capacitive WPT system can be approximated as:

$$\eta_{cpt} \approx 1 - \sqrt{\frac{\pi^2 P_{cpt}}{8V_{IN}V_{OUT}} \left(\frac{1}{\omega_{cpt} \frac{C_s}{2}} \right)}$$

2.21)

Where P_{cpt} is the transferred power, $\omega_{cpt} = 2\pi f_{cpt}$, and $Q_{L,cpt}$ is the quality factor of the matching network inductors. It can be seen from (2.20) and (2.21) that operating at a higher frequency lowers the efficiency of an inductive WPT system but increases the efficiency of capacitive WPT system. This is because a higher frequency increases the coupler reactance of the inductive WPT system ($\omega_{ipt} M$), requiring more compensation, but decreases the coupler reactance of the capacitive WPT system ($\frac{1}{\omega_{cpt} \frac{C_s}{2}}$), requiring less compensation.

2.3.4 Comparison Between IPT And CPT In Large Air-Gap

2.3.4.1 Power Transfer Capability

Reference [26] presents a comparison for ratio of the power transfer capability of an example capacitive WPT system to that of an example inductive WPT system with the same coupling area, as a function of the ratio of their operating frequencies; as shown in Figure 2.34. The systems having the same air-gap of 12 cm and the same coupling area A of 0.5 m × 0.5 m (the thickness of ferrite slab is assumed to be 5 cm).

As can be seen in Figure 2.34, the capacitive WPT system can achieve the same power transfer capability as the inductive WPT system by operating at about 900 times higher frequency. With the development of high-speed GaN transistors capable of efficiently switching at tens of MHz, and given that large air-gap inductive WPT systems typically operate at tens of kHz, capacitive WPT systems have the potential to operate at orders of magnitude higher frequencies, and achieve similar power transfer levels as inductive WPT systems [26].

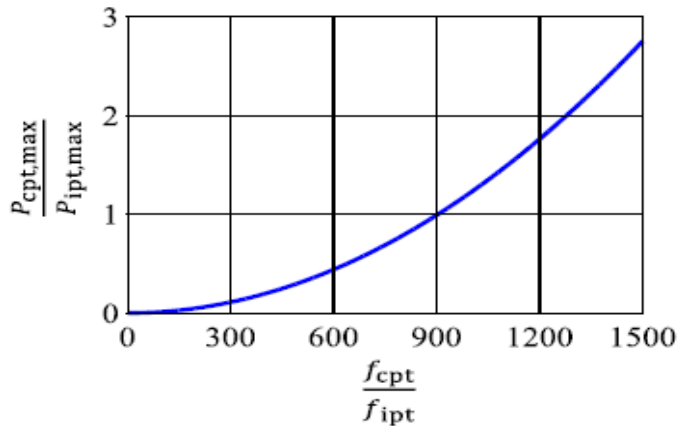


Figure 2.34 Ratio Of Power Transfer Capabilities Of An Inductive And A Capacitive WPT System Having The Same Air-Gap And Same Coupling Area [26]

2.3.4.2 Achievable Efficiency

In [26], the maximum efficiency of two example capacitive and inductive WPT systems, both having an air-gap of 12 cm, are shown below as a function of their power transfer density (defined as the power transferred per unit coupling area) for three different operating frequencies. The matching network inductors of both the systems and the coupling coil of the inductive WPT system all are assumed have a quality factor of 500.

The comparison is done for a system with 12 cm air-gap and $30\text{ cm} \times 30\text{ cm}$ plates as a function of their power transfer density for three different operating frequencies: 100 kHz [Figure 2.35], 1 MHz [Figure 2.36] and 10 MHz [Figure 2.37].

As expected, with increasing frequency, the efficiency of the capacitive WPT system rises and that of the inductive WPT system falls. At 10 MHz, the capacitive WPT efficiency is higher than the inductive WPT efficiency for the whole range of power transfer density [26].

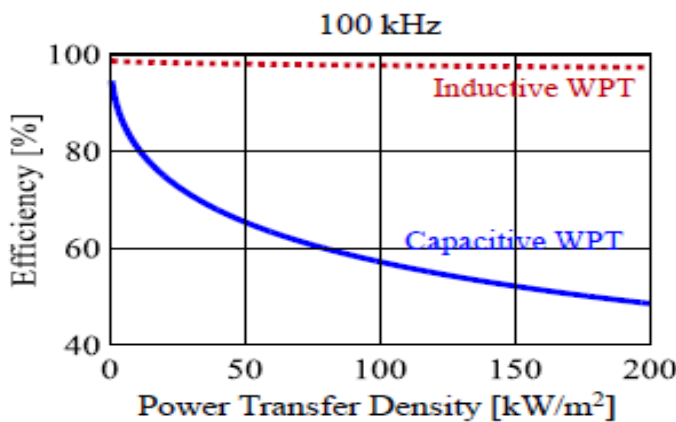


Figure 2.35 Efficiency Of An Inductive And A Capacitive Systems With 100 kHz [26]

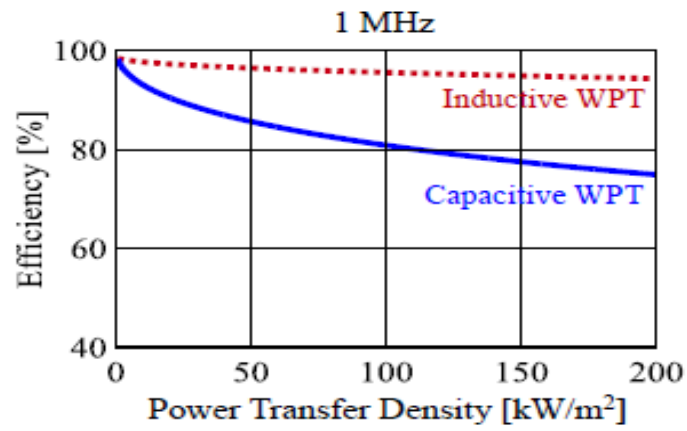


Figure 2.36 Efficiency Of An Inductive And A Capacitive Systems With 1 MHZ [26]

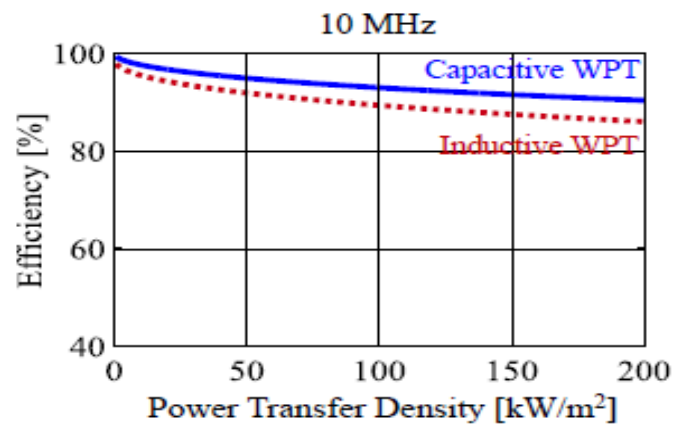


Figure 2.37 Efficiency Of An Inductive And A Capacitive Systems With 10 MHZ [26]

3 CHAPTER 3: RESONANT INDUCTIVE COUPLING

Resonance is a phenomenon where energy oscillates, generally, between two modes. In the case of an RLC circuit, energy oscillates between the electric field in the capacitor and the magnetic field in the inductor [38]. Matching the inductor's and capacitor's respective impedances allows an RLC circuit to operate in resonance. The values cancel out because they have the opposite signs, leaving the system with the lowest possible (pure resistive) impedance. The inductor and the capacitor or the circuit are resonating, the way the kinetic and potential energy in a pendulum resonate and empty into each other.

In ref[39], a distinction Between IPT and Resonance Inductive Coupling RIPT is discussed by summarizing their differences. It should be noted that they all conform to Faraday's and Ampere's law. So, the variations primarily include design approaches, system architectures, parameter selection and transfer characteristics.

- In RIPT, a variety of system topologies are used, which can help with impedance matching to improve system transfer properties. The coil's parasitic capacitance is typically used to generate an extremely high resonant frequency. IPT, in contrast, typically uses a system architecture with two coils, with the fundamental topologies being series-series, parallel-series, parallel-parallel, and series-parallel. To improve power transfer, the secondary coil of an IPT should be tuned at the operating frequency. The lumped capacitance of the primary coil should be specifically built to compensate for both the primary self-inductance and the reflected impedance in order to eliminate the imaginary power in particular topologies [39]. Except for the series-series topology, the compensation capacitance of the primary coil in the other three topologies are all affected by either mutual inductance values or load impedances [40];
- The operating frequency of RIPT is roughly in the MHz region since parasitic capacitances are typically used for tuning. The quality factors are therefore quite high. These high-quality variables can lessen the dramatic fall in transfer efficiency that is brought on by the reduced coupling coefficient as the transfer distance rises, allowing for the realization of high transfer efficiency in the meter scope. In contrast to RIPT, IPT typically operates in the KHz range, and ferromagnetic materials are frequently employed to enhance coupling and, hence, power transfer [39]. IPT quality factors are typically designed below 10 [40], [41] since higher quality factor values induce a sharp decline in transfer power [42];
- The frequency splitting phenomenon exists in both RIPT and IPT, but with different objectives. The former aims to maximize the transfer power, and the latter one aims to achieve a unity power factor [40]. AC sweep analysis results by executing Spice simulations are showed in Figure 3.1 [39]. P_{VS} , P_s and P_L represent the output power of the AC voltage source, the dissipation power of the source internal resistance and the load resistance. A and B represent the frequency splitting points based on achieving the unity power factor, D and E represent the frequency splitting points based on maximizing the transfer power, C_1 and C_2 are at the resonant frequency point. Obviously, the frequency splitting phenomenon appears in Figure 3.1, and A and D (or B and E) overlap with each other. But it should be noted that the premise is the equivalence between R_S and R_L , once this assumption is not satisfied, the misalignment between A and D (or B and E) will happen.

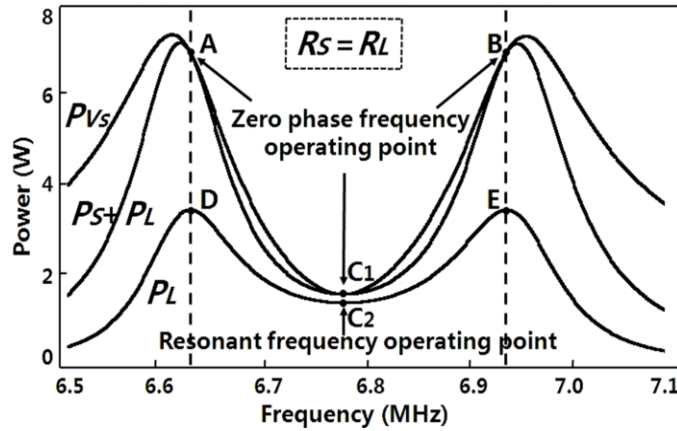


Figure 3.1 Frequency Splitting Phenomena in RIPT and IPT [39]

3.1.1 Models

3.1.1.1 Circuit Theory

Based on mutual inductance, the model is straightforward. Parallel-parallel and series-series compensations are the basic structures which have been well discussed in the literature. and additionally, their analysis and design methods are elaborated in [43], [44]. Hence, as an example to demonstrate Circuit Theory; Series-Series SS topology is chosen. Figure 3.2 shows the equivalent circuit model of a system architecture with two coils, in which, $R_S, R_2(R_3) = Z_p(Z_s), L_2(L_3) = L_p(L_s), C_2(C_3) = C_p(C_s), M_{23} = M$ and $R_L = Z_L$ represent the internal resistance of the voltage source, the coil parasitic resistances, the coil self-inductances, the resonant capacitors, the mutual inductance and the load resistance, respectively.

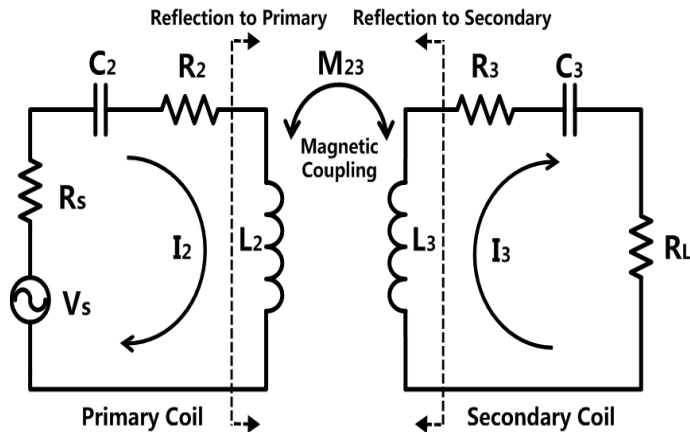


Figure 3.2 Equivalent Circuit Model Of System Architecture With Two Coils [39]

To further simplify the circuit all items can be referred to the primary as in Figure 3.3, then if the system is in the resonant state, the reflected impedance from the secondary coil to the primary coil, the transfer efficiency and the transfer power can be drawn as [43], [44]:

$$Z_r = R_{ref} = \frac{\omega^2 M_{23}^2}{Z_3} = \frac{\omega^2 M^2}{Z_s} \quad 3.1)$$

$$\eta = \frac{\omega^2 M_{23}^2 R_L}{R_3 + [R_L M_{23}^2 + (R_2 + R_s)(R_3 + R_L)]} \quad 3.2)$$

$$P_L = \frac{\omega^2 M_{23}^2 V_s^2 R_L}{[R_L M_{23}^2 + (R_2 + R_s)(R_3 + R_L)]} \quad 3.3)$$

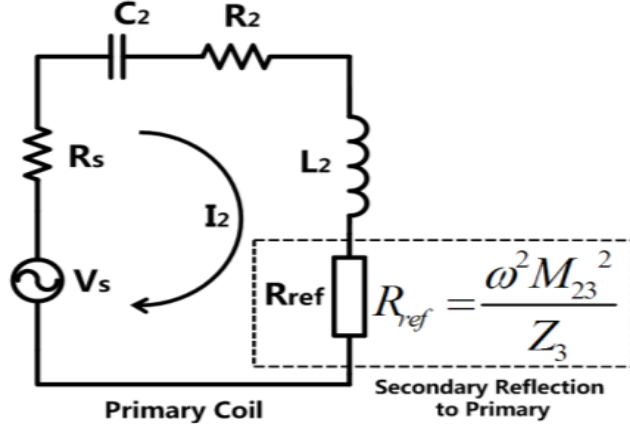


Figure 3.3 Simplified Circuit Model By Referring The Secondary Coil To Be The Equivalent Impedance In The Primary Side [39]

3.1.1.2 Coupled Mode Theory

According to Coupled Mode Theory, the physical processes of power transferring from one resonant object to another can be described in (2.10). If the intrinsic decay rate is not considered, the energy exchange between two resonant objects will be lossless. When considering the loss during the energy exchange, we use:

$$\begin{cases} \frac{da_m(t)}{dt} = (i\omega_m - \Gamma_m)a_m(t) + iK_{mn}a_n(t) + F_m(t) \\ \frac{da_n(t)}{dt} = (i\omega_m - \Gamma_m - \Gamma_L)a_n(t) + iK_{nm}a_m(t) \end{cases} \quad 3.4)$$

Where \$\Gamma_L\$ represents the additional energy decay rate due to the load. Suppose that the properties of these two resonant objects are identical, then \$\omega_m\$ and \$\omega_n\$ equal \$\omega_r\$, \$K_{mn}\$ and \$K_{nm}\$ equal \$K\$, and make the driving terms \$F_m(t)\$ be \$Ve^{i\omega t}\$ simultaneously, Equation (3.4) can be re-written as:

$$\begin{cases} a_m(t) = \frac{[(\Gamma_n + \Gamma_L) + i(\omega - \omega_r)]Ve^{i\omega t}}{K^2 + (i\omega - i\omega_r + \Gamma_m)(i\omega - i\omega_r + \Gamma_n + \Gamma_L)} \\ a_n(t) = \frac{iKVe^{i\omega t}}{K^2 + (i\omega - i\omega_r + \Gamma_m)(i\omega - i\omega_r + \Gamma_n + \Gamma_L)} \end{cases} \quad 3.5)$$

The transfer efficiency and transfer power expressions in CMT can be described as follows [30]:

$$\eta = \frac{\Gamma_L |a_n(t)|^2}{(\Gamma_m |a_m(t)|^2 + (\Gamma_n + \Gamma_L) |a_n(t)|^2)} \quad 3.6)$$

$$P_L = 2\Gamma_L |a_n(t)|^2$$

3.7)

3.1.2 Compensation Networks

The resonance converter topology plays a vital role in the amount of power transfer and distance [45]–[47]. An inductive power transfer system without resonance is less efficient. In addition, the voltage and current stress across the semiconductor devices and the rating depends on the configuration of the resonance topology. The arrangement of energy storage elements determines the order, size and shape of the waveforms [48].

To transmit power wirelessly, using a loosely coupled transformer it involves a large winding separation which has a relatively large leakage inductance, as well as proximity effect and winding resistance, even magnetising flux is significantly reduced [49]. Thus, additional compensation capacitors are needed to form the resonant tanks in both primary as well as secondary side [49]. Usually, the primary side inductance is compensated/-tuned to decrease the apparent power supply rating and the secondary inductance is compensated/tuned to maximize power transfer [50].

The most basic requirement of a compensation capacitor is to resonate with primary/secondary inductance to provide the reactive power required for the generation of adequate magnetic fields [51].

Ref [49] discussed requirements for compensation as follows:

- Minimum VA rating and maximized power transfer capability
 - Minimises apparent power / VA rating of power supply
 - Cancels the secondary inductance to maximize transfer capability
- Constant-Current (CC) / Constant-Voltage (CV)
 - Compensation topology can be selected as per the output requirement CC or CV
- High Efficiency
 - It is mainly decided by coupling coefficient and quality factor of the windings
- Bifurcation Resistant
 - To guarantee system stability by having unique zero phase angle (ZPA)

3.1.2.1 Higher Order Resonance

There is more freedom in the tuning of a higher-order resonance converter than in the tuning of the second order circuit. In general, in a higher-order resonance circuit, the number of storage elements will be more than two. Hence, more space is required in order to perform the same function [52].

3.1.2.2 Second Order

The primary compensation of the SS, SP, PS, PP resonance topologies are second order topologies [52]. Similarly, the secondary side follows the same. The power level, application and impedance of various combinations give an overall idea for how to select the switches for the IPT system [52].

- Series-Series SS.
- Series-Parallel SP.
- Parallel-Series PS.
- Parallel-Parallel PP.

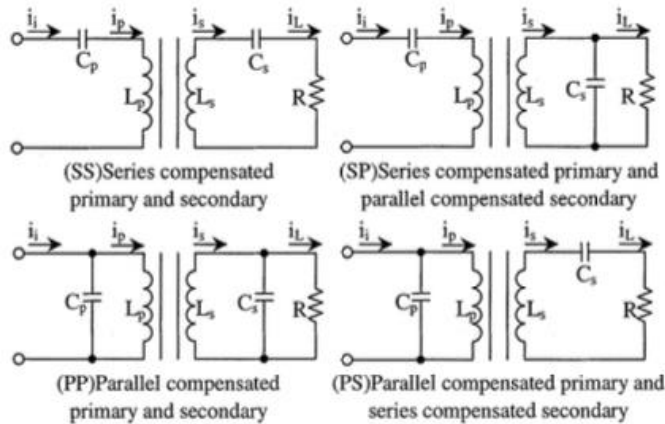


Figure 3.4 The Topologies Of The Basic Compensation Techniques Of The Primary And The Secondary [40]

When the compensation capacitor is connected in series in the primary side it acts as a voltage generator and when connected in parallel with an inductor the capacitor becomes a current generator.

On the secondary side the capacitor is dimensioned in order with the secondary coil inductance so as to minimize the circulating apparent power.

3.1.2.2.1 Series-Series SS

In this scheme the compensation capacitance is placed in series with the winding inductance both in the primary as well as secondary side as shown in Figure 3.4.

$$C_p = \frac{1}{\omega_o^2 L_p} \quad 3.8)$$

3.1.2.2.2 Series-Parallel SP

Here the primary side is connected in series to the compensation capacitance and secondary side is connected in parallel. This design is usually adopted for a constant-voltage output as shown in Figure 3.4.

$$C_p = \frac{1}{\omega_o^2 \left(L_p - \frac{M^2}{L_s} \right)} \quad 3.9)$$

3.1.2.2.3 Parallel-Series PS

Here the primary side is connected in parallel to compensation capacitance and secondary side is connected in series as shown in Figure 3.4.

$$C_p = \frac{\frac{L_p - \frac{M^2}{L_s}}{\left(\frac{M^2 R}{L_s^2} \right) + \omega_o^2 \left(L_p - \frac{M^2}{L_s} \right)}}{3.10)$$

3.1.2.2.4 Parallel-Parallel PP

In this scheme the compensation capacitance is placed in parallel with the winding inductance both in the primary as well as secondary side as shown in Figure 3.4.

$$C_p = \frac{L_p}{\left(\omega_o^2 \frac{M^2}{R}\right) + \omega_o^2 L_p^2}$$

3.11)

The comparison of different resonance combinations of second order has been listed in Table 3.1

| Circuit Topologies | | | | |
|--|--|---|---|---|
| Parameters | SS | SP | PS | PP |
| Inverter voltage rating | Lower DC link voltage (More than SP) | Less DC link voltage | High voltage is needed in comparison with SS and SP | High voltage is needed in comparison with SS and SP |
| Impedance(z) | Decrease along with misalignment | Decrease along with misalignment | Increases along with misalignment | Increases along with misalignment |
| Output independent by load | Voltage and current | Voltage and current | Voltage | Current |
| Efficiency for larger distance between coil | Low | Low | High | High |
| Advantages | <ul style="list-style-type: none"> • Output current is not dependent on the load at resonance • High-power transfer efficiency at higher frequencies | <ul style="list-style-type: none"> • Smaller pickup coil self-inductance than SS • Secondary parallel resonant converter gives stable current | Tuning is easy | Tuning is easy |

Circuit Topologies

| Parameters | SS | SP | PS | PP |
|--------------|--|--|---|---|
| Drawbacks | <ul style="list-style-type: none"> • Larger pickup coil • During partial loading condition, load is independent of voltage transfer ratio • High-frequency current flows through capacitor leads to high voltage across the capacitor | <p>DC components are not blocked</p> | <ul style="list-style-type: none"> • Need current source input to eliminate momentary changes in voltage • Need high voltage input voltage to transfer large amount of power due to high input resistance | <ul style="list-style-type: none"> • Low power factor • Required large current source • Need high voltage input voltage to transfer large amount of power due to high input resistance |
| Applications | Static and Dynamic IPT for EV | <ul style="list-style-type: none"> • Biomedical Applications • Low power Transport | High-power EV buses | High-power EV buses |
| Power level | High | Low and Medium | High | High |

Table 3.1 Comparison Between Different Resonance Combinations [53]

3.1.2.3 Hybrid

Considering the primary and secondary circuit as a whole, all the IPT systems are higher in the order of resonance. However, if the primary and secondary sides are separately considered, the order will be reduced. The hybrid circuit is a combination of series and parallel resonance. The compensation method gives more consistent performance. The tuning of the resonance capacitor is more precise and gives more control freedom[52].

This basic arrangement of energy storage element can be connected in the primary and secondary side of the IPT system. In such conditions, the cumulative performance of the system would be different. However, for a higher-power level, the best primary compensation is the series-series combination. It can be perfectly tuned and can bring the desired performance if there is a series of parallel combinations[52].

3.1.2.3.1 LCC

In order to achieve more flexible operations, such as Zero Voltage Switching ZVS, Zero Current Switching ZCS and Zero Phase Angle ZPA, the LCC compensation was proposed as shown in Figure 3.5 by tuning the compensation network parameters [54]. In the LCC symmetrical T-type compensation network, shown in the primary side of Figure 3.5, constant current or constant voltage can be achieved practically regardless of the impedance of the load [55]

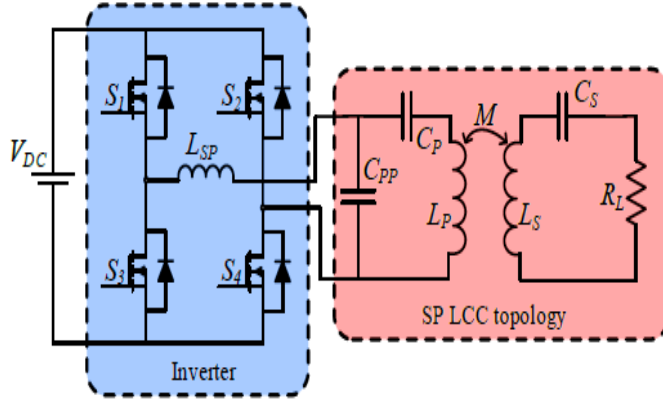


Figure 3.5 SS LCC Topology [54]

In order to achieve lower turn-off losses and switching stresses, the near ZCS with ZPA was derived for the LCC compensation topology by inserting the series-connected inductor L_{sp} and parallel-connected capacitor C_{pp} [56] Contrary to traditional topology, the ZCS operation has a different parameters design process. The nominal main power P_p and secondary side resonant frequency ω_o should be identified first. Thus, the primary coil current I_p and the calculation of the parallel compensation capacitor's C_{pp} is as follows:

$$I_p = \sqrt{\frac{P_p}{R_{ref}}} \quad 3.12)$$

$$C_{pp} = \frac{I_p}{\omega_o V_{inv}} \quad 3.13)$$

Where R_{ref} is the reflected resistance to primary as in (3.1) and V_{inv} is the output voltage of the inverter.

Consequently, the series-connected inductor L_{sp} and the resonant capacitor C_P can be expressed as:

$$L_{sp} = \frac{1}{\omega_o^2 C_{pp}} \quad 3.14)$$

$$C_p = \frac{C_{pp}}{\frac{L_p}{L_{sp}} - \frac{\pi^2}{8}} \quad 3.15)$$

The maximum transmission efficiency can be harvested within a certain distance by changing the ratio of series and parallel-connected compensation capacitors. Nevertheless, the main drawback is that the system performance is sensitive to parameter changes [54].

3.1.2.3.2 LCL

Moreover, the reflected capacitive reactance in the PP topology can be tuned out by the series-connected inductor as shown in Figure 3.6. There are several advantages for the LCL compensation networks. One is that the converter for LCL only supplies the active power required by the load when the system is under the resonant frequency. The LCL resonant tank is supplied by a DC voltage source, it leads to a major advantage that the output current is directly related to the input voltage supply and independent of the load variation. These make the controller design more simplified and easy to regulate the output power [54].

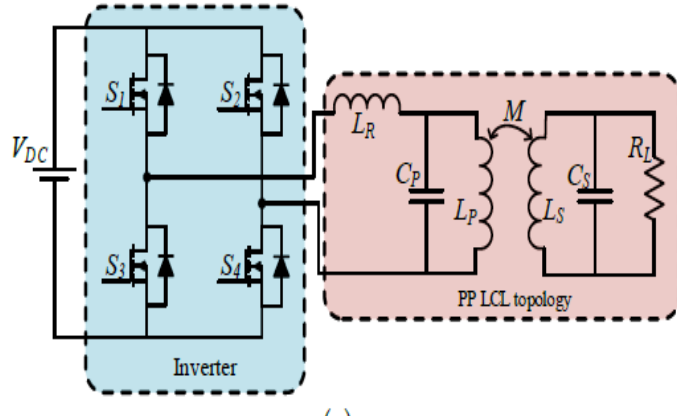


Figure 3.6 PP LCL Topology [54]

These make the controller design more simplified and easier to regulate the output power. Besides, the LCL topology can be operated with continuous and discontinuous current [57]. Furthermore, inverter working close to unity power factor (UPF) can be achieved by variable frequency control method [54].

The primary equivalent inductance is written as:

$$L_{p,eq} = L_p - \frac{1}{\omega^2 C_{pL}} - \frac{1}{\omega^2 C_r} \quad 3.16)$$

C_r is the reflected capacitance; C_{pL} is the primary series tuning capacitor. The primary series capacitor is written as:

$$L_{s,eq} = \frac{1}{\omega^2 C_{pp}} \quad 3.17)$$

$$C_{ps} = \frac{L_{s,eq}}{\omega_0^2 [L_{\Delta p} L_{s,eq} - M^2]} \quad 3.18)$$

Where M is the mutual inductance between the coils. The series capacitance in the circuit and the primary inductor are modified as an equivalent primary inductance. The bridge inductor L_R limits the current flowing from the inverter. The capacitor C_p is in resonance with the primary equivalent inductor $L_{p,eq}$.

The diode bridge at the receiving end is non-linear. An equivalent linear approximated resistance for the diode bridge is calculated based on the ratio of fundamental rms voltage to the fundamental rms current [52]. In LCL-based IPT systems, the equivalent resistance is written as:

$$R_{eq} = \frac{\pi^2 R_L}{8} \quad 3.19)$$

The tuning of the primary compensations capacitances allows the LCL-based IPT system to operate over a wide load range. The reflected capacitance is a function of misalignment. The changes in equivalent inductance due to the significant changes in misalignment are limited. This eventually reduces the change needed in the frequency of the operation to maintain the condition of resonance under misalignment[52].

As the LCL topology remains high transmission efficiency at low-quality factor Q, it is more preferred in high-power applications. In order to achieve operation closer to the UPF, normally, an additional series compensation capacitor can be added in series with L_R as shown in Figure 3.6 to compose the LCCL topology, which help the circuit block DC current from flowing in the inductor [54]. However, the inductor saturation is easy to occur in high power applications due to heavy and high frequency current [58].

3.1.3 Influence Of The Quality Factor On The Power Transferred

With the inductive and capacitive requirements of the system cleared, the maximum current in the circuit is dictated by its quality factor. The quality factor is the ratio of the power stored in a circuit to the power lost from it. Figure 3.7 shows the effect of the quality factor on the maximum current in a circuit.

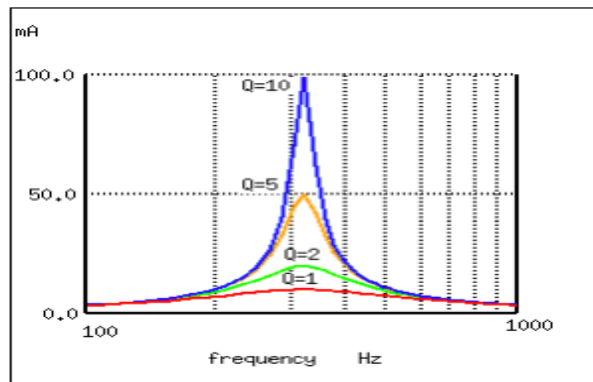


Figure 3.7 Effect Of The Dimensionless Quality Factor, Q, On The Maximum Current In A Circuit [59]

When proposing a deviation from the resonance peak, this dependence of the shape of the power curve on the quality factor makes it difficult to state a general recommendation for the allowable deviation, as it differs from one operational quality factor to the other. For high quality factors, the tolerance is smaller, as the curve is steeper. Consider an example of a secondary with a quality factor allowing a 2% deviation. [58]

3.1.4 Effect Of Misalignment On RIPT

In [60], using LCL based system shown in Figure 3.8; the effect of misalignment on RIPT parameters; including: Mutual Inductance, Operating (Resonance) Frequency, Power Transfer and Efficiency.

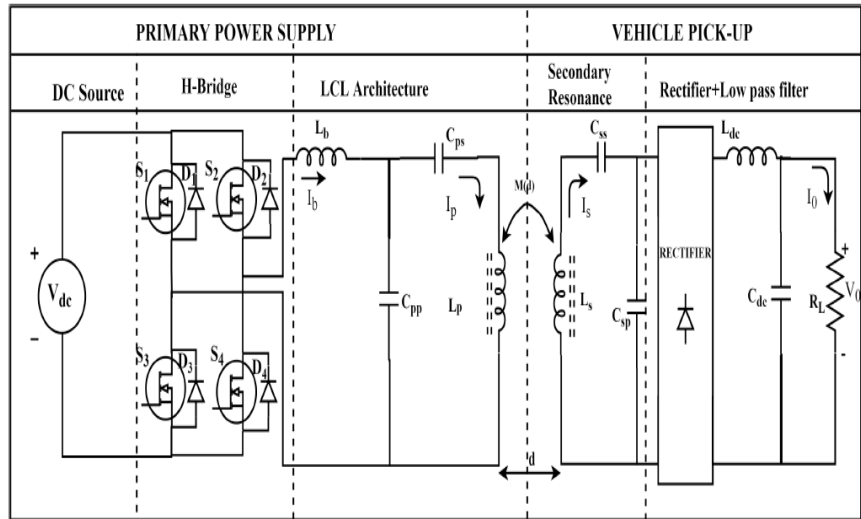


Figure 3.8 LCL Based RIPT System [60]

Circuit Parameter of the circuit was set as follows:

| Parameter | Value |
|---|-------------------------------|
| Power, P | 1 kW |
| Operating frequency, f | 85 kHz |
| Primary Inductance, L_p | 110 μH |
| Secondary Inductance, L_s | 110 μH |
| Minimum coupling coefficient, k_{min} | 0.08 |
| Controller | Texas Delfino (TMS320F28377S) |
| MOSFET | SPW47N60C3 |
| Diode | MUR1560G |
| Capacitor, C_{sp} | 50 nF |
| Capacitor, C_{ss} | 85 nF |
| Capacitor, C_{ps} | 53.2 nF |

| Parameter | Value |
|---------------------|--------------|
| Capacitor, C_{ss} | 85 nF |
| Capacitor, C_{dc} | 2200 μF |
| Inductor, L_{dc} | 135 μH |

Table 3.2 Circuit Parameter and values as set in [60]

3.1.4.1 Variation In Mutual Inductance

Contingent movement in the pickup coil with respect to the primary coil leads to the variation in mutual inductance [61]. The coil is physically displaced vertically, as well as horizontally, from the centre axis [52].

The coil is physically displaced vertically, as well as horizontally, from the center axis. The vertical misalignment is shown in Figure 3.9 (a); the horizontal misalignment is shown in Figure 3.9 (b). The mutual inductance variation leads to a variation in reflected capacitor value, which, in turn, changes the region of resonance. As a result, the current drawn by the inductive coil varies. The prevailing circumstances are quite often addressed in the literature. The resonance frequency is affected by the variation in mutual inductance [52]. Similarly:

$$M_{ij} = \frac{\mu_0}{\pi} \sqrt{R_p R_s} \int_0^\pi \frac{(1 - \frac{d}{R_s} \cos\varphi) \psi(k)}{\sqrt{V^3}} d\varphi \quad 3.20)$$

Where i and j are the primary and secondary turns in the corresponding coils. d is the distance between the center axis of the primary and secondary coil. R_s and R_p is the radius to the center of primary and secondary coil, $\Psi(k)$ is the function of elliptical integral of first and second kind.

The variation in mutual inductance is expressed as

$$\psi(k) = (1 - \frac{k^2}{2}) K(m) - E(m) \quad 3.21)$$

Similarly,

$$V = \sqrt{1 - \frac{2d}{R_s} \cos\varphi + \frac{d^2}{R_s^2}} \quad 3.22)$$

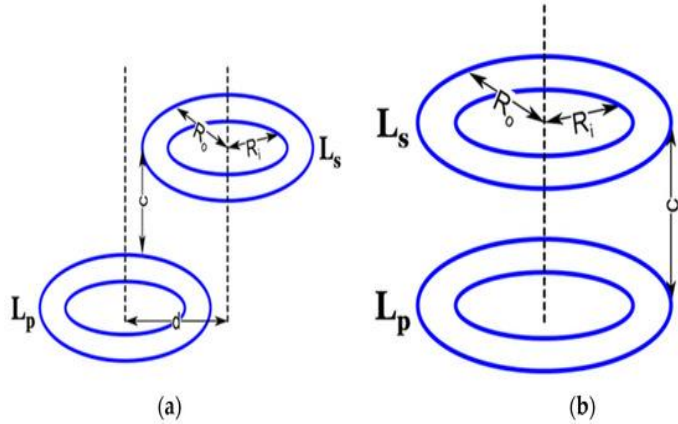


Figure 3.9 Size, Shape And Position Of Pickup Coil. (a) Horizontal Misalignment. (b) Vertical Misalignment [52]

The elliptical integral of first kind is written as:

$$K(m) = \int_0^{\pi} \frac{1}{\sqrt{1 - msin^2\theta}} d\theta \quad 3.23)$$

Similarly, the elliptical integral of the second kind is written as:

$$E(m) = \int_0^{\pi} \sqrt{1 - msin^2\theta} d\theta \quad 3.24)$$

Finally, the mutual inductance is written as:

$$M = \sum_{i=1}^{N1} \sum_{j=1}^{N2} M_{ij} \quad 3.25)$$

In [60], using the circular pancake inductive coils, used for the IPT system, a numerical simulation is performed aiming to examine the effect of misalignment on mutual inductance; The coil was typically displaced vertically by 20 cm. Similarly, the pickup coil was horizontally displaced by 16 cm. The range was chosen according to the average clearance of the conventional vehicles in the market. The elliptical integrals in the analytical expressions can be expanded in Taylor series expansions; the higher-order differential terms were omitted for fast convergence, and the effect was neglected in the expression. In general, the mutual inductance increased while the pickup coil approached the primary coil. Similarly, mutual inductance falls rapidly when the horizontal misalignment increases [60].

The coupling coefficient corresponding to the misalignment is noted in Figure 3.10. The coupling coefficient vs. the horizontal misalignment is shown in Figure 3.10 (a); vertical misalignment is shown in Figure 3.10 (b). The information is further used for the analysis when the coil is subjected to the coupling coefficient variations. In the case of dynamic IPT systems, the misalignment is an expected course of action. However, the variation in the primary current due to the variation in mutual inductance is always expected. Further, a proper compensation, as well as a proper selection operating frequency, stabilizes the entire IPT system under the contingency in misalignment [52].

Moreover, due to the symmetric nature of the coils, due to misalignment, the flux linkage in the parallel fields is also degraded significantly [62]. The change in mutual inductance changes the frequency of resonance, unlike the conventional resonance circuit. Which will be discussed in 3.1.4.2 below.

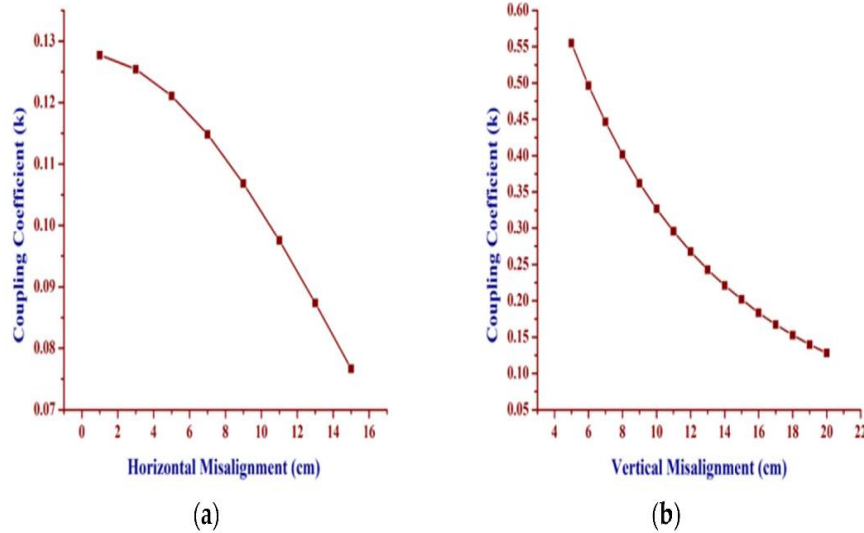


Figure 3.10 Coupling Coefficient Against Misalignment (a) Horizontal Misalignment. (b) Vertical Misalignment.[60]

3.1.4.2 Variation In Resonance Frequency

Operating frequency and resonance frequency is determined to comprehend the efficient operating region [61]–[63]

Resonance Frequency can be written as:

$$\omega_r = \frac{1}{\sqrt{L_{eq}C_{eq}}} \quad 3.26)$$

Where L_{eq} is the effective equivalent inductance. Similarly, C_{eq} is the equivalent capacitance. The values of $L_{p,eq}$ and C_{eq} are determined based on the circuit topology.

The operating frequency corresponding to maximum power transfer is identified based on the conditions of resonance, as per the design equation of an LCL based IPT system shown in Figure 3.8 is:

$$\omega L_b = \frac{1}{\omega C_{pp}} = \omega L_{p,eq} \quad 3.27)$$

An IPT system with $14 \mu H$ mutual inductance is excited with an 85 kHz operating frequency and $25 \mu H$ mutual inductance with an 87.7 kHz operating frequency. The corresponding voltage and current through the primary and secondary inductive tracks was observed in the simulation and shown in Figure 3.11 and Figure 3.12 [60].

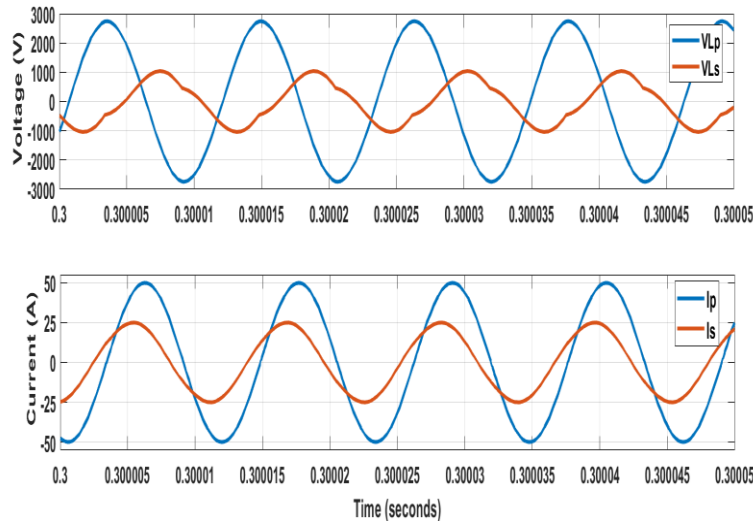


Figure 3.11 Voltage And Current Waveform Of The Inductive Track At $M = 14 \mu\text{H}$ And $f = 85 \text{ kHz}$ [60].

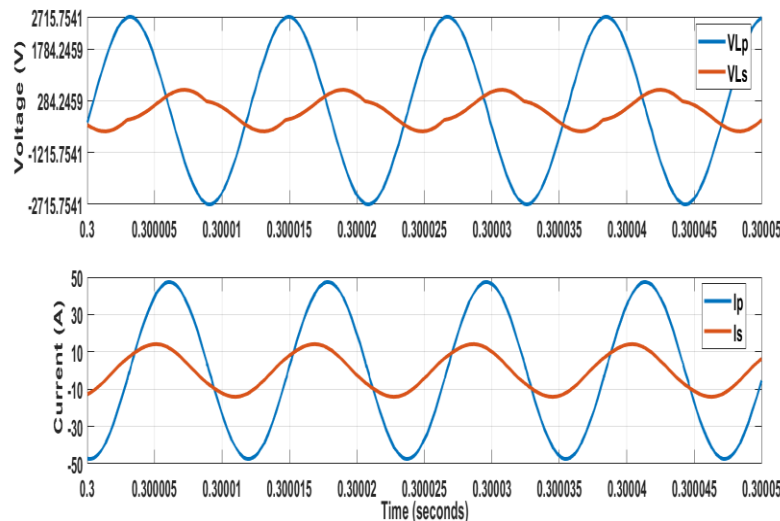


Figure 3.12 Voltage And Current Waveform Of The Inductive Track At $M = 25 \mu\text{H}$ And $f = 87.7 \text{ KHz}$ [60]

Then An IPT system with $25 \mu\text{H}$ mutual inductance is tuned from 85 kHz to 87.7 kHz , based on the obtained frequency plot and shown in Figure 3.13. An increase in the magnitude of current and voltage at 87.7 kHz , on the receiver side, was observed. Hence, the tuning had done its purpose completely. The operating frequency corresponding to the coupling coefficient is shown in Figure 3.14 [60].

The variation of frequency corresponding to the variation in misalignment is noted for Circuit shown in Figure 3.8. The obtained data is plotted in Figure 3.15 (a),(b). The circuit will sustain its condition for resonance under respective frequencies corresponding to the respective misalignment [60]. Increase in operating frequency increases the amount of power transfer capability to larger distances. Selection of switches according to the frequency of operation is quite essential in order to make sure that the circuit meets the needs [52].

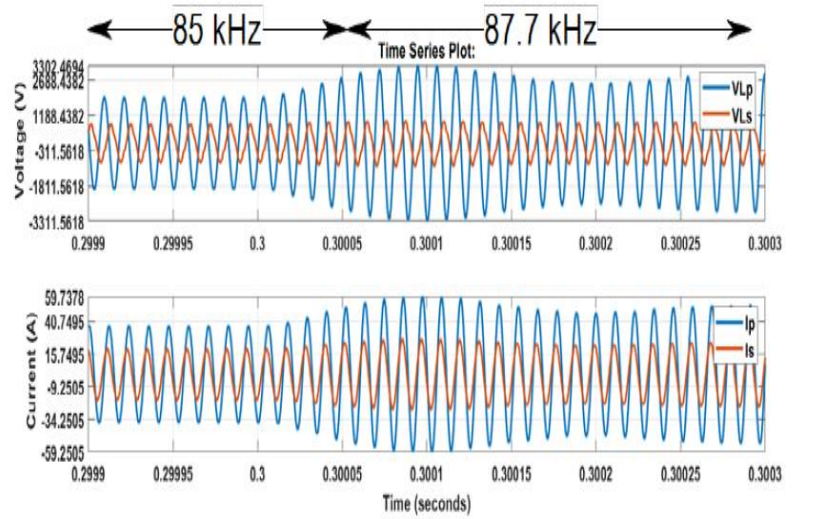


Figure 3.13 Voltage And Current Waveform Of Inductive Track At $M = 25\mu H$ While Tuning [60]

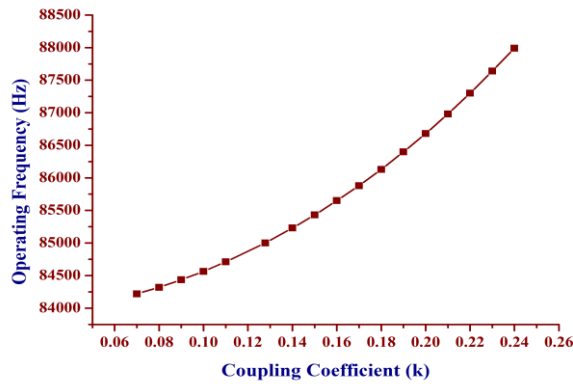


Figure 3.14 Operating Frequency Corresponding To Coupling Coefficient [60].

Normally, power IGBT cannot be used to attain this because of higher frequency. However, power MOSFET with less turn-on time is highly preferred. Additionally, the material used for power MOSFET also plays a vital role in the efficiency of the overall system. This further reduces the occurrence of switching losses in the system. For higher voltage stress, and with high operating frequency, SiC-based MOSFET would be preferred. If the speed of switching is a major concern, GaN-based MOSFETs are preferred. This, in turn, increases the power transfer level from one circuit to another [52].

3.1.4.3 Power Transfer Capability

For the same setting as 3.1.4.1 above the effect of misalignment on transferred power can be deducted, The power transferred to the reflected load will be:

$$P = \text{Re}\{I_p^2 Z_r\}$$

3.28)

Where Z_r is the reflected impedance from the secondary side. Further:

$$P = \frac{R_{eq}(\omega M I_p)^2 [\omega^2 C_{sp} L_{s,eq} - (\omega^2 C_{sp} L_{s,eq} - 1)]}{R_{eq}^2 (\omega^2 C_{sp} L_{s,eq} - 1)^2 + (\omega L_{s,eq})^2}$$

3.29)

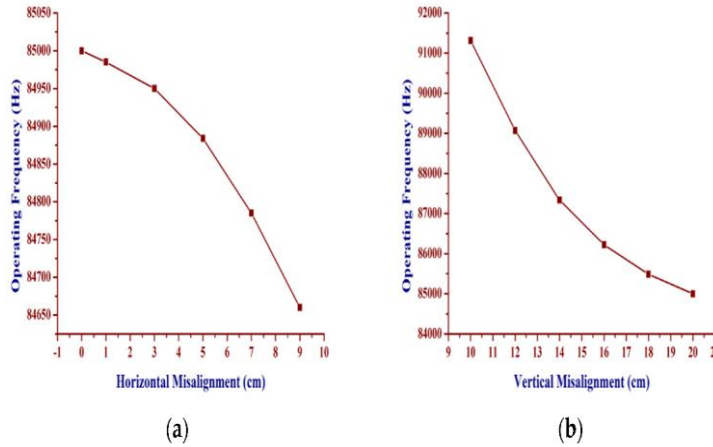


Figure 3.15 Operating Frequency Against Misalignment (a) Horizontal Misalignment. (b) Vertical Misalignment [60]

Now, the mutual inductance is the function of vertical and horizontal misalignment by Neumann's formula, and the power transferred to the reflected load is the function of mutual inductance. Hence, the power transferred from primary to the secondary, according to the misalignment, was plotted and the improvement in power transfer level is observed in Figure 3.16 (a),(b).

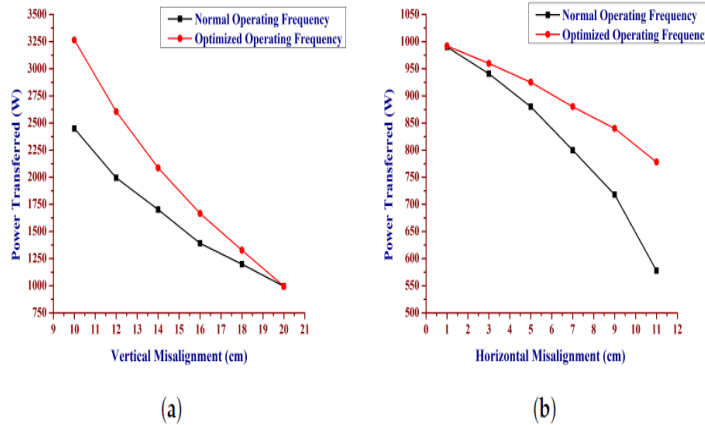


Figure 3.16 Power Transfer Level Corresponding To The Misalignment. (a) Vertical(b)Horizontal [60]

3.1.4.4 Efficiency

In [60], An experimental prototype was built to evaluate the real-time performance of the system. High frequency switching MOSFETs (SPW47N60C3) were used for inverting purposes, whereas high frequency diodes (MUR1560G) were used as un-controlled rectifier switches. A co-axial pancake circular coil, made of copper, was mounted on a ferrite spoke, in order to enhance the flux linkage on the pickup coil. High-frequency poly-polypropylene power film capacitors were used as resonance capacitors for the system. The dynamic structure of the coils made a wide range of misalignment possible in the vertical and horizontal directions. The resistive bank, equivalent to the steady state equivalent resistance of the battery, was considered as load.

The experiments were conducted for static, as well as dynamic, movements of the pickup coil. The primary and secondary currents were distorted, due to the perturbations in the position of the pickup coil. Power transfer efficiency of the IPT system was recorded from the experimental prototype under various misalignments [60].

| Vertical Misalignment (cm) | Efficiency % | | | | | |
|----------------------------|-----------------|-----------------|-----------------|-----------------|-----------------|-----------------|
| | $f = 91,315$ Hz | $f = 89,070$ Hz | $f = 87,337$ Hz | $f = 86,223$ Hz | $f = 85,990$ Hz | $f = 85,000$ Hz |
| 20 | 73.5 | 75.01 | 76.4 | 78.1 | 79.5 | 80.36 |
| 18 | 79.2 | 80.8 | 82.17 | 84.47 | 85.75 | 81.05 |
| 16 | 83.05 | 85.14 | 87.12 | 88.4 | 87.3 | 82.18 |
| 14 | 87.67 | 89.48 | 90.5 | 89.13 | 88.1 | 83.57 |
| 12 | 91.68 | 92.33 | 91.32 | 89.32 | 88.40 | 85.76 |
| 10 | 93.5 | 93.1 | 91.9 | 89.88 | 88.11 | 86.85 |

Table 3.3 Efficiency Corresponding To The Vertical Misalignment Under Various Operating Frequencies [60].

| Horizontal Misalignment (cm) | Efficiency % | | | | | |
|------------------------------|-----------------|-----------------|-----------------|-----------------|-----------------|-----------------|
| | $f = 84,985$ Hz | $f = 84,950$ Hz | $f = 84,884$ Hz | $f = 84,785$ Hz | $f = 84,660$ Hz | $f = 84,440$ Hz |
| 1 | 79.5 | 79.1 | 78.5 | 78.2 | 77.6 | 77.1 |
| 3 | 77.3 | 78.23 | 77.98 | 76.8 | 76.1 | 75.5 |
| 5 | 75.93 | 76.91 | 77.41 | 76.5 | 75.6 | 74.8 |
| 7 | 74.75 | 75.1 | 75.58 | 76.31 | 75.2 | 74.3 |
| 9 | 73.5 | 73.8 | 74.35 | 74.8 | 75 | 74.1 |
| 11 | 71.15 | 71.6 | 72.3 | 72.7 | 73.05 | 73.36 |

Table 3.4 Efficiency Corresponding To The Horizontal Misalignment Under Various Operating Frequencies [60].

3.2 THE NEED OF POWER CONVERTERS

The magnitude, phase and frequency of the current waveform in IPT system is decided by the load, as well as the converter topology connected to it. The need for the high-frequency alternating current to produce a high-frequency electromagnetic field in the transmitting coil is engendered by the high-frequency inverter[64], [65]. Similarly, the generated high-frequency-induced voltage in the secondary coil is rectified before being connected to the battery. The aforementioned conversion process is to be attained with minimum losses. This eventually ends with the utilization of power in semiconductor devices. Furthermore, the DC input for the high-frequency inverter is fed from the rectified AC power supply connected to the grid or standalone sources. In order to achieve a high-power factor, an uncontrolled rectifier followed by a DC–DC boost converter is typically used in converter topologies [52].

The state-of-the-art technology of the resonant circuits, including the non-resonant converters with a resonant tank and resonant inverters, will be reviewed and discussed in 4 below.

4 CHAPTER 4: POWER CONVERTER MODELLING

The AC-DC-AC power conversion is widely used in the primary side which involves an AC-DC converter in series with a DC-AC converter (commonly called an inverter). The AC-DC converter serves to convert the AC power from the grid to stable DC power. Then, the inverter produces high-frequency AC power to feed the resonant circuit where it is classified as the resonant inverter[54] as shown in Figure 4.1.

Obviously, this two-stage topology shows some drawbacks such as the costly and bulky DC-link, and higher switching losses. In order to eliminate the DC-link, the direct one-stage AC-AC converter is a good option for providing the desired high-frequency AC power[54].

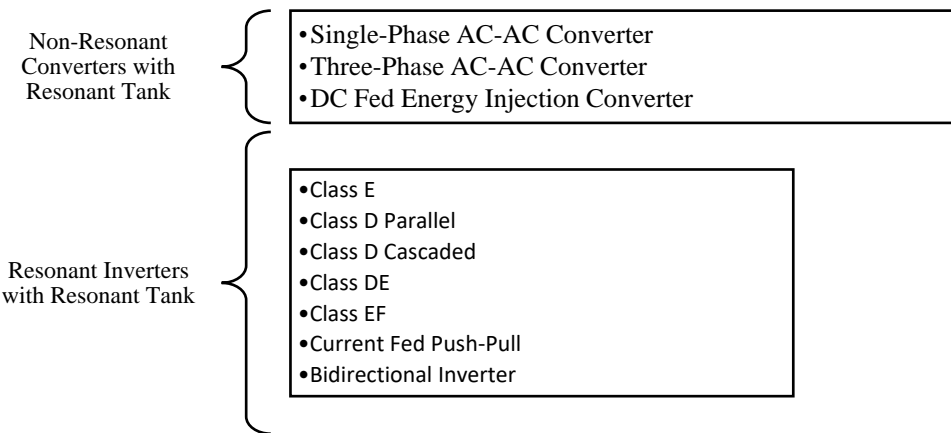


Figure 4.1 Classification Of Resonance Circuit

4.1 NON-RESONANT CONVERTERS WITH RESONANT TANK

4.1.1 Single-Phase AC-AC Converter

The single-phase AC-AC converter is shown in Figure 4.2, which is based on free oscillation and energy-injection control. This one-stage converter can simplify the controller design with a low switching frequency without reverse power flow [66]. The switches S_1 and S_2 are mainly used to control the power flow, and the S_3 and S_4 operate to constitute the resonant loop during the S_1 and S_2 Off.

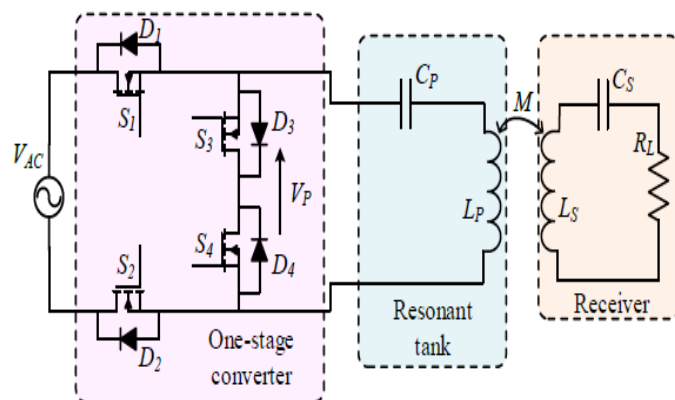


Figure 4.2 Single-Phase AC-AC Converter [54]

The number of oscillations can be controlled by the switching frequency of S_1 and S_2 . In the meantime, the ratio of the nominal resonant frequency to the switching frequency can be used to control the power flowing into the resonant circuit. A variable-frequency method can be applied to follow the circuit resonance, which makes the switching operation achieve zero-current switching (ZCS) easily [67]. This topology takes the definite advantage that the DC link and its bulky energy-storage element can be eliminated [68]. However, current sags around the zero-crossing points of the AC source are inevitable.

4.1.2 Three-Phase AC-AC Converter

Normally, the single-phase AC-AC converter suffers from great current sags around the AC source zero-crossings, especially under a high ratio of the nominal resonant frequency to the switching frequency. For some three-phase AC source applications, a similar one-stage AC-AC converter can be structured based on the same principle of free oscillation and energy injection control [54].

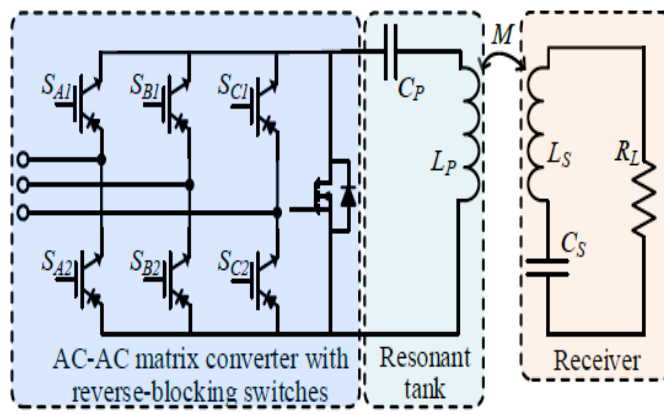


Figure 4.3 Three-Phase AC-AC Converter [54]

The three-phase AC-AC converter as shown in Figure 4.3 incorporates a matrix converter with six reverse-blocking switches and one regular MOSFET or IGBT. The operation includes eight modes with six energy-injection modes and two free oscillation modes [69], [70]. Basically, the energy injection control is the same as that of the single-phase AC-AC converter. Aiming to avoid the voltage zero-crossing, the LC tank terminals are altered between the most positive and the most negative input phases[54].

Significantly, by controlling the energy injected into the LC tank accumulated in each half-cycle of the resonant current until reaching the reference value, the output current, voltage and power regulation control can be realized [71]. Naturally, this converter inherits the advantages of the single-phase AC-AC converter, but with better current sags and higher power capability. Since the number of power switches increases, the control difficulty rises inevitably[54].

4.1.3 DC Fed Energy Injection Converter

Another non-resonant converter, the DC fed energy injection converter, is depicted in Figure 4.4 where the resonant circuit is used as an intermediate energy storage element [72]. The energy is injected into the LC tank when the switch S_1 is turned off. At the beginning, the switch S_1 is turned on to charge the inductor L_D with the current increasing at the rate of V_{DC}/L_D for several cycles of the LC resonance [73]. After the S_1 is turned off, the energy is injected into the C_D so that the LC tank performs oscillations via the C_P , L_P and D_1

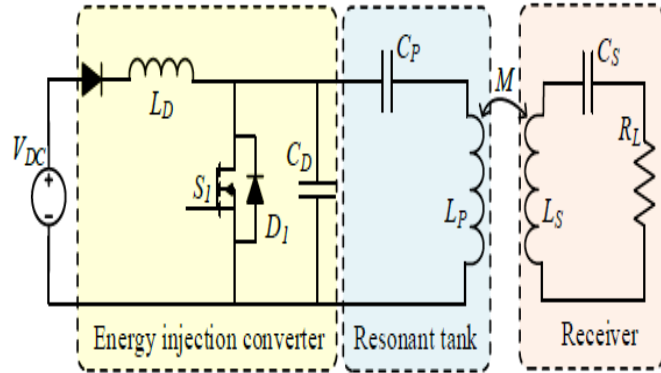


Figure 4.4 Dc Fed Energy Injection Converter[54]

Unlike the conventional inverter, the operating frequency of the LC tank is no longer determined by the switching frequency. This topology takes the advantage that the switching frequency can be lower than the nominal resonant frequency of the LC tank, which helps reduce the switching losses. However, the overall transmission efficiency and power level are limited by the energy reflow during the damping oscillation; consequently, the output voltage is unstable [54].

4.1.4 Comparison Between Non-Resonant Converters

The three mentioned non-resonant converters boost the resonant frequency equivalently with a lower switching frequency for some switches. A comparison of these three non-resonant inverters is shown in Table 4.1. However, they suffer from a common drawback that high current ripples in the resonant tank are inevitable during the energy oscillation.

Non-Resonant Converter

| | Single-Phase AC-AC Converter | Three-Phase AC-AC Converter | DC Fed Energy Injection Converter |
|---------|---|--|---|
| Factors | <ul style="list-style-type: none"> • Structure of matrix converter • Switching synchronization • Energy injection control • Zero current switching operation • Free oscillation time <ul style="list-style-type: none"> • Current sags • Input voltage variation • Switching frequency • Output voltage ripple (around input AC voltage zero crossings) | <ul style="list-style-type: none"> • Reverse blocking switches • Switching synchronization • Zero current switching operation • Free oscillation time <ul style="list-style-type: none"> • Current sags • Input voltage variation • Switching frequency • Output voltage ripple (around input AC voltage zero crossings) • Current, voltage and power regulation control | <ul style="list-style-type: none"> • Energy injection • Energy oscillation • Switching technique at high-Q regimes • Energy reflow problems • Zero voltage switching turn-off control • Output voltage ripple (determined by switching time) • Transient response analysis |

Non-Resonant Converter

| | Single-Phase AC-AC Converter | Three-Phase AC-AC Converter | DC Fed Energy Injection Converter |
|-----------------|---|--|---|
| Features | <ul style="list-style-type: none"> • Single-phase AC supply <ul style="list-style-type: none"> • No DC link • Less bulky energy storage <ul style="list-style-type: none"> • 4 modes of operation • Low power level • Medium control difficulty | <ul style="list-style-type: none"> • Three-phase AC supply <ul style="list-style-type: none"> • No DC link • Medium power level • Less bulky energy storage <ul style="list-style-type: none"> • More switches • 8 modes of operation • Lower electromagnetic interference • High control difficulty | <ul style="list-style-type: none"> • DC power supply • Only one switch • Low power level • 1 switching mode • Low control difficulty • Eliminating the impact of loading in the transmitter circuit |

Table 4.1 Comparison Of Non-Resonant Converters With Resonant Tank For WPT System As Discussed In [54].

4.2 RESONANT INVERTERS WITH RESONANT TANK

For most WPT applications, the one-stage AC-AC converter with resonant tank is not suitable mainly due to its high control difficulty and unstable output. Thus, the DC-link buffer is necessary to improve the system's power level, stable output, and flexibility. With the help of DC-link, the resonant circuit can be driven at the resonant frequency by using resonant inverters

4.2.1 Class E Resonant Inverter

The Class E resonant inverter topology is the same as the DC fed energy injection converter but employing a special switching technique as shown in Figure 4.4. Normally, the Class E resonant inverter is driven at the nominal resonant frequency of LC tank without DC energy injection. The simplified single switch structure is famous for the high efficiency at high operating frequency and high power level to several kilowatts [74]. By optimizing the circuit parameters properly, it is guaranteed that the transistor S_1 is switched ON with zero-voltage switching (ZVS) and zero-voltage derivative switching (ZVDS), and therefore the switching losses and stresses are reduced significantly [75], [76].

For high power level WPT applications, this topology can control the output power via manipulating the duty cycle control or varying the switching frequency with an efficiency sacrifice [77]. However, the main disadvantage of the Class E resonant inverter is its high peak voltage across the switch, reaching up to 3.5 times DC voltage at a duty cycle of 0.5. Consequently, less power will be produced by the Class E inverter than other resonant inverters with the same voltage and current stresses. For some high DC power supply occasions, the high peak voltage may result in efficiency drop or permanent damage to the inverter

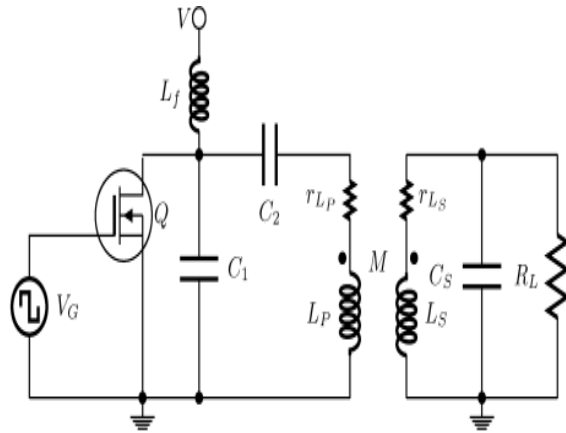


Figure 4.5 Class E Inverter With An Inductive Link [77]

4.2.2 Class D Resonant Inverter

The Class D inverter employs two switches and a series-resonant LC tank, which results in lower switching frequency than the Class E inverter. It should be noted that the peak voltage across the switch in the full-bridge Class D is as twice higher as the DC supply voltage. Thus, this topology can output twice the voltage to feed the LC resonant circuit, especially suitable for low DC supply WPT applications. Obviously, the Class D resonant inverter with two switches has lower voltage stress across the switch since the peak voltage is as high as the DC supply [54].

4.2.2.1 Parallel

In order to provide higher and more flexible output levels for WPT, the parallel inverter with two full-bridge Class D inverters was proposed as shown in Figure 4.6. Each full-bridge Class D inverter is controlled by the clamped-mode switching technique, which results in controllable output voltage, rather than by the duty cycle control [78]. By taking the advantage that power is distributed evenly by the parallel inverters, the heat dissipation becomes easier than the single inverter topology.

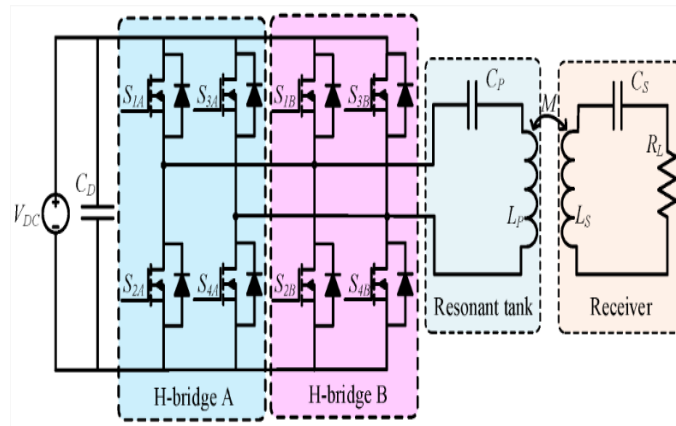


Figure 4.6 Parallel Full-Bridge Class D Resonant Inverter [54]

Furthermore, this topology has high fault-tolerant ability. When one of the parallel bridge is in the open circuit fault, another bridge can still make the system work properly [79]. However, if the fault type is short circuit, there is no option for the LC resonant operating properly except shutting down the whole system.

4.2.2.2 Cascaded

By the same token, the output power can be enhanced under the same switching capacity by the cascaded inverter [80] as shown in Figure 4.7. The cascaded structure has saliency preponderance in terms of reducing the voltage stress and alleviating the harmonic contamination of the output voltage, namely, with a lower THD. Furthermore, more operating modes can be achieved with higher flexibility in the cascaded structure; therefore the switching losses can be reduced effectively [81].

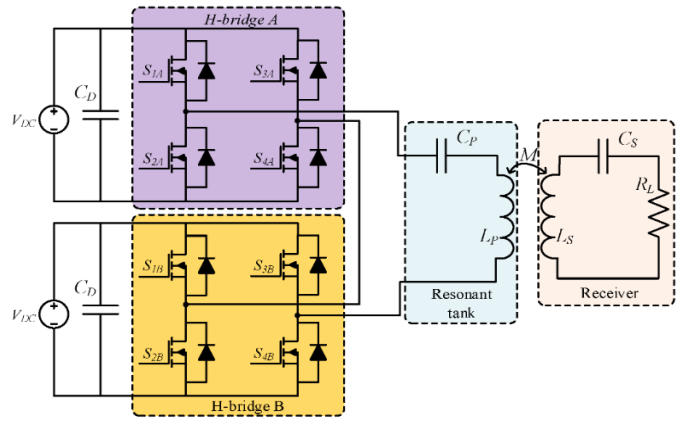


Figure 4.7 Cascaded Full-Bridge Class D Resonant Inverter [54].

4.2.3 Class DE Resonant Inverter

By combining the lower switching stress of Class D and high efficiency of Class E [82], the Class DE topology is created as shown in Figure 4.8. The Class DE inverter is quite similar to the Class D inverter, only with two additional parallel-connected capacitors [83]. Thus, the Class DE inverter realizes low switching voltage within the DC supply to reduce the switching losses. Furthermore, the shunt capacitors enable high-frequency operation with ZVS and ZVDS.

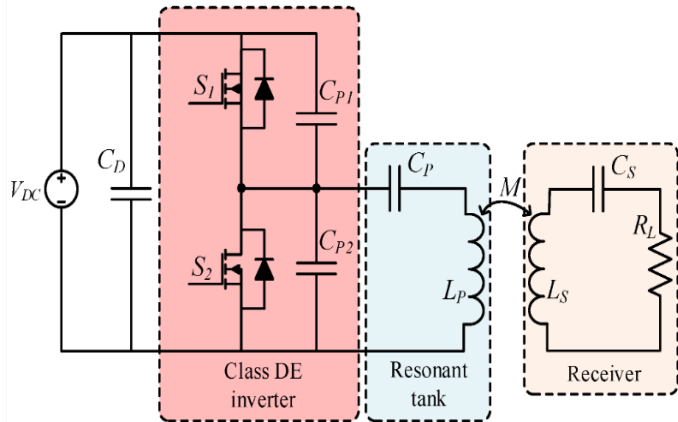


Figure 4.8 Class DE Resonant Inverter[54]

4.2.4 Class EF_n Resonant Inverter

In order to inherit the advantages of the Class E inverter and reduce the number of switches, an inverter topology called the Class EF_n was proposed as shown in Figure 4.9. It consists of a choke inductor L_D , shunt capacitor C_1 , and two parallel-connected LC resonant tanks, where the L_2C_2 resonant tank is tuned to n times the operating resonant frequency f_o of $L_P C_P$ [84]. Typically, the subscript n is set to two, namely the EF_2 resonant inverter. Hence, the peak voltage stress across the switch can be reduced to 2 times the input DC supply. Besides, the class EF_2 inverter has a higher

power output capability and efficiency than the Class E and other EF_n inverters with the same voltage stresses on their switches [54].

Comparing with the Class D inverter or full-bridge Class D inverter, the Class EF_2 inverter can be designed to achieve ZVS and ZVDS, which makes the single switch operate efficiently up to the megahertz range [85]. Other two benefits of this topology are that the switch's drain voltage and the output current do not contain a second harmonic component, and has an improved electromagnetic interference performance. However, the corresponding feasibility is limited by the requirement of additional resonant tank [54].

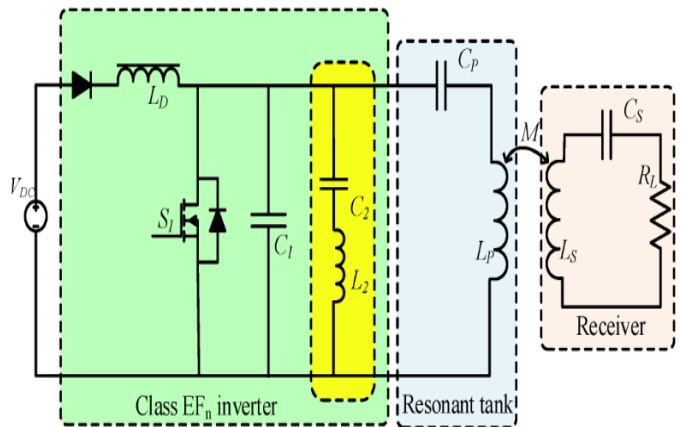


Figure 4.9 Class Efn Resonant Converter [54]

4.2.5 Other Resonant Converters

4.2.5.1 Current-fed push-pull resonant inverter

In general, the switches in the inverter should be driven by externally controlled signal for WPT applications. Recently, an autonomous current-fed push-pull resonant inverter with ZVS operation was proposed in which the driving signal was generated automatically without external gate control and kept running at the steady state [86] as shown in Figure 4.10. In this topology, the start-up should be analysed, since the two switches S_1 and S_2 tend to turn ON simultaneously once the DC power supply is turned ON. In a practical system, the two switches would not act at the identical speed due to some parameter differences, hence once a switch is ON first, the other one will be turned OFF. However, it is hard to control which switch should be ON first in the start-up process. Moreover, the RC circuit with C_{Si} and R_i should be calculated carefully to make sure that the requirements of switching frequency and circuit losses are fulfilled. By using two or more autonomous push-pull resonant inverters with various phase shifts, a rotating magnetic field can be generated for rotary WPT applications [87]. More details on this Converter is discussed in 4.4 below.

4.2.5.2 Bidirectional resonant inverter

With the EV wireless charging becoming more and more popular, combining the vehicle-to-grid (V2G) or vehicle-to-home (V2H) technology [88] and the WPT technique is a viable solution for shaving the peak demand in the power grid. In order to charge or discharge EVs in the V2G or V2H system, a current-source bidirectional resonant inverter was developed in [89]. A typical bidirectional resonant inverter for WPT is shown in Figure 4.11. In order to improve the power level and the fault tolerant ability, a bidirectional WPT system consisting of two resonant inverters was also proposed with optimized control method [90], [91]. Such structure makes it more effective and suitable to modify the power flow direction.

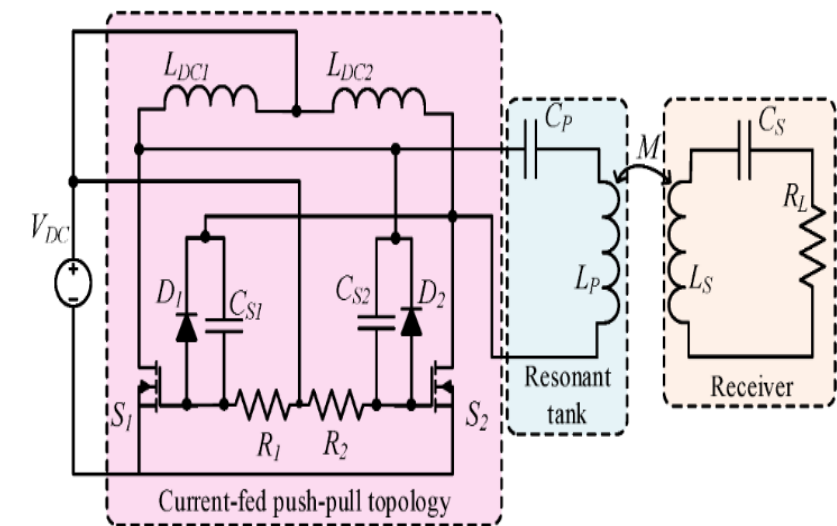


Figure 4.10 Current-Fed Push-Pull Resonant Inverter [54]

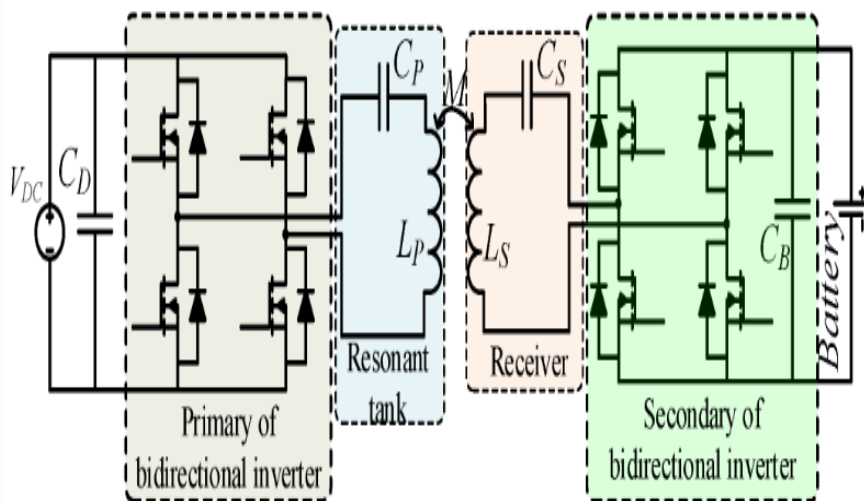


Figure 4.11 Bidirectional Resonant Inverter [54]

4.3 COMPARISON OF RESONANT CIRCUITS

The aforementioned resonant circuits are qualitatively compared as shown in Table 4.2 . This comparison focuses on assessing some key features for WPT, namely the voltage stress, power level, high frequency operation, control difficulty, switching loss, and effective cost.

| Type | Voltage Stress ¹ | Power Level ² | High Frequency Operation ³ | Control Difficulty | Switching Loss | Effective Cost |
|---|-----------------------------|--------------------------|---------------------------------------|--------------------|----------------|----------------|
| Single-phase AC-AC converter | Low | Low | Medium | Medium | Low | Medium |
| Three-phase AC-AC converter | Medium | Medium | Medium | High | Medium | Medium |
| DC fed energy injection converter | Low | Low | High | Medium | Low | Low |
| Class D Parallel resonant inverter | Medium | High | Medium | High | High | High |
| Class D Cascaded resonant inverter | Medium | High | Medium | High | High | High |
| Class E resonant inverter | High | High | High | Low | Low | Low |
| Class DE resonant inverter | Low | Medium | High | Medium | Low | Medium |
| Class EF ₂ resonant inverter | Low | Medium | High | Low | Low | Low |
| Current-fed push-pull resonant inverter | Medium | Medium | Medium | NA | Low | Low |

Table 4.2 Comparison Of Resonant Circuits For WPT As Shown In [54].

4.4 PUSH-PULL CURRENT-FED RESONANT INVERTER

Among various wireless link topologies proposed in 4.1 & 4.2 above , current source parallel-resonant inverter has short-circuit protection and better performance under no load condition due to its current limiting dc-link characteristic[92]. Another advantages include less components, ease of implementation at high switching frequency [93], and a simple gate driving circuit [94]. Moreover, the output voltage is not a square wave but a sinusoid, which minimizes EMI harmonics[95].

¹ Voltage stress can range from 1 to 3.5 times voltage supply.

² Power level can range from 50 W to 20 kW. Generally, medium power level represents power higher than 300 W but lower than several kilowatts, and high power level represents power higher than several kilowatts.

³ Generally, the switching frequency for wireless power transfer is above several dozen kHz, which is in the medium frequency range. In addition, the high frequency can reach several megahertz for some low power applications and far field transmission.

4.4.1 Basic Structure

The dc voltage source is in series with two large dc inductors as compared with the resonant inductor acting as a quasi-current source. The two input inductors divide the DC current in half under steady-state conditions, so that the current flowing into the resonant tank is approximately a square waveform with half the magnitude of the DC current. [86]

In total, the converter is configured as two main switches S_1 & S_2 , and it comprises of a parallel tuned resonant circuit that consists of a primary inductor L_p and a tuning capacitor C_p . Primary Coil is magnetically coupled to the secondary power pickup with inductance L_S . A secondary power converter is then used to realize circuit tuning, rectification, and power regulation according to the load requirements. At steady state, when the secondary pickup coil is fully tuned, the reactive impedance reflected back to the power supply would be very small and can be compensated when designing the primary inductor [86]. Therefore, for the steady-state conditions of the power supply, it is sufficient to simplify the reflected impedance of the secondary pickups as a pure resistive load R_{eq} , as shown in Figure 4.12.

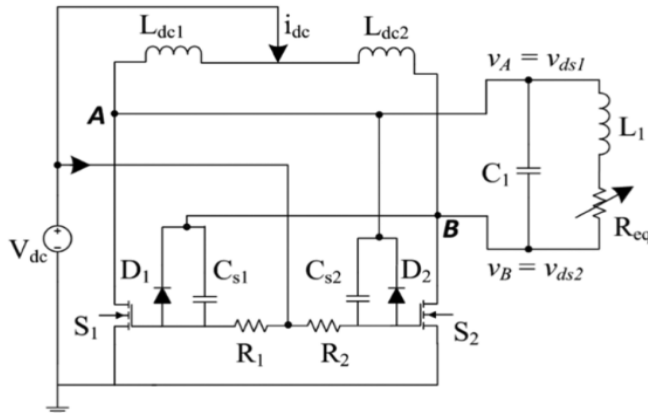


Figure 4.12 Equivalent Circuit for Push-Pull Current Fed Inverter [86].

4.4.2 Gate Signal Analysis

Referring to Figure 4.12, at steady state, when the voltage at one side of the tank, say v_B is high, the voltage at terminal-K of D_1 is higher than the voltage at its terminal-A, which is equal to the voltage at the gate. During this time, the diode is reverse biased and therefore, keeping the voltage at the gate of S_1 high (V_{G1}). For the second half-cycle, when $v_B = 0 V$, the voltage at terminal-K of D_1 also goes to zero and consequently the voltage at the gate of S_1 . Similar scenario occurs for the other side of the circuit with 180 phase shift.

It can be observed that depending on the voltage level on both sides of the resonant tank, the voltage at the gates goes high and low following the frequency of the resonant tank, as shown in Figure 4.13. The cross-coupled diodes D_1 and D_2 play an important role in achieving the ZVS operation, as summarized in Table 4.3.

For the converter in Figure 4.12, the current limiting resistors are needed to prevent the shorting of the dc source regardless of the operating frequency [86]. These resistors in combination with the input capacitances of the switches provide an RC circuit, which largely determines the turning ON speed. For a given switch with a certain input capacitance C_{iss} , a smaller resistance results in a smaller time constant and a faster charging speed of the input capacitor. However, smaller resistances increase the circuit losses, particularly at a high V_{dc} . This is mitigated by adding two speedup capacitors (C_{S1} and C_{S2}) in parallel with D_1 and D_2 , as shown in Figure 4.12.

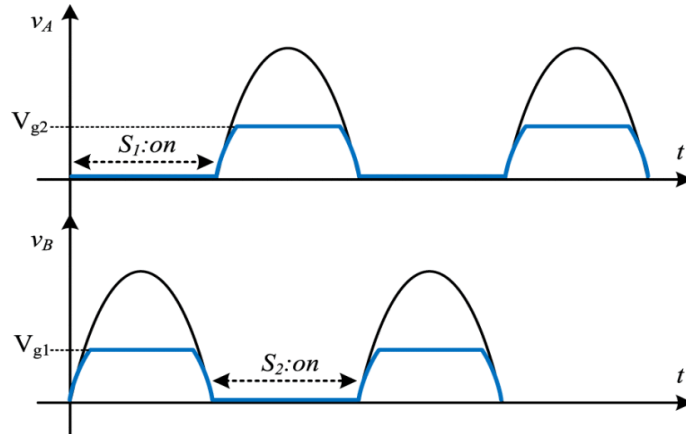


Figure 4.13 Conceptual Illustration Of Gate Signals Operation Following The Frequency Of The Resonant Tank [86].

| Parameter | First Half-Cycl | Second Half-Cycle |
|-----------|-----------------|-------------------|
| v_A | Low | High |
| v_B | High | Low |
| D_1 | OFF | ON |
| D_2 | ON | OFF |
| V_{g1} | High | Low |
| V_{g2} | Low | High |

Table 4.3 Logic Of The ZVS Circuit For Push-Pull Converter

The gate drive circuit dynamics during half a period to turn ON the switch can be modeled with two voltage sources, as shown in Figure 4.14. From this model, the voltage at the gate v_g is contributed by both the sources V_{dc} and $v_{ds} = \pi V_d \sin(\omega t)$ (for a push–pull topology), which can be found by applying the superposition theorem [96]

$$v_g(t) = V_{dc} \left(1 - e^{-\frac{t}{\tau}} \right) + \left(V_{dc} \frac{\pi C_s R_\omega}{1 + \tau^2 \omega^2} \right) (\cos \omega t + \tau \omega \sin \omega t) - \left(V_{dc} \frac{\pi C_s R_\omega}{1 + \tau^2 \omega^2} \right) e^{-\frac{t}{\tau}} \quad 4.1)$$

Where $\tau = R(C_{iss} + C_s)$ is the time constant of the gate driving circuit.

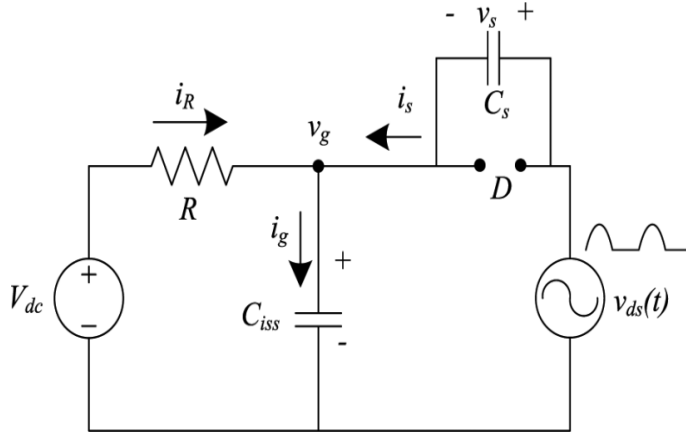


Figure 4.14 Basic Gate Driving Circuit With Speedup Capacitor [86].

4.4.3 Startup Analysis

The switching operation presented in the previous section is based on the steady-state conditions when the converter passed the transient stage of the startup time. At steady state, the zero crossing points exist and detected by the cross-connected diodes allowing the switching operation to be employed based on the frequency of the resonant tank [86]. At startup, however, this is not the case as initially there is no energy in the tank circuit and no zero point to be detected. Therefore, an initial energy is essential for starting up the circuit because without any initial energy in the circuit, the resonant voltage would have no zero crossings points, so automatic turning ON and OFF of the switches would not occur [97].

Initially, the two switches S_1 and S_2 are turned OFF. After the dc source is turned ON, both the switches tend to turn-ON by V_{dc} and the gate resistors R_1 and R_2 , so some initial current on the equivalent dc inductance from L_{dc1} and L_{dc2} would be established. However, S_1 and S_2 cannot stay ON all the time because the ON-state of one switch will short circuit the gate of the other one and try to turn the other side OFF. In a practical circuit, the two switches would not act at exactly the same speed due to parameter differences, noise, and disturbances; the side that turns ON faster will win the competition to short circuit the gate voltage of the other side, and further strengthen its ON-state [86].

For instance, a lower voltage, say V_A , due to faster turning ON of S_1 , will provide a lower voltage at the gate of S_2 , thus S_2 will turn-OFF resulting in a higher voltage drop V_B , which will further increase the voltage at terminal-K of D_1 assuring that S_1 remains ON until the resonant voltage changes the polarity. Consequently, this positive feedback (negative resistance) leads to the bistable circuit oscillation and full ZVS operation [86], as shown in Figure 4.15.

The cross-coupled differential MOSFET pair presents a negative resistance to the resonator due to positive feedback. This negative resistance compensates for the equivalent resistance of the resonator and enables sustained oscillation [98], [99],[100]. The mathematical model governing the initial dc current building up when both the switches are ON can be approximately expressed as:

$$\frac{L_{dc}(di_{dc}(t))}{dt} = V_{dc}$$

4.2)

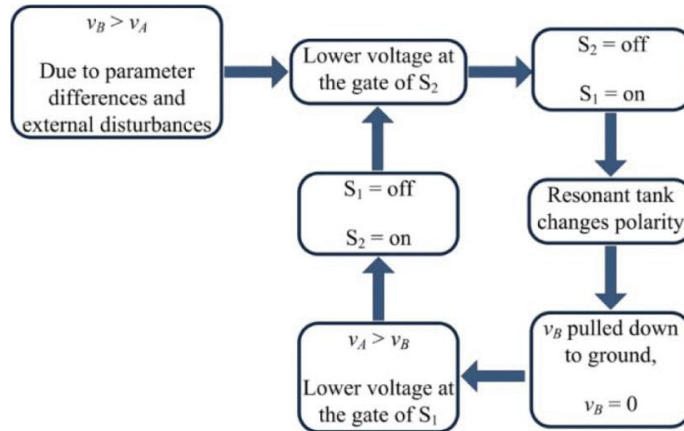


Figure 4.15 Flowchart Of The Autonomous Regenerative Process [86]

Where L_{dc} is the equivalent dc inductance from $L_{dc1} = L_{dc2}$ (for uncoupled inductors) given by:

$$L_{dc1} = (L_{dc1} \parallel L_{dc2}) = \frac{L_{dc1}}{2} = \frac{L_{dc2}}{2} \quad 4.3)$$

Therefore, for a short time (startup time t_o), i_{dc} increases linearly and it can be expressed by:

$$i_{dc} = \frac{V_{dc}}{L_{dc}} t_o \quad 4.4)$$

The accurate ZVS operating frequency at steady state can be determined by analysing a half cycle. In each half cycle, one of the two separate inductors (L_{dc1} or L_{dc2}) is in series with the resonant tank and on average it carries half of the DC current. The other inductor is parallel with the DC source, so in principle it does not affect the resonant tank. As the normally the inductances of DC inductors L_{dc1} and L_{dc2} are much larger than that of the resonant inductor L_1 , the switching network injects approximately constant DC current into the resonant tank in a half cycle. Which can be simplified in Figure 4.16

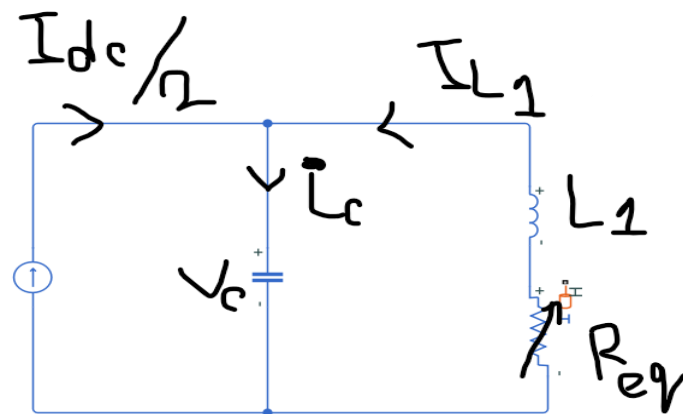


Figure 4.16 Simplified Circuit for Current-Fed Converter

By analyzing the circuit above, and starting from second order differential equation as:

$$L_1 C_1 \frac{d^2 v_c}{dt^2} + RC \frac{(dv_c)}{dt} + v_c = \frac{I_{dc}}{2} R$$

4.5)

By taking initial Conditions as in 4.6).

$$v_c(0) = 0, \frac{dv_c}{dt}(0) = \frac{I_{dc}/2 + IL(0)}{C_1}$$

4.6)

Solve for t and then find the time t_z which is the in which $v_c = 0$. Then Solution can be obtained as in [96] to be:

$$f_{ZVS} = \frac{2}{t_z}$$

4.7)

4.5 PROPOSED MODEL FOR PUSH-PULL CURRENT FED RESONANT INVERTER.

As have been presented in 4.4 above, the chosen resonant inverter has the drawback of the need to apply a gate driving circuit; in order to achieve ZVS. Yet a problem may happen because of the need of Initial Energy as mentioned above. Solution to this problem is to ensure that during starting up there's always some energy in the circuit. One way to achieve this is by using a polyphase approach to ensure the availability of energy during start-up phase which has been discussed in [86], [101]. In which the coupling between phases should be unified[86].

Another way is by combining the benefits of the Cascaded Class D inverter discussed in 4.2.2.2 above that decreases the voltage stress; which is one of the problems facing the Current-fed Converters- with the advantages of the mentioned resonant inverters mentioned in 4.4 above as shown in Figure 4.17.

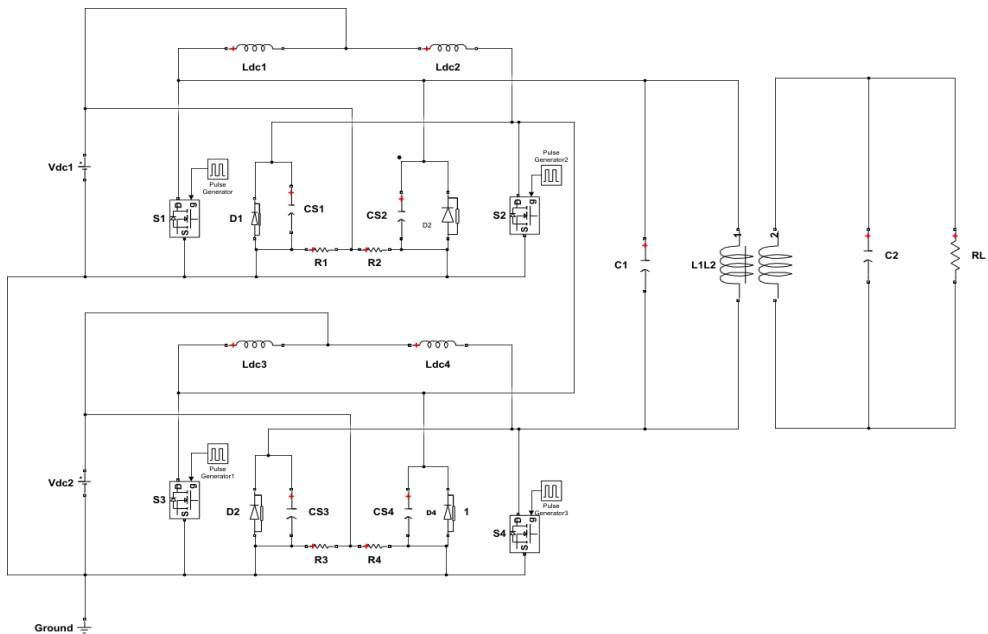


Figure 4.17 Proposed Inverter Topology

The main idea is to maintain the circuit energised with respect to the resonant topology and with this topology the resonance circuit is always connected to active elements; whether it's positive or negative.

4.6 RESONANCE TUNING FOR PUSH–PULL PARALLEL-RESONANT INVERTER

In practical applications, self-inductance of TX is deviated from its nominal value due to various reasons. One of the reasons could be the distance variation between TX and RX coils because the metallic and shielding structure in RX affects the TX inductance. These cause detuning of resonant frequency, power fluctuations, high-voltage stress on switch, and low efficiency [95].

Figure 4.18 shows conventional current-fed parallel-resonant inverter. Figure 4.19 shows the narrow pulselength and high peaking of V_{d1} due to smaller value of $C_{TX} \times L_{TX}$. This causes high-voltage stress on switches and degraded effective output voltage of inverter, all of which limits the output power of wireless link. On the other hand, if the L_{TX} is detuned to high value as in Figure 4.20 the ZVS fails for M_1 and M_2 , thus degrading efficiency [95].

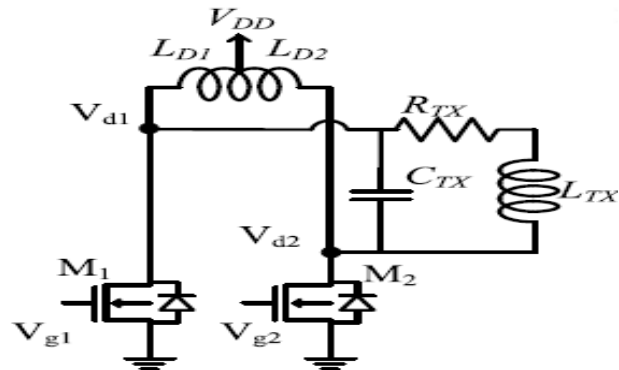


Figure 4.18 Schematic Of Conventional Push–Pull Parallel-Resonant inverter [95].

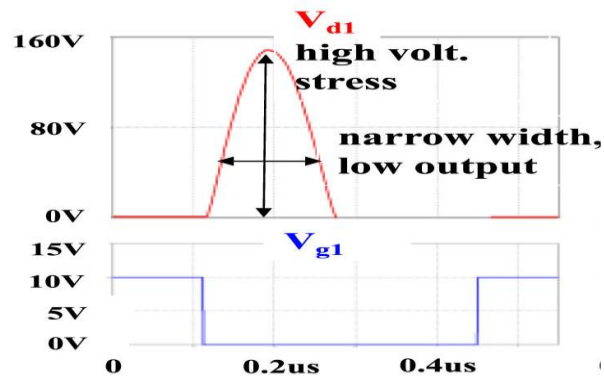


Figure 4.19 When L_{TX} Is Detuned To Low Value. The Effective Output Voltage Of Inverter Is Low, Voltage Stress On M_1 Is High [95].

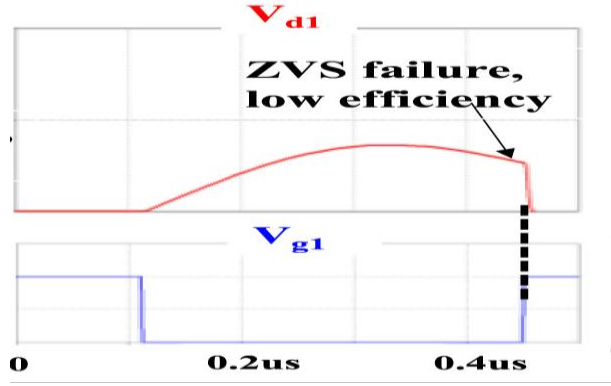


Figure 4.20 When LTX Is Detuned To High Value. The V_{d1} Does Not Drop To Zero Before Gate Turns On, Which Causes Zero-Voltage Switching Failure [95]

Reference [95] suggests a tunable resonant tank and its control method for push-pull parallel-resonant inverters shown in Figure 4.21. The parallel tuning capacitor is controlled using pulsedwidth modulation, and its duty cycle is determined by the sensing of drain voltage waveshape. Soft switching is ensured at both the turn-on and turn-off for every switches in the proposed inverter: zero voltage turn-on and low $\frac{dv}{dt}$ turn-off. The waveforms of autotuning inverter are presented in Figure 4.22.

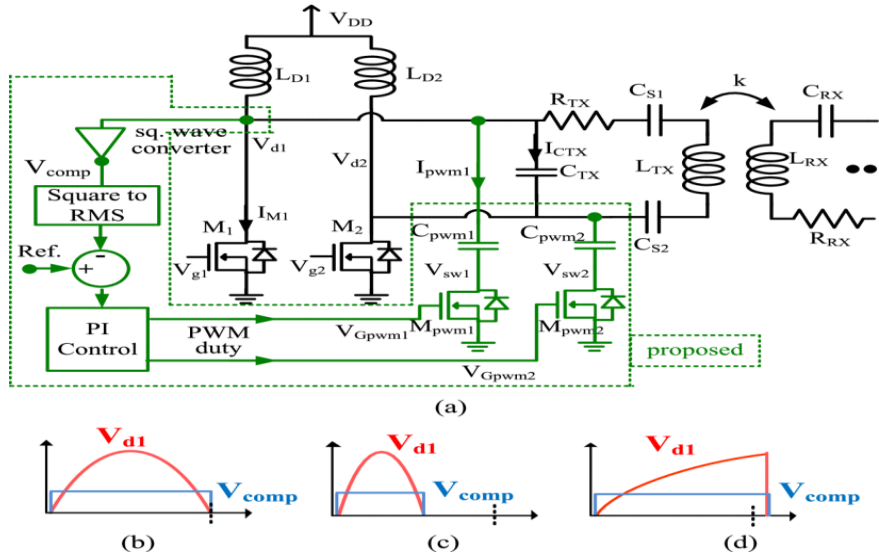


Figure 4.21 Proposed Tuning Control For Parallel-Resonant Inverter. (A) When M_{pwm1} Is On, L_{TX} Resonates Both With C_{TX} And C_{pwm1} . V_{d1} And Comparator's Output V_{comp} . (B) At Perfect Resonant Condition. (C) When L_{TX} Is Detuned To A Lower Value. (D) When L_{TX} Is Detuned To A Higher Value [95]

The real-time tuning minimizes the voltage stress on switches and maximizes the output power, and guarantees soft switching regardless of detuning of parallel-resonant inverter. The voltage stress on the tunable element is lower than the stress on the main inverter part [95].

Moreover, all the MOSFETs are connected to ground. Hence, the MOSFETs do not experience large resonant voltage swing across negative and positive levels. These also simplify the gate driving circuitry. The proposed tuning achieves higher efficiency than conventional switch-controlled capacitor due to the elimination of back-to-back two-series MOSFETS [95].

The experimental setup which is comprised of current-fed push-pull resonant inverter, TX and RX coils, RX rectifier, sensor board, and TMS320F28335 as MCU. The detuning of L_{TX} with respect to

TX-to-RX distance is presented in Figure 4.23. The coil diameter is 15 cm. The operating frequency is a fixed 85 kHz which is suitable for small-sized devices [95].

Figure 4.24 presents the improvement in RX received power at different RX distances. The voltage stress on switch is regulated to be identical between conventional and proposed for comparison purpose. At TX–RX distance of 8 cm, the received power is doubled at proposed inverter.

Figure 4.25 compares the TX-to-RX efficiency between the systems with and without the proposed tuning. For the conventional case of black square curve in Figure 4.25 , efficiency drops when TX–RX distance is short due to the failure of ZVS caused by detuning of L_{TX} , which is as illustrated in Figure 4.20.

Figure 4.26and Figure 4.27 shows the loss breakdown analysis of proposed and conventional. In conventional system, decreasing TX–RX distance causes ZVS failure, resulting in high switching losses of $M_1 + M_2$.

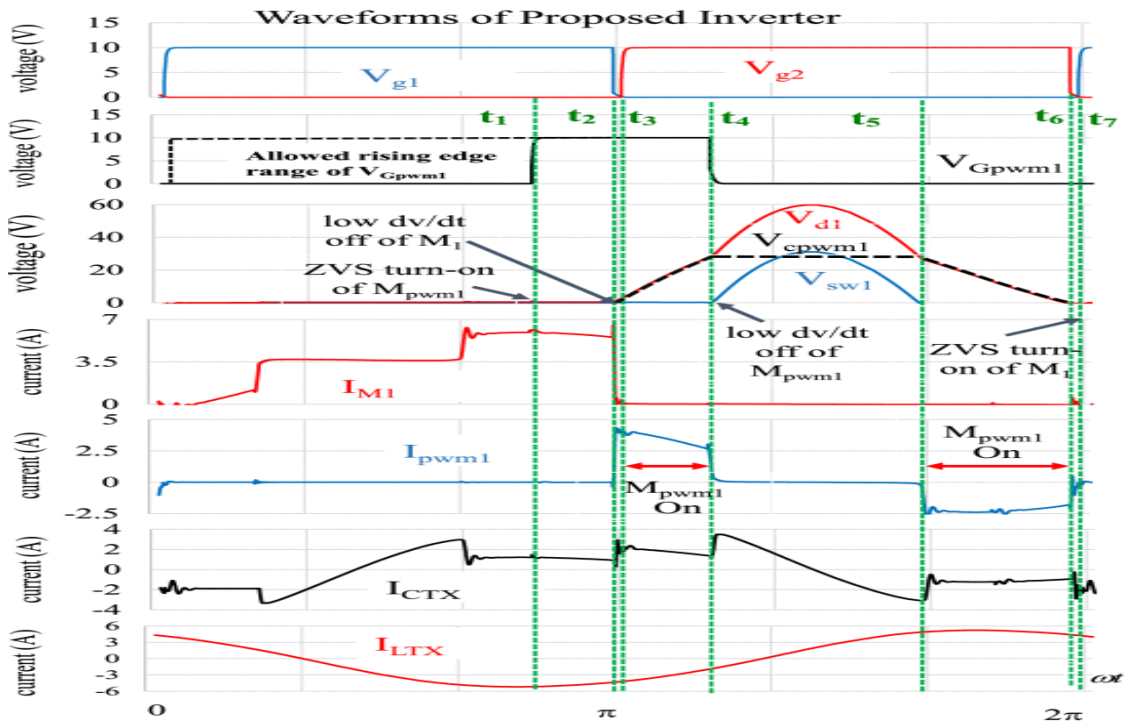


Figure 4.22 Waveforms Of Autotuning Inverter [95].

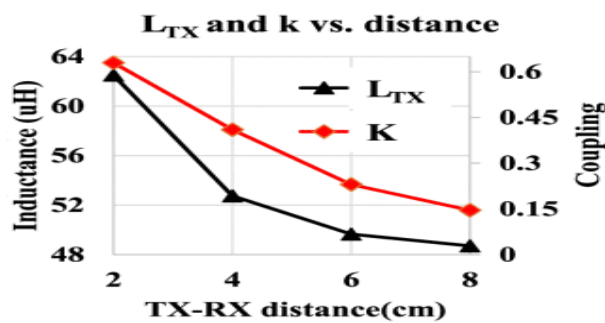


Figure 4.23 Variation Of L_{TX} And Coupling k With Respect To TX–RX Distance [95].

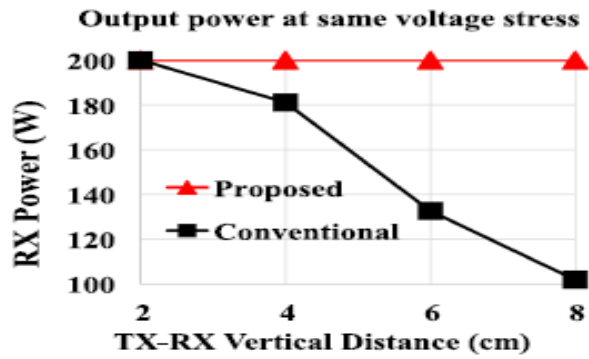


Figure 4.24 RX power with respect to distance [95].

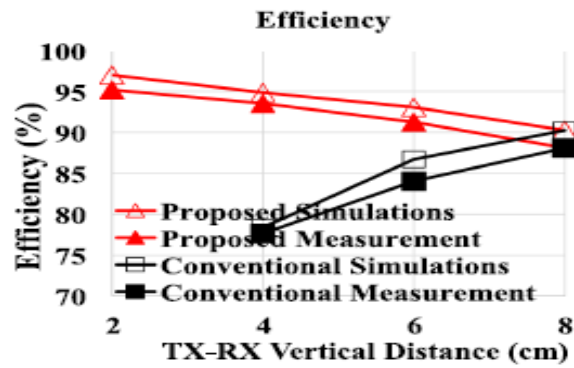


Figure 4.25 TX-to-RX efficiency comparison between the conventional [95].

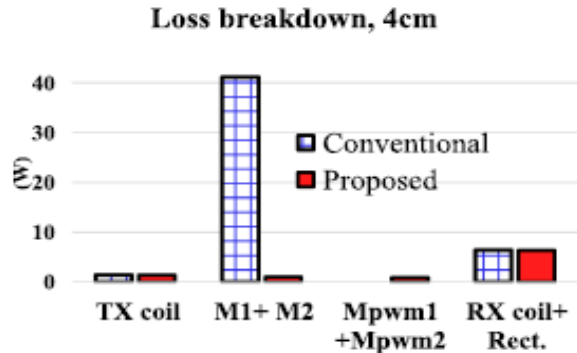


Figure 4.26 Loss break down at TX-RX distance of 4 cm [95].

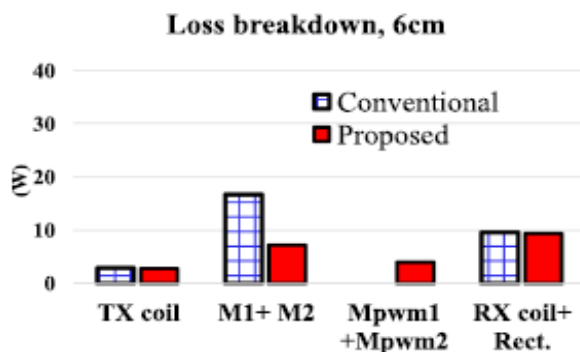


Figure 4.27 Loss break down at TX-RX distance of 6 cm [95].

The measurements verified that the proposed method achieves maximum 1.96 times higher output power and 15.86% higher efficiency with the same voltage stress on switches [95].

5 CONCLUSION AND FUTURE WORK

5.1 CONCLUSION

Wireless Power Transfer is becoming a reality sooner or later, in order to get rid off difficulties that may face the wired charging. And as we are transferring into the modern technology world that includes Internet of Things, Electric Cars, advanced medical devices and possible new mobility trends like Electric Air Vehicles, Hyperloops and Super-fast Electric Trains- it's mandatory that new technology for delivering electric energy should be developed, as well as achieving Nikola Tesla dream of using whole earth as conductor as mentioned in 1.1 above.

The principles of WPT analysed in 2.2 above shows that the far field topologies used now are ineffective and face a lot of problems. That makes the Near field methods more convenient for use. Then Capacitive and Inductive were further investigated. An established decision suggests that Capacitive are better in High frequency application because the higher the frequency the lower the capacitive reactance. This decision rises a question of the safety of this technology since high Electric fields are dangerous for living being which might limit the range of applications for such a technology.

Through the research it's found out that The Resonance Magnetic Coupling (RIPT) is the most useful technique to transfer electric power wirelessly. Since it utilizes the resonance phenomenon which cancels out the reactance from the active components as discussed in 3 above. The resonance is realised by the use of compensation topologies which are discussed briefly in 3.1.2 above. It's established that the use of hybrid topologies will combine the benefits of the basic Compensation topologies.

Then it's concluded that the misalignment that may occur during lifetime application of the technology- that may affect both Mutual Inductance and Operating Frequency, Power Transferred and Efficiency as discussed in 3.1.4 above; this will result in the diminishing of resonance idea as a whole. To solve this problem, it's suggested to use power converters in order to tune the frequency according to circuit parameters.

There's a wide variety of Power converters, the power converters that may be used are established in 4 above some of the converters are a combination of other types. The main idea behind a Resonant converter is the ability to achieve Zero Current Switching ZCS, Zero Voltage Switching ZVS and Zero Phase Angle ZPA; by using these techniques the resonant frequency can be retrieved by comparing the wave forms through these techniques. It's found out that Current-fed push-pull Resonant Converter evaluated in 4.2.5.1 above is the most useful option since it automatically generates the driving signal as well as it's economically feasible in regards to other options.

The Conventional Current-Fed converter requires a gate driving circuit, suffers from high voltage stress and it loses energization in some cases of Resonance frequency change; hence, the solution is to always keep the circuit active, it can be achieved by implementing poly-phase scheme or as presented a combination from the Class D Cascaded topology. This will keep Circuit Energized and will reduce voltage stress on the converter.

Still under misalignment the chosen push-pull converter still suffers degradation in performance, so a control scheme is suggested as found in literature. This scheme proved to improve the efficiency of the system in case misalignment occurs.

5.2 FUTURE WORK

In the field of novel approach for Wireless power transfer methods this thesis is a step forward towards selecting the best option available Further studies include the tuning methods used in the converter selected, along with the control techniques that will make the selected options the most valuable. In addition to application of the proposed topology.

In addition to comparison between different resonant converters under different applications and various inputs; to determine the optimum selection for each use and to eliminate the uncertainty behind further implementation of near-field wireless power as one of the main methods for electricity transfer

REFERENCES

- [1] W. C. Brown, ‘The history of wireless power transmission’, *Solar Energy*, vol. 56, no. 1, pp. 3–21, Jan. 1996, doi: 10.1016/0038-092X(95)00080-B.
- [2] N. Tesla, “Apparatus for transmitting electrical energy,” 1,119,732, Dec. 01, 1914 [Online]. Available: <https://patentimages.storage.googleapis.com/8a/95/f3/1b1780c6941fb9/US1119732.pdf>
- [3] W. C. Brown, ‘The History of Power Transmission by Radio Waves’, *IEEE Transactions on Microwave Theory and Techniques*, vol. 32, no. 9, pp. 1230–1242, Sep. 1984, doi: 10.1109/TMTT.1984.1132833.
- [4] A. S. Marincic, ‘Nikola Tesla and the Wireless Transmission of Energy’, *IEEE Transactions on Power Apparatus and Systems*, vol. PAS-101, no. 10, pp. 4064–4068, Oct. 1982, doi: 10.1109/TPAS.1982.317084.
- [5] A. Mahesh, B. Chokkalingam, and L. Mihet-Popa, ‘Inductive Wireless Power Transfer Charging for Electric Vehicles—A Review’, *IEEE Access*, vol. 9, pp. 137667–137713, 2021, doi: 10.1109/ACCESS.2021.3116678.
- [6] S. Y. R. Hui, W. Zhong, and C. K. Lee, ‘A Critical Review of Recent Progress in Mid-Range Wireless Power Transfer’, *IEEE Transactions on Power Electronics*, vol. 29, no. 9, pp. 4500–4511, Sep. 2014, doi: 10.1109/TPEL.2013.2249670.
- [7] ‘Wireless Power for Medical Devices’. Accessed: Jun. 27, 2022. [Online]. Available: <https://www.mddionline.com/components/wireless-power-medical-devices>
- [8] ‘Witricity System’. Accessed: Jun. 27, 2022. [Online]. Available: available:%20http://top-news.in/usa/unique-manmade-%20materials-could-ease-wireless-power-transfer-210164
- [9] H. Feng, R. Tavakoli, O. C. Onar, and Z. Pantic, ‘Advances in High-Power Wireless Charging Systems: Overview and Design Considerations’, *IEEE Transactions on Transportation Electrification*, vol. 6, no. 3, pp. 886–919, Sep. 2020, doi: 10.1109/TTE.2020.3012543.
- [10] ‘Witricity Electric Vehicle Wireless Charging’. Accessed: Jun. 27, 2022. [Online]. Available: <https://witricity.com/wp-content/uploads/2021/12/witricity-assembly-diagram.jpg>
- [11] M. E. Baghdadi, Y. Benomar, O. Hegazy, Y. Yang, and J. Van Mierlo, ‘Design approach and interoperability analysis of wireless power transfer systems for vehicular applications’, in *2016 18th European Conference on Power Electronics and Applications (EPE’16 ECCE Europe)*, Sep. 2016, pp. 1–11. doi: 10.1109/EPE.2016.7695695.
- [12] N. Kuyvenhoven, C. Dean, J. Melton, J. Schwannecke, and A. E. Umenei, ‘Development of a foreign object detection and analysis method for wireless power systems’, in *2011 IEEE Symposium on Product Compliance Engineering Proceedings*, Oct. 2011, pp. 1–6. doi: 10.1109/PSES.2011.6088250.
- [13] ‘ISO. Ergonomics of the thermal environment. Methods for the assessment of human responses to contact with surfaces Part 1: Hot surfaces.’ Accessed: Jun. 27, 2022. [Online]. Available: <https://www.iso.org/standard/43558.html>
- [14] S. D. Barman, A. W. Reza, N. Kumar, Md. E. Karim, and A. B. Munir, ‘Wireless powering by magnetic resonant coupling: Recent trends in wireless power transfer system and its applications’,

Renewable and Sustainable Energy Reviews, vol. 51, pp. 1525–1552, Nov. 2015, doi: 10.1016/j.rser.2015.07.031.

- [15] P. Venugopal, S. Bandyopadhyay, P. Bauer, and J. Ferreira, ‘A Generic Matrix Method to Model the Magnetics of Multi-Coil Air-Cored Inductive Power Transfer Systems’, *Energies*, vol. 10, p. 774, Jun. 2017, doi: 10.3390/en10060774.
- [16] K. Knaisch and P. Gratzfeld, ‘Comparison of magnetic couplers for inductive electric vehicle charging using accurate numerical simulation and statistical methods’, in *2015 5th International Electric Drives Production Conference (EDPC)*, Sep. 2015, pp. 1–10. doi: 10.1109/EDPC.2015.7323223.
- [17] S. Chopra and P. Bauer, ‘Analysis and design considerations for a contactless power’, in *Analysis and design considerations for a contactless power*, 2011, pp. 1–6.
- [18] S. Lukic and Z. Pantic, ‘Cutting the Cord: Static and Dynamic Inductive Wireless Charging of Electric Vehicles’, *IEEE Electrification Magazine*, vol. 1, no. 1, pp. 57–64, Sep. 2013, doi: 10.1109/MELE.2013.2273228.
- [19] T. Kan, Y. Zhang, Z. Yan, P. P. Mercier, and C. C. Mi, ‘A Rotation-Resilient Wireless Charging System for Lightweight Autonomous Underwater Vehicles’, *IEEE Transactions on Vehicular Technology*, vol. 67, no. 8, pp. 6935–6942, Aug. 2018, doi: 10.1109/TVT.2018.2836988.
- [20] Z. Bi, T. Kan, C. C. Mi, Y. Zhang, Z. Zhao, and G. A. Keoleian, ‘A review of wireless power transfer for electric vehicles: Prospects to enhance sustainable mobility’, *Applied Energy*, vol. 179, pp. 413–425, Oct. 2016, doi: 10.1016/j.apenergy.2016.07.003.
- [21] X. Lu, P. Wang, D. Niyato, and E. Hossain, ‘Dynamic spectrum access in cognitive radio networks with RF energy harvesting’, *IEEE Wireless Communications*, vol. 21, no. 3, pp. 102–110, Jun. 2014, doi: 10.1109/MWC.2014.6845054.
- [22] K. Jin and W. Zhou, ‘Wireless Laser Power Transmission: A Review of Recent Progress’, *IEEE Transactions on Power Electronics*, vol. 34, no. 4, pp. 3842–3859, Apr. 2019, doi: 10.1109/TPEL.2018.2853156.
- [23] X. Lu, P. Wang, D. Niyato, D. I. Kim, and Z. Han, ‘Wireless Charging Technologies: Fundamentals, Standards, and Network Applications’, *IEEE Communications Surveys & Tutorials*, vol. 18, no. 2, pp. 1413–1452, Secondquarter 2016, doi: 10.1109/COMST.2015.2499783.
- [24] M. P. Theodoridis, ‘Effective Capacitive Power Transfer’, *IEEE Transactions on Power Electronics*, vol. 27, no. 12, pp. 4906–4913, Dec. 2012, doi: 10.1109/TPEL.2012.2192502.
- [25] H. Zhang, F. Lu, H. Hofmann, W. Liu, and C. C. Mi, ‘A Four-Plate Compact Capacitive Coupler Design and LCL-Compensated Topology for Capacitive Power Transfer in Electric Vehicle Charging Application’, *IEEE Transactions on Power Electronics*, vol. 31, no. 12, pp. 8541–8551, Dec. 2016, doi: 10.1109/TPEL.2016.2520963.
- [26] S. Sinha, S. Maji, and K. K. Afridi, ‘Comparison of Large Air-Gap Inductive and Capacitive Wireless Power Transfer Systems’, in *2021 IEEE Applied Power Electronics Conference and Exposition (APEC)*, Jun. 2021, pp. 1604–1609. doi: 10.1109/APEC42165.2021.9487431.
- [27] A. Triviño-Cabrera, J. M. González-González, and J. A. Aguado, *Wireless Power Transfer for Electric Vehicles: Foundations and Design Approach*. Cham: Springer International Publishing, 2020. doi: 10.1007/978-3-030-26706-3.

- [28] C. Zheng, B. Chen, L. Zhang, R. Chen, and J. -S. Lai, ‘Design considerations of LLC resonant converter for contactless laptop charger’, in *2015 IEEE Applied Power Electronics Conference and Exposition (APEC)*, Mar. 2015, pp. 3341–3347. doi: 10.1109/APEC.2015.7104832.
- [29] R. Vaka and R. K. Keshri, ‘Review on Contactless Power Transfer for Electric Vehicle Charging’, *Energies*, vol. 10, no. 5, 2017, doi: 10.3390/en10050636.
- [30] A. Kurs, A. Karalis, R. Moffatt, J. D. Joannopoulos, P. Fisher, and M. Soljačić, ‘Wireless Power Transfer via Strongly Coupled Magnetic Resonances’, *Science*, vol. 317, no. 5834, pp. 83–86, Jul. 2007, doi: 10.1126/science.1143254.
- [31] C. Liu, C. Jiang, and C. Qiu, ‘Overview of coil designs for wireless charging of electric vehicle’, in *2017 IEEE PELS Workshop on Emerging Technologies: Wireless Power Transfer (WoW)*, May 2017, pp. 1–6. doi: 10.1109/WoW.2017.7959389.
- [32] D. Patil, M. K. McDonough, J. M. Miller, B. Fahimi, and P. T. Balsara, ‘Wireless Power Transfer for Vehicular Applications: Overview and Challenges’, *IEEE Transactions on Transportation Electrification*, vol. 4, no. 1, pp. 3–37, Mar. 2018, doi: 10.1109/TTE.2017.2780627.
- [33] ‘IPT Fact Sheet Series: No. 2 Magnetic Circuits for Powering Electric Vehicles’, 2014.
- [34] M. Budhia, G. Covic, and J. T. Boys, ‘A new IPT magnetic coupler for electric vehicle charging systems’, *IECON 2010 - 36th Annual Conference on IEEE Industrial Electronics Society*, pp. 2487–2492, 2010.
- [35] S. Kim, G. A. Covic, and J. T. Boys, ‘Tripolar Pad for Inductive Power Transfer Systems for EV Charging’, *IEEE Transactions on Power Electronics*, vol. 32, no. 7, pp. 5045–5057, Jul. 2017, doi: 10.1109/TPEL.2016.2606893.
- [36] Y. Liu, T. Wu, and M. Fu, ‘Interleaved Capacitive Coupler for Wireless Power Transfer’, *IEEE Transactions on Power Electronics*, vol. 36, no. 12, pp. 13526–13535, Dec. 2021, doi: 10.1109/TPEL.2021.3086629.
- [37] F. Lu, H. Zhang, H. Hofmann, and C. Mi, ‘A Double-Sided LCLC-Compensated Capacitive Power Transfer System for Electric Vehicle Charging’, *IEEE Transactions on Power Electronics*, vol. 30, no. 11, pp. 6011–6014, Nov. 2015, doi: 10.1109/TPEL.2015.2446891.
- [38] N. M. A. N.Ravishankar, ‘Analysis and design of noncontact charger using lc load resonant coupling for electrical vehicle system’, *The International Journal of Engineering and Science*, pp. 42–48, Mar. 2015.
- [39] X. Wei, Z. Wang, and H. Dai, ‘A Critical Review of Wireless Power Transfer via Strongly Coupled Magnetic Resonances’, *Energies*, vol. 7, no. 7, pp. 4316–4341, Jul. 2014, doi: 10.3390/en7074316.
- [40] Chwei-Sen Wang, G. A. Covic, and O. H. Stielau, ‘Power transfer capability and bifurcation phenomena of loosely coupled inductive power transfer systems’, *IEEE Transactions on Industrial Electronics*, vol. 51, no. 1, pp. 148–157, Feb. 2004, doi: 10.1109/TIE.2003.822038.
- [41] O. H. Stielau and G. A. Covic, ‘Design of loosely coupled inductive power transfer systems’, in *PowerCon 2000. 2000 International Conference on Power System Technology. Proceedings (Cat. No.00EX409)*, Dec. 2000, vol. 1, pp. 85–90 vol.1. doi: 10.1109/ICPST.2000.900036.

- [42] X. Huang, Q. Ji, L. Tan, W. Wang, J. Zhao, and Y. Zhou, ‘Study on series-parallel model of wireless power transfer via magnetic resonance coupling’, vol. 28, pp. 171–176+187, Mar. 2013.
- [43] L. Sandrolini, U. Reggiani, G. Puccetti, and Y. Neau, ‘Equivalent circuit characterization of resonant magnetic coupling for wireless transmission of electrical energy: CHARACTERIZATION OF RESONANT MAGNETIC COUPLING FOR ENERGY TRANSMISSION’, *Int. J. Circ. Theor. Appl.*, vol. 41, no. 7, pp. 753–771, Jul. 2013, doi: 10.1002/cta.1873.
- [44] Xun Liu, W. M. Ng, C. K. Lee, and S. Y. Hui, ‘Optimal operation of contactless transformers with resonance in secondary circuits’, in *2008 Twenty-Third Annual IEEE Applied Power Electronics Conference and Exposition*, Feb. 2008, pp. 645–650. doi: 10.1109/APEC.2008.4522790.
- [45] T. Nagashima, X. Wei, T. Suetsugu, M. K. Kazimierczuk, and H. Sekiya, ‘Waveform Equations, Output Power, and Power Conversion Efficiency for Class-E Inverter Outside Nominal Operation’, *IEEE Transactions on Industrial Electronics*, vol. 61, no. 4, pp. 1799–1810, Apr. 2014, doi: 10.1109/TIE.2013.2267693.
- [46] S. Aldhaher, P. C. Luk, K. E. K. Drissi, and J. F. Whidborne, ‘High-Input-Voltage High-Frequency Class E Rectifiers for Resonant Inductive Links’, *IEEE Transactions on Power Electronics*, vol. 30, no. 3, pp. 1328–1335, Mar. 2015, doi: 10.1109/TPEL.2014.2316170.
- [47] T. Nagashima, X. Wei, E. Bou, E. Alarcón, M. K. Kazimierczuk, and H. Sekiya, ‘Steady-State Analysis of Isolated Class-E\$^2\$ Converter Outside Nominal Operation’, *IEEE Transactions on Industrial Electronics*, vol. 64, no. 4, pp. 3227–3238, Apr. 2017, doi: 10.1109/TIE.2016.2631439.
- [48] P. C. K. Luk and S. Aldhaher, ‘Analysis and design of a Class D rectifier for a Class E driven wireless power transfer system’, in *2014 IEEE Energy Conversion Congress and Exposition (ECCE)*, Sep. 2014, pp. 851–857. doi: 10.1109/ECCE.2014.6953486.
- [49] W. Zhang and C. C. Mi, ‘Compensation Topologies of High-Power Wireless Power Transfer Systems’, *IEEE Transactions on Vehicular Technology*, vol. 65, no. 6, pp. 4768–4778, Jun. 2016, doi: 10.1109/TVT.2015.2454292.
- [50] A. Zaheer, H. Hao, G. A. Covic, and D. Kacprzak, ‘Investigation of Multiple Decoupled Coil Primary Pad Topologies in Lumped IPT Systems for Interoperable Electric Vehicle Charging’, *IEEE Transactions on Power Electronics*, vol. 30, no. 4, pp. 1937–1955, Apr. 2015, doi: 10.1109/TPEL.2014.2329693.
- [51] R. W. Erickson and D. Maksimović, *Fundamentals of Power Electronics*. Boston, MA: Springer US, 2001. doi: 10.1007/b100747.
- [52] S. Varikkottil, F. D. J. Lionel, M. K. Srinivasan, S. Williamson, R. Kannan, and L. I. Izhar, ‘Role of Power Converters in Inductive Power Transfer System for Public Transport—A Comprehensive Review’, *Symmetry*, vol. 14, no. 3, p. 508, Mar. 2022, doi: 10.3390/sym14030508.
- [53] V. Shevchenko, O. Husev, R. Strzelecki, B. Pakhaluk, N. Poliakov, and N. Strzelecka, ‘Compensation Topologies in IPT Systems: Standards, Requirements, Classification, Analysis, Comparison and Application’, *IEEE Access*, vol. 7, pp. 120559–120580, 2019, doi: 10.1109/ACCESS.2019.2937891.
- [54] C. Jiang, K. T. Chau, C. Liu, and C. H. T. Lee, ‘An Overview of Resonant Circuits for Wireless Power Transfer’, *Energies*, vol. 10, no. 7, 2017, doi: 10.3390/en10070894.

- [55] Q. Zhu, L. Wang, Y. Guo, C. Liao, and F. Li, 'Applying LCC Compensation Network to Dynamic Wireless EV Charging System', *IEEE Transactions on Industrial Electronics*, vol. 63, no. 10, pp. 6557–6567, Oct. 2016, doi: 10.1109/TIE.2016.2529561.
- [56] Z. Pantic, S. Bai, and S. M. Lukic, 'ZCS \$LCC\\$-Compensated Resonant Inverter for Inductive-Power-Transfer Application', *IEEE Transactions on Industrial Electronics*, vol. 58, no. 8, pp. 3500–3510, Aug. 2011, doi: 10.1109/TIE.2010.2081954.
- [57] Chwei-Sen Wang, G. A. Covic, and O. H. Stielau, 'Investigating an LCL load resonant inverter for inductive power transfer applications', *IEEE Transactions on Power Electronics*, vol. 19, no. 4, pp. 995–1002, Jul. 2004, doi: 10.1109/TPEL.2004.830098.
- [58] N. A. Keeling, G. A. Covic, and J. T. Boys, 'A Unity-Power-Factor IPT Pickup for High-Power Applications', *IEEE Transactions on Industrial Electronics*, vol. 57, no. 2, pp. 744–751, Feb. 2010, doi: 10.1109/TIE.2009.2027255.
- [59] 'Jason Starck. Lessons In Electric Circuits: Resonance.' Accessed: Jun. 29, 2022. [Online]. Available: https://www.ibiblio.org/kuphaldt/electricCircuits/AC/AC_6.html
- [60] S. Varikkottil and F. D. J. L, 'Estimation of Optimal Operating Frequency for Wireless EV Charging System under Misalignment', *Electronics*, vol. 8, no. 3, 2019, doi: 10.3390/electronics8030342.
- [61] N. Jamal, S. Saat, and A. Z. Shukor, 'A study on performances of different compensation topologies for loosely coupled inductive power transfer system', in *2013 IEEE International Conference on Control System, Computing and Engineering*, Dec. 2013, pp. 173–178. doi: 10.1109/IC-CSCE.2013.6719954.
- [62] Y. H. Sohn, B. H. Choi, E. S. Lee, G. C. Lim, G. Cho, and C. T. Rim, 'General Unified Analyses of Two-Capacitor Inductive Power Transfer Systems: Equivalence of Current-Source SS and SP Compensations', *IEEE Transactions on Power Electronics*, vol. 30, no. 11, pp. 6030–6045, Nov. 2015, doi: 10.1109/TPEL.2015.2409734.
- [63] B. X. Nguyen, W. Peng, and D. M. Vilathgamuwa, 'Multilevel converter topologies based high power inductive power transfer systems', in *2016 IEEE International Conference on Sustainable Energy Technologies (ICSET)*, Nov. 2016, pp. 264–269. doi: 10.1109/ICSET.2016.7811793.
- [64] 'IEC 60364-7; Requirements for Special Installations or Locations. IEC: Geneva, Switzerland, 2017'. Accessed: Jun. 30, 2022. [Online]. Available: <https://webstore.iec.ch/publication/33784>
- [65] J. M. Stankiewicz and A. Choroszucho, 'Comparison of the Efficiency and Load Power in Periodic Wireless Power Transfer Systems with Circular and Square Planar Coils', *Energies*, vol. 14, no. 16, 2021, doi: 10.3390/en14164975.
- [66] A. A. Khan, H. Cha, and H. F. Ahmed, 'High-Efficiency Single-Phase AC–AC Converters Without Commutation Problem', *IEEE Transactions on Power Electronics*, vol. 31, no. 8, pp. 5655–5665, Aug. 2016, doi: 10.1109/TPEL.2015.2494605.
- [67] H. Sarnago, O. Lucía, A. Mediano, and J. M. Burdío, 'Efficient and Cost-Effective ZCS Direct AC–AC Resonant Converter for Induction Heating', *IEEE Transactions on Industrial Electronics*, vol. 61, no. 5, pp. 2546–2555, May 2014, doi: 10.1109/TIE.2013.2262752.

- [68] H. L. Li, A. P. Hu, and G. A. Covic, ‘A Direct AC–AC Converter for Inductive Power-Transfer Systems’, *IEEE Transactions on Power Electronics*, vol. 27, no. 2, pp. 661–668, Feb. 2012, doi: 10.1109/TPEL.2011.2159397.
- [69] M. Moghaddami, A. Anzalchi, and A. I. Sarwat, ‘Single-Stage Three-Phase AC–AC Matrix Converter for Inductive Power Transfer Systems’, *IEEE Transactions on Industrial Electronics*, vol. 63, no. 10, pp. 6613–6622, Oct. 2016, doi: 10.1109/TIE.2016.2563408.
- [70] P. W. Wheeler, J. Rodriguez, J. C. Clare, L. Empringham, and A. Weinstein, ‘Matrix converters: a technology review’, *IEEE Transactions on Industrial Electronics*, vol. 49, no. 2, pp. 276–288, Apr. 2002, doi: 10.1109/41.993260.
- [71] Y. Zhang and X. Ruan, ‘Three-Phase AC–AC Converter With Controllable Phase and Amplitude’, *IEEE Transactions on Industrial Electronics*, vol. 62, no. 9, pp. 5689–5699, Sep. 2015, doi: 10.1109/TIE.2015.2410761.
- [72] X. Ju, L. Dong, X. Huang, and X. Liao, ‘Switching Technique for Inductive Power Transfer at High- \$Q\\$ Regimes’, *IEEE Transactions on Industrial Electronics*, vol. 62, no. 4, pp. 2164–2173, Apr. 2015, doi: 10.1109/TIE.2014.2361806.
- [73] F. del-Aguila-Lopez, P. Pala-Schonwalder, P. Molina-Gaudio, and A. Mediano-Heredia, ‘A Discrete-Time Technique for the Steady-State Analysis of Nonlinear Class-E Amplifiers’, *IEEE Transactions on Circuits and Systems I: Regular Papers*, vol. 54, no. 6, pp. 1358–1366, Jun. 2007, doi: 10.1109/TCSI.2007.896741.
- [74] M. Liu, M. Fu, and C. Ma, ‘Low-Harmonic-Contents and High-Efficiency Class E Full-Wave Current-Driven Rectifier for Megahertz Wireless Power Transfer Systems’, *IEEE Transactions on Power Electronics*, vol. 32, no. 2, pp. 1198–1209, Feb. 2017, doi: 10.1109/TPEL.2016.2551288.
- [75] M. Pinuela, D. C. Yates, S. Lucyszyn, and P. D. Mitcheson, ‘Maximizing DC-to-Load Efficiency for Inductive Power Transfer’, *IEEE Transactions on Power Electronics*, vol. 28, no. 5, pp. 2437–2447, May 2013, doi: 10.1109/TPEL.2012.2215887.
- [76] T. Nagashima, X. Wei, E. Bou, E. Alarcón, M. K. Kazimierczuk, and H. Sekiya, ‘Analysis and Design of Loosely Inductive Coupled Wireless Power Transfer System Based on Class-\$\rm E^2\$ DC-DC Converter for Efficiency Enhancement’, *IEEE Transactions on Circuits and Systems I: Regular Papers*, vol. 62, no. 11, pp. 2781–2791, Nov. 2015, doi: 10.1109/TCSI.2015.2482338.
- [77] S. Aldhaher, P. C. -K. Luk, A. Bati, and J. F. Whidborne, ‘Wireless Power Transfer Using Class E Inverter With Saturable DC-Feed Inductor’, *IEEE Transactions on Industry Applications*, vol. 50, no. 4, pp. 2710–2718, Aug. 2014, doi: 10.1109/TIA.2014.2300200.
- [78] H. Hao, G. A. Covic, and J. T. Boys, ‘A Parallel Topology for Inductive Power Transfer Power Supplies’, *IEEE Transactions on Power Electronics*, vol. 29, no. 3, pp. 1140–1151, Mar. 2014, doi: 10.1109/TPEL.2013.2262714.
- [79] A. Schonknecht and R. W. A. A. De Doncker, ‘Novel topology for parallel connection of soft-switching high-power high-frequency inverters’, *IEEE Transactions on Industry Applications*, vol. 39, no. 2, pp. 550–555, Apr. 2003, doi: 10.1109/TIA.2003.809453.
- [80] Y. Li, R. Mai, M. Yang, and Z. He, ‘Cascaded multi-level inverter based IPT systems for high power applications’, *Journal of Power Electronics*, vol. 15, no. 6, pp. 1508–1516, 2015.

- [81] B. X. Nguyen, D. M. Vilathgamuwa, G. Foo, P. Wang, and A. Ong, ‘A modified cascaded multi-level converter topology for high power bidirectional inductive power transfer systems with the reduction of switching devices and power losses’, 2015, pp. 93–97.
- [82] H. Koizumi and K. Kurokawa, ‘Analysis of the class DE inverter with thinned-out driving patterns’, *IEEE Transactions on Industrial Electronics*, vol. 54, no. 2, pp. 1150–1160, 2007.
- [83] T. Nagashima, X. Wei, and H. Sekiya, ‘Analytical design procedure for resonant inductively coupled wireless power transfer system with class-DE inverter and class-E rectifier’, in *2014 IEEE Asia Pacific Conference on Circuits and Systems (APCCAS)*, Nov. 2014, pp. 288–291. doi: 10.1109/APCCAS.2014.7032776.
- [84] Z. Kaczmarczyk, ‘High-Efficiency Class E,\$hbox{EF_2}\$, and\$hbox{E/F_3\$Inverters’}, *IEEE Transactions on Industrial Electronics*, vol. 53, no. 5, pp. 1584–1593, Oct. 2006, doi: 10.1109/TIE.2006.882011.
- [85] S. Aldhaher, D. C. Yates, and P. D. Mitcheson, ‘Modeling and Analysis of Class EF and Class E/F Inverters With Series-Tuned Resonant Networks’, *IEEE Transactions on Power Electronics*, vol. 31, no. 5, pp. 3415–3430, May 2016, doi: 10.1109/TPEL.2015.2460997.
- [86] A. Abdolkhani, A. P. Hu, and J. Tian, ‘Autonomous Polyphase Current-Fed Push–Pull Resonant Converter Based on Ring Coupled Oscillators’, *IEEE Journal of Emerging and Selected Topics in Power Electronics*, vol. 3, no. 2, pp. 568–576, Jun. 2015, doi: 10.1109/JESTPE.2014.2377171.
- [87] A. Abdolkhani, A. P. Hu, G. A. Covic, and M. Moridnejad, ‘Through-Hole Contactless Slipring System Based on Rotating Magnetic Field for Rotary Applications’, *IEEE Transactions on Industry Applications*, vol. 50, no. 6, pp. 3644–3655, Dec. 2014, doi: 10.1109/TIA.2014.2312998.
- [88] C. Liu, K. T. Chau, D. Wu, and S. Gao, ‘Opportunities and Challenges of Vehicle-to-Home, Vehicle-to-Vehicle, and Vehicle-to-Grid Technologies’, *Proceedings of the IEEE*, vol. 101, no. 11, pp. 2409–2427, Nov. 2013, doi: 10.1109/JPROC.2013.2271951.
- [89] U. K. Madawala and D. J. Thrimawithana, ‘A Bidirectional Inductive Power Interface for Electric Vehicles in V2G Systems’, *IEEE Transactions on Industrial Electronics*, vol. 58, no. 10, pp. 4789–4796, Oct. 2011, doi: 10.1109/TIE.2011.2114312.
- [90] M. J. Neath, A. K. Swain, U. K. Madawala, and D. J. Thrimawithana, ‘An Optimal PID Controller for a Bidirectional Inductive Power Transfer System Using Multiobjective Genetic Algorithm’, *IEEE Transactions on Power Electronics*, vol. 29, no. 3, pp. 1523–1531, Mar. 2014, doi: 10.1109/TPEL.2013.2262953.
- [91] A. K. Swain, M. J. Neath, U. K. Madawala, and D. J. Thrimawithana, ‘A Dynamic Multivariable State-Space Model for Bidirectional Inductive Power Transfer Systems’, *IEEE Transactions on Power Electronics*, vol. 27, no. 11, pp. 4772–4780, Nov. 2012, doi: 10.1109/TPEL.2012.2185712.
- [92] S. Chudjuarjeen, C. Koompai, and V. Monyakul, ‘Full-bridge current-fed inverter with automatic frequency control for forging application’, in *2004 IEEE Region 10 Conference TENCON 2004.*, Nov. 2004, vol. D, pp. 128-131 Vol. 4. doi: 10.1109/TENCON.2004.1414885.
- [93] H. Kobayashi, J. M. Hinrichs, and P. M. Asbeck, ‘Current-mode class-D power amplifiers for high-efficiency RF applications’, *IEEE Transactions on Microwave Theory and Techniques*, vol. 49, no. 12, pp. 2480–2485, Dec. 2001, doi: 10.1109/22.971639.

- [94] M. K. Kazimierczuk and D. Czarkowski, *Resonant power converters*, 2nd ed. Hoboken, N.J.: Wiley, 2011.
- [95] S. Ali Khan and D. Ahn, ‘Automatic Resonance Tuning With ON/OFF Soft Switching for Push–Pull Parallel-Resonant Inverter in Wireless Power Transfer’, *IEEE Transactions on Power Electronics*, vol. 37, no. 9, pp. 10133–10138, Sep. 2022, doi: 10.1109/TPEL.2022.3168978.
- [96] A. Abdolkhani and A. P. Hu, ‘Improved autonomous current-fed push–pull resonant inverter’, *IET Power Electronics*, vol. 7, no. 8, pp. 2103–2110, Aug. 2014, doi: 10.1049/iet-pel.2013.0749.
- [97] A. P. Hu, G. A. Covic, and J. T. Boys, ‘Direct ZVS start-up of a current-fed resonant inverter’, *IEEE Transactions on Power Electronics*, vol. 21, no. 3, pp. 809–812, May 2006, doi: 10.1109/TPEL.2006.873226.
- [98] J. -. C. Zhan, K. Maurice, J. Duster, and K. T. Kornegay, ‘Analysis and design of negative impedance LC oscillators using bipolar transistors’, *IEEE Transactions on Circuits and Systems I: Fundamental Theory and Applications*, vol. 50, no. 11, pp. 1461–1464, Nov. 2003, doi: 10.1109/TCSI.2003.818617.
- [99] A. Buonomo and A. L. Schiavo, ‘Modelling and analysis of differential VCOs’, *Int. J. Circ. Theor. Appl.*, vol. 32, no. 3, pp. 117–131, May 2004, doi: 10.1002/cta.270.
- [100] N. M. Nguyen and R. G. Meyer, ‘Start-up and frequency stability in high-frequency oscillators’, *IEEE Journal of Solid-State Circuits*, vol. 27, no. 5, pp. 810–820, May 1992, doi: 10.1109/4.133172.
- [101] A. E. L. Costa and R. L. Andersen, ‘High-gain three-phase current-fed push–pull DC–DC converter’, *IET Power Electronics*, vol. 13, no. 3, pp. 545–556, Feb. 2020, doi: 10.1049/iet-pel.2019.0843.